Thesis, FRANZEN Rachelle

Auteur : Grodent, Sarah
Promoteur(s) : Neirinckx, Virginie
Faculté : Faculté de Médecine
Diplôme : Master en sciences biomédicales, à finalité approfondie
Année académique : 2025-2026
URI/URL : http://hdl.handle.net/2268.2/26011

Master's Thesis

Validation of a PTK7-targeted, AAV-mediated Suicide-Gene Therapy for Glioblastoma

University of Liège
Faculty of Medicine
Laboratory of Nervous System Disorders and Therapies (GIGA Neurosciences)

Master's thesis presented in partial fulfilment of the requirements for the degree of Master in Biomedical Science, Research Focus

by **Sarah Grodent**

Promotor and Co-promotor:
Virginie **Neirinckx**
Bernard **Rogister**

Reading committee:
Akeila **Bellahcène**
Emmanuel **Di Valentin**
Arnaud **Lombard**

Academic year 2025-2026

LIÈGE université Médecine

LIÈGE université GIGA Neurosciences

Acknowledgments

To begin with, I would like to thank the members of my jury — Akeila Bellahcène, Emmanuel Di Valentin, and Arnaud Lombard — for the time devoted to reading and evaluating this work. I hope you will enjoy discovering it as much as I enjoyed writing it.

First and foremost, I wanted to thank Pr Bernard Rogister for his warm welcome, his kindness, and the many "Comment ça va miss?" and "Quoi de neuf?". It goes without saying that I am also infinitely grateful to my incredible promotor, Dr. Virginie Neirinckx. Thank you for your trust, your kindness, your availability, and your constant support throughout this project. I couldn't have asked for better supervision. I would also like to express my sincere thanks to Kim Mottard, who introduced me to this wonderful project and guided me through every step of it. My gratitude extends to all the team members including Célia Lemoine, Natasha Herremans, Amandine Kuppens, Julie Cokaiko, Damla Isci and lab buddies Matheo Dumont and Théo Cornet, for your support, your kindness, your interest in my work, and for your willingness to help whenever needed. I am also grateful to Céline Vanwinge from the GIGA Flow Cytometry platform for her help and patience during the many sessions on the CytoFlex. A special mention goes to Enéa, who has become a close friend during these two short months by her side. More broadly, I would like to thank everyone I have had the chance to meet over the past few years. Even if our paths have diverged, I will always remember the great atmosphere and the wonderful moments we shared. My thanks also go to Lola, who became a true friend during this master's degree, as well as to Liza, my SBIM partner over these last years. I hope we will one day walk these corridors again as PhD students.

Finally, I could not conclude this master's thesis without thanking my parents and my brother for their unwavering support during this emotionally intense year. Thank you for believing in me and for encouraging me, even when I doubted myself, both in my studies and in life more generally. We went through illness together and you know how being able to work on a project like this means to me. Thanks also to the rest of my family and to those true friends, who can be counted on one hand, but who are essential to my well-being. Last but not least, I wanted to thank my life partner, Antoine, for his patience, his encouragement, and his unconditional love from the very beginning of our journey together.

Résumé

Le glioblastome (GBM) est la tumeur cérébrale primitive la plus fréquente et la plus agressive chez l'adulte. Malgré les traitements standards incluant chirurgie, radiothérapie et chimiothérapie par témozolomide (TMZ), la survie médiane actuelle reste limitée à approximativement 9 mois et est caractérisée par des rechutes systématiques. Cette évolution défavorable s'explique notamment par une forte hétérogénéité intratumorale, un microenvironnement tumoral immunosuppressif, un passage limité des traitements à travers la barrière hémato-encéphalique, ainsi que par la persistance de cellules souches de glioblastome (CSG), impliquées dans la résistance thérapeutique et les récidives. Dans ce contexte, le laboratoire a développé une approche thérapeutique visant à cibler la protéine tyrosine kinase-7 (PTK7), fortement exprimée par les cellules de GBM. Au cours de ce mémoire, l'objectif principal était d'évaluer l'efficacité et la spécificité de cette stratégie thérapeutique. Pour répondre à cet objectif, nous avons caractérisé la cytotoxicité induite dans des lignées cellulaires $PTK7^+$, analysé la sélectivité de l'effet en conditions de coculture $PTK7^+/PTK7^-$, et validé ces observations dans des modèles translationnels de complexité croissante, incluant des modèles *in vivo*. Nous avons également développé un modèle de CSG murin exprimant PTK7, dans lequel nous avons étudié l'expression de la protéine et la spécificité du ciblage. Les résultats obtenus suggèrent une induction préférentielle de la mort cellulaire dans les cellules $PTK7^+$ exposées à la thérapie, associée à une activation de marqueurs apoptotiques, observée par western-blot et cytométrie en flux. En parallèle, la spécificité du ciblage a été confirmée en monocultures et cocultures de cellules $PTK7^+$ et $PTK7^-$. Ces observations ont été partiellement confirmées dans les tissus de xénogreffes intracérébrales, où des altérations morphologiques de la tumeur, ainsi que des foyers localisés positifs pour des marqueurs de mort cellulaire ont été observés. Enfin, un modèle murin de GBM exprimant PTK7 a été établi et validé pour de futures investigations translationnelles.

Abstract

Glioblastoma (GBM) is the most common and aggressive primary brain tumour in adults. Despite standard treatments, including surgery, radiotherapy, and chemotherapy with temozolomide (TMZ), the current median survival rate remains limited to approximately 9 months and is characterised by systematic relapses. This poor prognosis is primarily due to significant intratumoral heterogeneity, an immunosuppressive tumour microenvironnement (TME), limited penetration of treatments through the blood-brain barrier (BBB), and the persistence of glioblastoma stem cells (GSCs), which are implicated in treatment resistance and recurrence. In this context, the laboratory has developed a therapeutic approach aimed at targeting protein tyrosine kinase-7 (PTK7), which is highly expressed by GBM cells. The primary objective of this master thesis was to evaluate the efficacy and specificity of this therapeutic strategy. To achieve it, we characterised the cytotoxicity induced in $PTK7^+$ cell lines, analysed the selectivity of the effect under $PTK7^+/PTK7^-$ co-culture conditions, and validated these observations in translational models of increasing complexity, including *in vivo* models. We have also developed a mouse GSC model expressing PTK7, in which we examined protein expression and targeting specificity. The results suggest a preferential induction of cell death in $PTK7^+$ cells exposed to the therapy, associated with the activation of apoptotic markers observed by western blot and flow cytometry. Concurrently, the specificity of the targeting was confirmed in monocultures and co-cultures of $PTK7^+$ and $PTK7^-$ cells. These observations were partially validated in intracerebral xenograft tissues, where morphological alterations in the tumour, as well as localised foci positive for a cell death marker were recorded. Finally, a murine model of GBM expressing PTK7 was established and validated for future translational investigations.

Table of contents

Acknowledgments i
Résumé ii
Abstract iii
Glossary* vi
List of abbreviations viii
CHAPTER 1 - INTRODUCTION .....
1. GENERAL BACKGROUND ON PRIMARY BRAIN TUMOURS 1
1.1. Overview 1
1.2. Focus on Gliomas 1
1.2.1. General Features and Clinical Relevance of Gliomas 1
1.2.2. Integrated Histo-Molecular Diagnosis of Gliomas 2
A. The Founding Histopathological Era (1926-2007) 2
B. Towards Integrated Diagnostics (WHO 2016) - The Molecular Revolution 3
C. The 2021 WHO Edition (CNS5) - The Dominant Molecular Taxonomy 3
D. Diagnostic Methods and Limitations 4
E. Key Molecular Signatures in Adult Diffuse Gliomas 4
2. GLIOBLASTOMA 7
2.1. Epidemiology and Pathogenesis 7
2.2. Clinical and Molecular Features 8
2.3. Standard of Care 9
Maximal Safe Resection 9
Radiotherapy 9
Chemotherapy 10
Supportive care 10
2.4. The Main Mechanisms of Resistance and Recurrence in GBM 10
2.4.1. Concept of Glioblastoma Stem Cells 11
2.4.2. The Tumour Microenvironment 11
2.5. Treatment Prospects based on Immunotherapy 12
3. TARGETED THERAPIES 14
3.1. Surface Proteome in GBM 14
3.1.1. Diversity of Surface Proteins and Biological Implications 14
3.1.2. Brief Functional Role of Surface Proteins in GBM Signalling 15
3.1.3. GSCs as a key targeting issue 15
3.1.4. Identification and Validation of Surface Targets 16
3.2. Focus on PTK7 and Targeting Modalities 17
3.2.1. PTK7 functions in health and disease 17
3.2.2. PTK7 Targeting Strategies 18
Antibody-Drug Conjugates (ADCs) 18
CAR T-cells 18
Aptamer-Based Therapies 19
4. ADENO-ASSOCIATED VIRUSES (AAVS) AS TARGETED THERAPY TOOLS 20
4.1. Structure and Biological Characteristics of AAVs 20
4.2. Recombinant AAVs and Therapeutic Applications 20
5. WORK PERFORMED IN THE HOST LABORATORY 21
5.1. Identification and Validation of PTK7 as a Candidate Target 21
Surface Proteomic Identification of PTK7 in GSCs 21
Biological Relevance of PTK7 in GBM treatment 22
5.2. Generation and Validation of Anti-PTK7 Nanobodies 22
What is a Nanobody? 22
Production and validation of the anti-PTK7 Nb5 23
5.3. Concept of Suicide-Gene Therapy 23
5.4. Assembly of AAV-Nanobody-TK Construct and Initial Validations 23
Construction of the rAAV 23
CHAPTER 2 - OBJECTIVES .....
1. HYPOTHESES AND OBJECTIVES 25

2. Experimental Strategy 25
Chapter 3 - Materials & Methods .....
1. Cell cultures 26
1.1. Patients-derived GSCs cultures 26
1.2. U87MG cell line 26
1.3. m005 cell line 26
1.4. Generation of modified cell lines by lentiviral transduction 27
2. Immunoblotting 27
2.1. Preparation of protein samples 27
Suicide-gene therapy in vitro, using U87 and T033 27
Validation of PTK7 expression in m005 27
Protein extraction and quantification 28
2.2. SDS-PAGE and immunodetection 28
3. Flow Cytometry analysis 28
3.1. PTK7 membrane expression in m005 cells 29
3.2. Annexin V/DAPI apoptosis assay in cells upon SGT in vitro 29
3.3. Co-culture assays 29
Evaluation of PTK7 expression and AAV-Nb5 specific binding upon co-culture 29
Evaluation of viability for assessment of the "bystander effect" 29
4. Immunostainings 30
4.1. Brain tissue processing 30
4.2. Immunofluorescence on cryosections 30
5. Quantification and Statistical analysis 30
Chapter 4 - Results .....
1. Evaluation of SGT-induced cytotoxicity in GBM cells 31
1.1. Characterisation of cell death marker expression 31
1.2. Quantitative analysis of cell death using Annexin V/DAPI staining 32
2. Evaluation of therapeutic specificity in $PTK7^+$/$PTK7^-$ co-culture 33
2.1. Evaluation of PTK7 expression and AAV-Nb5 specific binding 33
2.2. Evaluation of viability for assessment of the "bystander effect" 34
3. Validation of AAV-based SGT efficacy in xenograft tissues 36
4. Establishment and validation of a PTK7-expressing murine model for Nb5-VHH targeting 37
Chapter 5 - Discussion .....
SGT strategy induces selective apoptotic cell death in $PTK7^+$ cells 39
AAV-Nb5 vector mediates PTK7-dependent targeting 40
SGT reduces tumour volume in vivo and alters tissue organization and integrity 42
PTK7 expression and specific recognition by Nb5-VHH are confirmed in the m005 tumour model 43
Perspectives for the AAV-Nb5-TK/GCV strategy 44
Bibliography 46
Appendix .....

Glossary*

Blood-Brain Barrier (BBB): A physiological structure formed by endothelial cells connected by tight junctions, together with supporting cells including astrocytes and pericytes, creating a highly selective interface that regulated the passage of various substances between the bloodstream and the brain, such as toxins, pathogens, therapeutic agents, nutrients, oxygen and water.

Cancer: A malignant neoplasm, characterised by deregulated cell proliferation, which can result in an ability to invade surrounding tissues and, in many cases, spread to distant organs (metastasis) leading to progressive destruction of healthy tissues.

Cancer Stem Cells (CSCs): A small subpopulation of cells within a tumour capable of self-renewal and differentiation that sustains malignancy and contributes critically to its progression and metastasis.

Chemoradiotherapy: A combination of chemotherapy and radiotherapy.

Chemotherapy: A treatment which can be administered alone or in combination with other therapies, using different routes depending on the stage of the cancer. Its aim is to block tumour progression by either killing cancer cells or preventing them from dividing.

Extracellular Matrix (ECM): A network of extracellular proteins and molecules that surrounds cells and provides structural support, while regulating processes such as cell adhesion, migration, signalling and damage repair. In cancer, ECM can be altered and participates in tumour progression.

Glioblastoma (GBM): The most common malignant primary brain tumour in adults. It is an aggressive, high-grade diffuse astrocytic glioma characterised by rapid growth and infiltrative behaviour.

Intratumoral heterogeneity: The variability among cells within a single tumour, resulting in distinct morphological features and genetic profiles, underpinning variable behaviour and treatment response. *(Definition adapted from current literature)*

Interpatient heterogeneity: Differences between tumours from different patients, even when they share the same histopathological diagnosis, including variations in molecular alterations, aggressiveness, and clinical outcome *(Definition adapted from current literature)*

Prognosis: The prediction on the outcome of a disease or health condition.

Radiotherapy: A local cancer treatment in which high-energy radiation (for example X-rays or proton beams) is directed at the tumour region to damage DNA in cancer cells and block their ability to divide or survive. It is mostly delivered from a machine outside the body in repeated sessions (EBRT).

Targeted Therapy: A type of cancer treatment that uses drugs or other agents, designed to act on specific molecular features which support cancer cells survival and proliferation. These therapies can be used

either to block growth signals, inhibit tumour blood supply, deliver toxic payloads to cancer cells, interfere with essential hormones, enhance immune mediating killing, or directly induce cancer cells death. Most targeted therapies are either small-molecule inhibitors or monoclonal antibodies.

Tumour Microenvironment (TME): A complex network of cells, molecules, and blood vessels, which surrounds and interacts with the tumour, participating in cancer progression and response to therapy.

* Unless otherwise specified, definitions are adapted from the National Cancer Institute (NCI) Dictionary of Cancer Terms.

Use of generative AI

Generative AI tools were used as paraphrasing and editorial support tools, particularly for text correction, reformulation, and assistance in structuring ideas. All scientific content, including source verification, interpretation of results, and final decisions regarding the manuscript content remains the author's responsibility and is based on an in-depth bibliographic investigation. The cover page image was obtained from Adobe Stock.

List of abbreviations

A	**AA**	Amino Acid
	AAV	Adeno-Associated Virus
	Ab	Antibody
	ABC	ATP-Binding Cassette
	ADC	Antibody-Drug Conjugate
	ATRX	Alpha Thalassemia/Mental Retardation Syndrome X-linked
B	**BBB**	Blood-Brain Barrier
	BCNU	Carmustine or bis-chloroethylnitrosourea
	BMDM	Bone Marrow-Derived Macrophage
	BPP	Bipotential Progenitor
C	**CAR**	Chimeric Antigen Receptor
	CASP-3	Caspase-3
	CCK-4	Colon Carcinoma Kinase-4
	CCNU	Lomustine or *N*-(2-Chloroethyl)-*N*-cyclohexyl-*N*-nitrosourea
	CD	Cluster of Differentiation / Cytosine Deaminase
	CDR	Complementary Determining Region
	CDKN2A/B	Cyclin-Dependent Kinase Inhibitor 2A and 2B
	CGGA	Chinese Glioma Genome Atlas
	cIMPACT-NOW	Consortium to Inform Molecular and Practical Approaches to Central Nervous System Tumor Taxonomy-Not Official WHO
	CNS	Central Nervous System
D	**DAMP**	Damage-Associated Molecular Pattern
	DAPI	4',6-diaminido-2-phenylindole
	DNA	Desoxyribonucleic Acid
E	**ECD**	Extracellular Domain
	ECM	Extracellular Matrix
	EGFR	Epidermal Growth Factor Receptor
	EMT	Epithelial-Mesenchymal Transition
F	**FDA**	Food and Drug Administration
G	**GBM**	Glioblastoma
	GCV	Ganciclovir
	GDEPT	Gene-Directed Enzyme/Prodrug Therapy
	GFP	Green Fluorescent Protein
	GLOBOCAN	Global Cancer Observatory
	GPC	Glial Progenitor Cell
	GSC	Glioblastoma Stem Cell
H	**HGG**	High-Grade Glioma
	HIF	Hypoxia-Inducible Factor
	HMGB1	High Mobility Group Box 1
	HSV1-TK	Herpes Simplex Virus-1 Thymidine Kinase
I	**IARC**	International Agency for Research on Cancer
	IDH	Isocitrate Dehydrogenase
	Ig-like	Immunoglobulin-like
	ITR	Inverted Terminal Repeat
K	**KO**	Knock-Out
M	**mAb**	Monoclonal Antibody
	MDSC	Myeloid-Derived Suppressor Cell
	MFI	Mean Fluorescent Intensity
	MGMT	O6-Methylguanine-DNA Methyltransferase
	MHC	Major Histocompatibility Complex
	MMP	Matrix Metalloproteinase

	MPP	Multipotent Progenitor
	MRI	Magnetic Resonance Imaging
	MS	Mass Spectrometry
	MVP	Microvascular Proliferation
N	**Nb**	Nanobody
	NGS	Next-Generation Sequencing
	NPC	Neural Progenitor Cell
O	**OE**	Overexpression
	OPC	Oligodendrocyte Progenitor Cell
	OS	Overall Survival
P	**PARP**	Poly(ADP-ribose) Polymerase
	PCP	Planar Cellular Polarity
	PDGFRA	Platelet-Derived Growth Factor Receptor Alpha
	PTEN	Phosphatase and TENsin homolog
	PTK7	Protein Tyrosine Kinase 7
R	**RNA**	Ribonucleic Acid
	RT	Room Temperature
	RTK	Receptor Tyrosine Kinase
	RT-PCR	Reverse Transcription Polymerase Chain Reaction
S	**SGT**	Suicide Gene Therapy
	SLC	Solute Carrier
T	**TAM**	Tumour-Associated Macrophage
	TCGA	The Cancer Genome Atlas
	TERT	Telomerase Reverse Transcriptase
	TIL	Tumour Infiltrating Lymphocyte
	TK	Thymidine Kinase
	TME	Tumour Microenvironment
	TP53	Tumour Protein 53
U	**UPP**	Unipotent Progenitor
V	**VHH**	Variable domain of the Heavy chain of Heavy-chain-only Antibodies
	VTE	Venous Thromboembolism
W	**WB**	Western Blot
	WHO	World Health Organization
	WT	Wild Type
	α-KG	α-Ketoglutarate
	5-FC	5-Fluorocytosine
	5-FU	5-Fluorouracil

Chapter 1 - Introduction

Presented by Sarah Grodent, based on an in-depth bibliographic exploration

1. General Background on Primary Brain Tumours

1.1. Overview

As reported by the International Agency for Research on Cancer (IARC) in 2022, 321,731 cases of brain central nervous system (CNS) cancers and 248,500 deaths were recorded across both sexes and all ages. Age-standardised incidence of brain tumours differs from region to region and is the highest in Western Europe (5.56 per 100,000), Northern America (5.46 per 100,000) and Eastern Asia (3.95 per 100,000) with lower rates across Africa. Scenario analyses using the Global Cancer Observatory (GLOBOCAN) indicate approximately 474,000 cases by 2045 (~ +47% vs 2022) if age-specific rates remain unchanged, an increase driven especially by ageing and population growth.[1]

These patterns underscore the clinical weight of CNS tumours worldwide. Indeed, despite advances and the intensification of therapeutic research, tumours of the CNS remain challenging to treat and particularly resistant to standard treatments by surgery, radiotherapy, and chemotherapy. This refractoriness reflects several brain specific factors: (1) the limited extent of tumoral resection due to diffuse infiltration; (2) the restricted drug delivery across the highly selective blood-brain barrier (BBB); and (3) the reality of a complex, immunosuppressive tumour microenvironment, against a backdrop of developmental programmes and genetic as well as epigenetic alterations.[2,3] In addition to these resistance mechanisms, there are characteristics specific to brain tumours, namely the existence of a strong intra-tumour heterogeneity, an invasive potential and a disorganised vascular network.[3]

Among primary CNS tumours, gliomas represent the most common malignant entities in adults and account for a substantial proportion of CNS cancer-related mortality[4], justifying a specific focus in the following section.

1.2. Focus on Gliomas

1.2.1. General Features and Clinical Relevance of Gliomas

Gliomas are the most frequent primary brain tumours affecting adults, accounting for ~80% of malignant primary CNS tumours, although brain metastases are the most common type of brain malignancies. They occur within the CNS (brain and spinal cord) and are thought to arise from glial progenitor cells (GPCs)[4,5], broadly classified into multipotent progenitors (MPPs) that can develop into a subset of cell types, bipotential progenitors (BPPs) that generate either oligodendrocyte progenitor cells (OPCs) and neural progenitor cells (NPCs), and unipotent progenitors (UPPs) that give rise to a single differentiated lineage, such as oligodendrocytes, astrocytes or ependymal cells, which support neuronal function[5,6]. However, although gliomas are known to arise from glial cells, the exact origin remains unclear. Therefore, a specific glioma subtype can reflect a certain phenotype or differentiation state rather than the precise cell type from it originated.[7,8] Clinically, gliomas exhibit interpatient variability, with both

focal symptoms (e.g., motor impairment, aphasia, ataxia) and general/non-specific symptoms (e.g., headache, vomiting, weakness, mental status change, seizures). Non-specific onsets are hard to attribute to a brain tumour, however chronic and persistent headache associated to vomiting, nausea, seizures or even an alteration of mental state should raise suspicion. Focal signs help localize the impact of the lesion on specific brain regions, while systemic symptoms are much more complex and non-localizing. These manifestations stem from broader processes affecting the brain and such variability relates to size and tumour location, though size does not predict severity.[9]

1.2.2. Integrated Histo-Molecular Diagnosis of Gliomas

Historically, before the 2021 World Health Organization (WHO) classification of CNS tumours, gliomas were classified primarily by histology and clinical grade, comparing microscopic similarities to the presumed lineage of originate cells[10]. This type of classification relied mainly on the presence of cellular anaplasia, mitotic activity, microvascular proliferation (MVP) and necrosis.[11] More recently, it has become clear that classifying brain tumours considering molecular characteristics yields greater diagnosis and prognosis accuracy, and facilitates the implementation of personalised therapy[12]. In this section, we mainly focus on adult diffuse gliomas, which carry most of the malignant burden and set the stage for the subsequent focus on glioblastoma (GBM).

A. The Founding Histopathological Era (1926-2007)

Glioma classification has undergone a profound revision process over almost a century, evolving from a more descriptive approach to the progressive integration of more complex molecular features. In 1926, Bailey and Cushing published a major classification of gliomas based on microscopic resemblance to the putative cells of origin. The characterisation of histological similarities depended mainly on features observed under light microscopy on sections stained with haematoxylin-eosin, as well as on the immunohistochemical expression of proteins associated with specific cell lineages. It was only in 1979 that this framework was codified by the WHO, which underwent several updates, with incorporation of several molecular markers in 2016 and a comprehensive revision in 2021.[10,13]

Thus, until 2016, tumour grading was the main tool for predicting the biological behavior of a lesion, used as a scale of malignancy, ranging from I to IV. Typically, regarding neoplasms in general, **grade I** tumours correspond to slow-growing lesions that are often easy to cure by surgery alone, whereas **grade II** tumours have a low proliferative potential but a greater propensity for invasion and may evolve into higher-grade malignancies. **Grade III** lesions, such as anaplastic astrocytomas, are considered high-grade cancers, growing and spreading more aggressively and characterised by nuclear atypia and a high mitotic index. Finally, **grade IV** tumours, such as GBM, represent the highest level of aggressiveness, showing high mitotic activity, marked proliferative and invasive potential, MVP, and/or necrosis, with a high risk of fatal outcome.[14]

Although this diagnostic system served as a reference for years, it suffered from significant weaknesses, particularly the difficulty of assigning a lesion to a specific glial lineage (astrocytic, oligodendroglial, mixed). As a consequence, histological diagnostic alone did not invariably predict the clinical outcome[15] and the 2007 WHO revision was the last to be based strictly on histology.

B. Towards Integrated Diagnostics (WHO 2016) - The Molecular Revolution

Compared with the 2007 WHO CNS glioma classification, the WHO 2016 revision integrated molecular markers, including Isocitrate Dehydrogenase (IDH) mutations and 1p/19q codeletion, while histology was still playing a key role in the glioma subtype categorization. We therefore moved from a virtually purely morphological system to a histomolecular system, with the aim of better reflecting tumour biology and thereby improving diagnosis accuracy and patient care. A good example of this editing is the historically vague category of "oligoastrocytomas", which almost disappears when these molecular criteria are applied: most cases are reclassified as diffuse IDH-mutant astrocytomas or IDH-mutant, 1p/19q-codeleted oligodendrogliomas, with only rare cases retaining a truly mixed profile. However, the counterpart to this stricter classification is the emergence of less well-defined groups not otherwise specified (NOS)[10] and even the traditional malignancy assigned to diffuse gliomas needs to be reconsidered in light of these molecularly refined tumour subsets.[10,16]

C. The 2021 WHO Edition (CNS5) - The Dominant Molecular Taxonomy

The transition from the WHO 2016 edition (CNS4) to the WHO 2021 edition (CNS5) marked a real turning point in the way of diagnosing diffuse gliomas, moving from a classification mainly based on morphological features to a much more comprehensive integration of molecular markers. This fifth edition has thus enabled the emergence of a new approach, by introducing revised diagnostic and grading criteria while including major changes in prognosis and treatment management.[17] First, the reduction of the number of main categories, with adult diffuse gliomas now assigned to 3 distinct tumour types (IDH-mutant astrocytomas, IDH-mutant 1p/19q-codeleted oligodendrogliomas and IDH-wildtype (WT) GBM), compared to 15 entities in CNS4, thereby reducing dependence on traditional histological classification.[18] Second, the removal of the oligoastrocytomas category, referring to a mix between oligodendrogliomas and astrocytomas properties, because the molecular characterisation of these gliomas genetically corresponded either to oligodendroglioma or to astrocytoma.[19] Finally, the term GBM is now reserved exclusively for IDH-WT gliomas, and grading system has been harmonised from Roman numbers to Arabic numbers in line with the recommendations of the Consortium to Inform Molecular and Practical Approaches to CNS Tumor Taxonomy—Not Official WHO (cIMPACT-NOW).[18,20] **(Figure 1)**

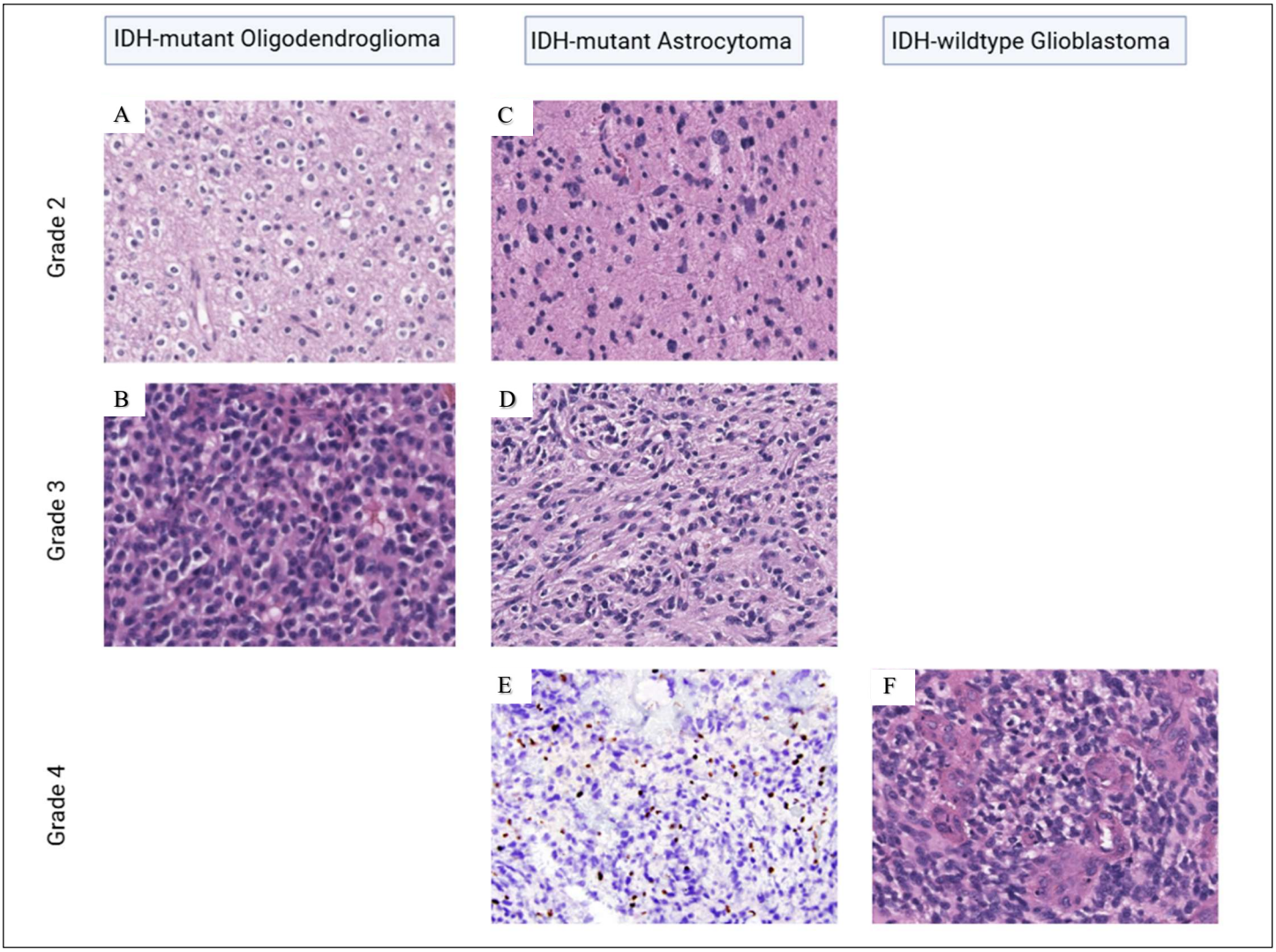

Figure 1. Histologic Grading of Adult-diffuse Gliomas. Histological characterisation of IDH-mutated 1p/19q codeleted Oligodendroglioma (**A** WHO grade 2 with "fried-egg" appearance cells; and (**B**) WHO grade 3 (anaplasic) with a high cellular density, hyperchromatic nuclei and MVP; IDH-mutated Astrocytoma (**C**) WHO grade 2 with mild hypercellularity and nuclear atypia; (**D**) WHO grade 3 with similar pattern, but higher cellularity and more frequent mitosis; (**E**) WHO grade 4 with additional MVP and/or necrosis; and IDH-wildtype GBM (**F**) WHO grade 4 characterised by high mitotic activity, marked proliferative and invasive potential, MVP, and/or necrosis. *Adapted from M Zuo et al. (2025) and Virchows et al. (2017).* [ref 21: 5]

D. Diagnostic Methods and Limitations

Current diagnostic tools mainly combine neuroimaging by magnetic resonance imaging (MRI), positron emission tomography (PET) and computed tomography, and histopathology on biopsy. Unfortunately, imaging remains non-specific, and struggles with determining precise tumour subtypes, treatment response assessment and margin definition of the tumour.[22] Consequently, the implementation of molecular diagnostic tools including next-generation sequencing (NGS), quantitative polymerase chain reaction (qPCR) or even methylome profiling remains necessary to better characterise tumour types and inform treatment option.[17]

E. Key Molecular Signatures in Adult Diffuse Gliomas

As mentioned in the previous sections, molecular markers allowed a re-classification of tumour types. Adult-diffuse gliomas are now classified in the first place by their IDH status (WT or mutated) as it seems that mutations in IDH genes are one of the earliest genetic events in gliomagenesis[23]. Mutated IDH tumours are divided into two main subtypes: **(1) astrocytomas** characterised by alteration in the tumour protein p53 (TP53) gene and alpha thalassemia/mental retardation syndrome X-linked (ATRX) loss, and **(2) oligodendrogliomas** characterised by the concomitant deletion of both the short arm of chromosome 1 (1p) and the long arm of chromosome 19 (19q) (1p/19q codeletion) and by the mutation of the telomerase reverse transcriptase (TERT) promoter. Regarding GBM, this term is assigned to IDH-WT tumours, while previously classified IDH-mutant GBM is currently classified as IDH-mutated astrocytoma grade 4. So, although IDH status is a primary indicator, other biomarkers are analysed to assess tumour type and prognosis.[17,20,24] **(Figure 2)**

IDH mutation

IDH is an enzyme which plays an essential role in metabolic pathways, essentially in the Krebs cycle (or tricarboxylic acid cycle), and has three main isoforms (IDH1, IDH2 and IDH3) encoded by distinct genes and situated throughout the cell in different locations; IDH1 is in cytoplasm and peroxisome, while IDH2 and IDH3 are in mitochondria. In normal conditions, IDH catalyses the conversion of isocitrate into α-ketoglutarate (α-KG), a key intermediate metabolite which acts as a cofactor of 2-oxoglutarate-dependent dioxygenases, enzymes involved in epigenetic regulation, deoxyribonucleic acid (DNA) repair, metabolites biosynthesis etc.[25] This reaction also generates NADH from NAD^+ via IDH3 and NADPH from $NADP^+$ via IDH1/2. The NADPH produced by IDH1/2 is the principal source of energy in many tissues, acting as a reducing agent, sustaining antioxidant defence mechanisms, by keeping the glutathione and thioredoxin in a reduced state. In addition to their role in Krebs cycle, IDH enzymes participate in metabolite exchanges between mitochondria and the cytosol and in electron transfer[26]. While IDH3 is rarely mutated in cancers[25], IDH1/2 are frequently mutated, especially in hematopoietic cancers and several solid tumours (e.g., acute myeloid leukemia, intrahepatic cholangiocarcinoma, gliomas), allowing the production of 2-hydroxyglutarate (2-HG), an

oncometabolite which mimics α-KG and leads to the inhibition of α-KG-dependent dioxygenases, disrupting essential cellular functions. Those IDH1/2 mutations often occur to an arginin of the catalytic site. On IDH1, the most common mutation involves a change from arginine to histidine at position 132 (R132H), although other variants exist (R132C, R132S, R132G, R132L), while in IDH2, the mutation occurs mainly at arginine 172 or 140. In gliomas, IDH mutations are associated with other mutations, including ATRX, TP53, TERT and 1p/19q codeletion. Interestingly, IDH enzymes function as WT-mutant heterodimers, leading to an efficient conversion of α-KG into 2-HG, which probably explains why heterozygosity is common.[27] Finally, IDH-mutant gliomas seem to be characterised by extensive hypermethylation of DNA at CpG islands; this is referred to as Glioma CpG island methylator phenotype (G-CIMP), associated with a better prognosis compared to IDH-WT gliomas.[25,28]

1p/19q codeletion

1p/19q codeletion is another key biomarker of adult diffuse gliomas, characteristic of IDH-mutated oligodendrogliomas, graded as CNS WHO grade 2 (non-anaplastic) or 3 (anaplastic). It is associated with additional tumour features such as ATRX retention and TERT gene promoter mutations, with a better prognosis and improved responsiveness to chemotherapy and radiotherapy.[29]

ATRX and TP53 status

ATRX acts as a critical molecular feature of diffuse gliomas, mainly expressed in IDH-mutant astrocytomas, mutually exclusive with 1p/19q codeletion and TERT promoter mutations, involved in the compaction of the chromatin in inactive regions of the genome, such as pericentric chromatin and telomeres, in association with a death-domain associated protein (DAXX). Mutations on the ATRX gene manifest by loss-of-function (ATRX retained), preventing telomeres to shortening, thus allowing cells to divide infinitely.[29,30]

TP53 is a well-known tumour suppressor gene that encodes for p53, a transcription factor which plays a crucial role in cell defences by protecting DNA integrity in response to stress, by regulating cell cycle and when required, triggers apoptosis. TP53 is mutated in most human cancers, which typically leads to accumulation in nucleus and interaction with oncoproteins, causing tumour development. In gliomas, as for ATRX, TP53 mutations occur particularly in lower-grades IDH-mutant astrocytomas. It has been demonstrated that depending on the mutation on TP53, it can lead to a better response to chemotherapy. For example, mutations on the codon 273 are associated to a high chemosensitivity and a higher survival rate.[31]

TERT promoter mutation

As ATRX, TERT is another gene involved in telomeres maintenance, by encoding for the catalytic subunit of the telomerase complex. It is expressed at high levels in both IDH-WT GBM and IDH-

mutated 1p/19q-codeleted oligodendrogliomas. Consequently, mutation on TERT promoter is not sufficient to make a diagnostic.[32]

EGFR amplification

Epidermal Growth Factor Receptor (EGFR) is a member of the receptor tyrosine kinase (RTK) family, encoded by a gene located on chromosome 7.[33] It is frequently mutated, resulting in an amplification in IDH-WT GBM and it acts as a key factor of mesenchymal conversion, which increases the infiltration capacity of glioma cells. However, EGFR can also be activated by signals from infiltrating immune cells such as tumour-associated monocytes (TAMo). In this context, we refer to EGFR-WT, although it may display aggressiveness similar to EGFR-amplified tumours.[34]

Gain of chromosome 7 and loss of chromosome 10

The gain of chromosome 7 and loss of chromosome 10 (7+/10-) is a phenomenon which frequently occurs in IDH-WT GBM, since, according to several studies, this appears to be a tumour evolutionary mechanism. The initial loss of chromosome 10 prevents the tumour of using genes essential to its survival. A way of countering this process consists in a chromosome 7 gain, to compensate for lost functions. This compensatory mechanism is predominant in specific brain regions such as the cerebral cortex, which can be an explanation for the preferential GBM development in this zone.[35]

CDKN2A/B homozygous deletion

Cyclin-Depend Kinase Inhibitor 2A (CDKN2A) and 2B (CDKN2B) are genes located on chromosome 9, respectively encoding for p14/p16 and p15 proteins, which take part into the cell cycle blockade by inhibiting CDKs, enzymes involved into the control of cell division.[36] Similarly to other markers, CDKN2A/B homozygous deletion is a factor of poor prognosis, characteristic of IDH-mutant astrocytomas grade 4.[37]

Before WHO 2021 classification, IDH-WT GBM were diagnosed based on the presence of necrosis and/or MVP.[33] Through the integration of molecular features, it is therefore possible to diagnose IDH-WT GBM based on these histological characteristics or on the presence of one of these 3 molecular markers : EGFR gene amplification, TERT promoter mutation, or a 7+/10- signature, even if histology shows no signs of aggressiveness. Concerning IDH-mutant astrocytomas, WHO 2016 classification distinguished between three types, based on histology: diffuse astrocytomas, anaplastic astrocytomas and IDH-mutant GBM. Under WHO 2021, they are classified as a single entity: IDH-mutant astrocytomas of grade 2, 3 or 4. The grade is no longer only histological; for example, a homozygous deletion of CDKN2A/B is sufficient to classify an astrocytic tumour as grade 4, even in the absence of necrosis and/or MVP.[18]

Other molecular markers

Although the previous points briefly describe the main molecular markers involved in the 2021 WHO classification of adult diffuse gliomas, other markers can be used for diagnosis.

For example, the O6-methylguanine-DNA methyltransferase promotor (p-MGMT) allows the production of MGMT, an enzyme involved in the repair of damage to DNA caused by alkylation, a type of chemical modification induced by substances known as alkylating agents (e.g. chemotherapy by Temozolomide). This gene promoter is made of CpG islands, sequences rich in guanine (G) and cytosine (C) bases, crucial for gene regulation, typically unmethylated in normal cells, which allow accessibility of transcription machinery to DNA. In tumours, those regions are frequently methylated, leading to gene silencing. In our context, p-MGMT is found to be methylated in ~46% of GBM cases and is associated to a better response to Temozolomide (TMZ).[3,4,17]

Phosphatase and TENsin homolog (PTEN) is a tumour suppressor gene, which encodes for a protein involved into regulation of cell cycle and DNA repair. PTEN loss can be found in GBM and is a poor prognosis factor.[6,17]

2. Glioblastoma

After outlining the histo-molecular framework for adult-diffuse gliomas, we will now focus specifically on glioblastoma (GBM), detailing its epidemiology, clinical-molecular landscape, current standard of care, and the main elements involved in resistance mechanisms, that motivate the experimental work presented in this master's thesis.

2.1. Epidemiology and Pathogenesis

Among gliomas, GBM is the most aggressive form. It accounts for >50% of glial tumours, with an incidence of ~3.9 cases per 100,000 people, predominantly affecting males and those ≥ 65. GBM arises mainly in the supratentorial region, particularly the frontal and temporal lobes. Despite standard therapy, median survival is ~9 months and the 5-year survival rate is 7.1%, with near-universal relapse.[38,39] This therapeutic failure can be explained by several factors, including marked intratumoral heterogeneity, an immunosuppressive and hypoxic microenvironnement, and the persistence of GBM stem cells (GSCs) capable of self-renewal and developing treatment resistance. Although the cause of GBM remains unknown in most cases, suggested risk factors include exposure to ionizing radiation[40] and certain hereditary genetic syndromes (e.g., Li-Fraumeni syndrome, Neurofibromatosis 1, Lynch syndrome). By contrast, for putative environmental exposures such as obesity, diabetes, smoking, exposure to electromagnetic fields or cell phones, no consistent association has yet been established; conversely, atopy/allergic predisposition has been associated with a protective effect.[39]

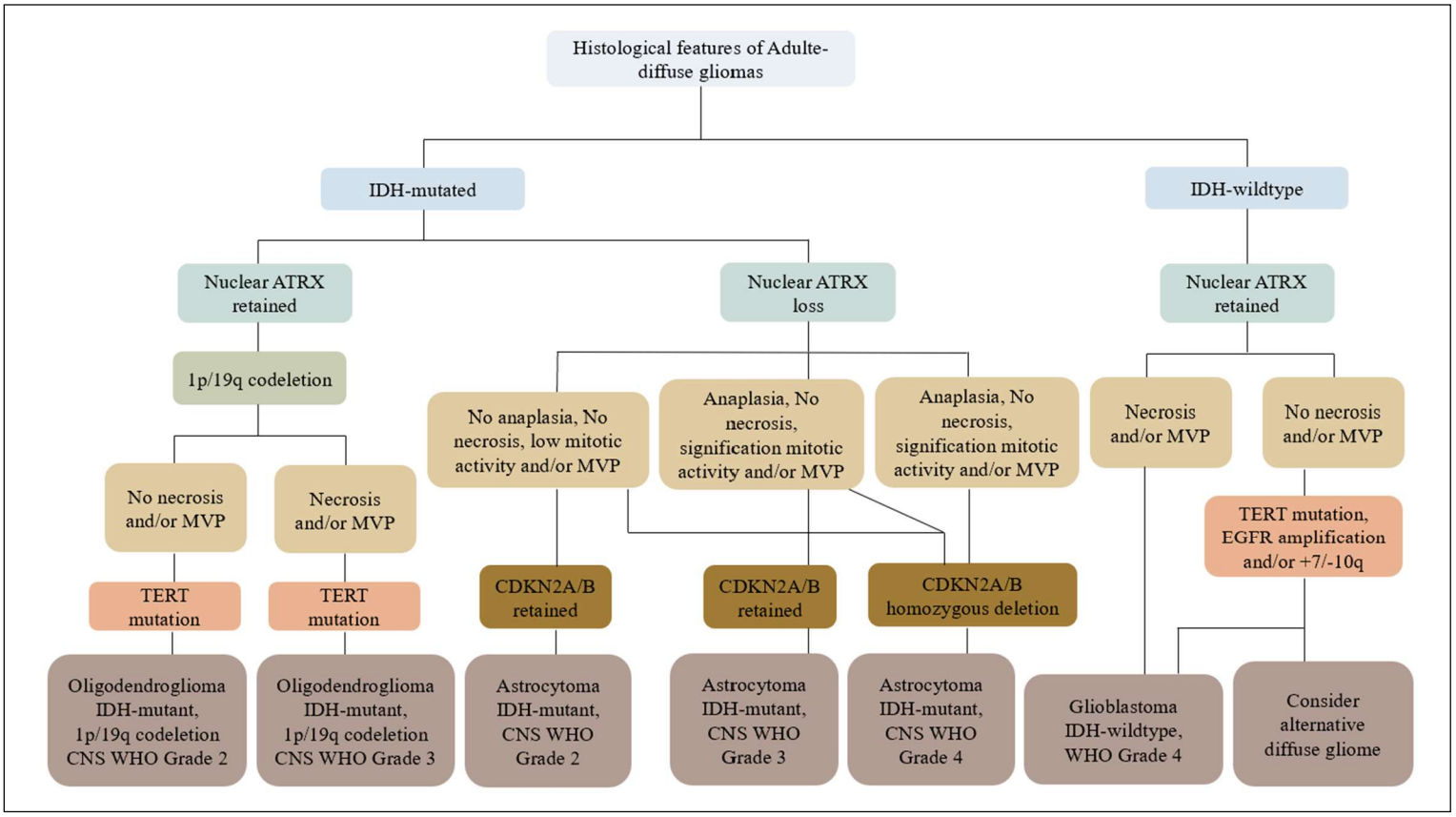

Figure 2. The WHO 2021 Classification of Adult-type Diffuse Gliomas. Integration of key molecular markers, including IDH mutation status, ATRX expression, 1p/19q codeletion, and additional alterations, to distinguish between major glioma subtypes and grades, including astrocytomas, oligodendrogliomas, and GBM. *Adapted from M. Antonelli, P.L. Poliani (2022).* [ref 19]

2.2. Clinical and Molecular Features

Symptoms in GBM largely overlap with those of other primary brain tumours, ranging from focal neurological and motor deficits to more systemic clinical manifestations such as seizures, headache, weakness and memory loss. Those symptoms have been identified in different studies to be predictive factors of survival and treatment efficacy, acting as non-invasive indicators, which is a significant advantage, unlike molecular biomarkers, which require the use of a more invasive surgical biopsy. As an example, a study published in 2021 used patients data and found out that patients with memory problems and generalised weakness had reduced survival, consistent with these deficits indicating decreased ability for self-care and a poorer overall prognosis.[41]

Though evaluation of symptoms is a first indicator, diagnosis of GBM and extent-of-disease (EOD) assessment require the use of standardised diagnostic methods, among which MRI is described as the gold standard. For diagnosis, this technique allows the distinction between normal tissue and tumour mass, as well as the detection of necrotic core and BBB disruption through contrast medium (gadolinium).[38] **(Figure 3)** However, conventional MRI faces limits for monitoring treatment response by distinguishing a real progression from pseudoprogression (distinction between tumour growth and post-treatment inflammatory response), identifying radionecrosis or even analysing tumour physiology. Those limitations can be overcome by using complementary techniques: (1) diffusion MRI, which enables visualization of water molecules diffusion in tissues, revealing their microstructure, (2) MR spectroscopy which visualizes specific metabolites as lactate or choline, or even (3) PET Scan which uses radiotracers to measure metabolic activity.[38,42]

Before WHO 2021 edition, GBM used to be classified into “primary” and “secondary” forms with distinct genetic features: primary GBM arose *de novo* and commonly showed EGFR amplification, PTEN mutation and loss of chromosome 10, while secondary GBM evolved from a pre-existing lower-grade astrocytoma or anaplastic astrocytoma with frequent IDH1/2 and TP53 mutations.[43] In the current taxonomy, the term GBM is strictly reserved to IDH-WT tumours (grade 4), while IDH-mutated diffuse gliomas are classified as astrocytoma (grades 2-4) or oligodendroglioma (grades 2-3).[18] Beyond this histomolecular designation, GBM can be grouped by bulk sample analyses based on genetic markers, and by single-cell cellular states. Initial bulk expression studies (e.g., TCGA) grouped GBMs into **4 main subtypes**—classical (CL), mesenchymal (MES), proneural (PN) and neural (NE)—each with distinct genomic profiles. But based on Wang et al. (2018), the NE category was abandoned as non-tumour specific, partly because the sample analysed contained a large amount of non-tumoral tissue and partly because it was the only subtype lacking hallmark GBM genetic abnormalities.[3,44,45] The **CL subtype** shows a gene expression profile similar to astrocytes and is typically characterised by EGFR amplification and CDKN2A loss, which are associated with a poorer prognosis. The **PN subtype** shares features with oligodendrocytes and neural progenitor cells and is often linked to IDH1 and TP53

mutations as well as markers such as platelet-derived growth factor receptor alpha (PDGFRA). Overall, it is associated to better outcomes and longer overall survival (OS). Finally, at relapse, or under the influence of treatments or the tumour microenvironment (TME), tumour cells may shift towards a **MES subtype** through an epithelial-mesenchymal transition (EMT), also associated to NF1 gene mutation, as well as to a highly invasive potential and resistance to therapy.[45] However, this bulk classification conceals internal cellular diversity. At the single-cell level, dynamic cellular states coexist in varying proportions: **neural progenitor-like (NPC-like), oligodendrocyte progenitor-like (OPC-like), astrocyte-like (AC-like) and mesenchymal-like (MES-like) states**.[46] Cells can switch between states in response to environmental conditions and treatment. For example, the MES-like state can be overrepresented under hypoxic or inflammatory conditions and is associated to a strong glycolytic status.[47] In summary, GBM exhibits marked intratumoral heterogeneity, adopting a basic profile, where coexist cellular states that shift under therapy and TME.[48]

2.3. Standard of Care

Maximal Safe Resection

Gross total resection constitutes the first step in GBM treatment.[49,50] It not only provides a histological diagnosis, but also achieves substantial tumour cytoreduction, while preserving the patient's neurological function—the principle of **maximal safe resection**.[51] To optimise the extent of resection (EOR), neurosurgeons may use neuronavigation, awake mapping, fluorescence-guided resection by 5-aminolevulinic acid (5-ALA), and less commonly in routine practice, intraoperative MRI (i-MRI).[51,52] Although molecular predictive factors and patients characteristics, both age and gender, are important tools to inform surgical planning, the EOR is the main modifiable surgical variable, even if it is not the best indicator of survival. Residual tumour volume seems to be a stronger indicator of survival than percentage resected.[53] But, because GBM is highly infiltrative, complete resection of the tumour remains challenging. When tumour involves eloquent brain areas, carrying out surgery is tough to perform, and the achievable resection is often limited, which can affect prognosis.[39,51]

Radiotherapy

After performing maximal safe resection, the standard of care for GBM includes adjuvant radiotherapy which consists of delivering **60 grays (Gy) in 2.0-Gy fractions (30 fractions over six weeks)**.[48] However, radiotherapy regimen can vary with patient characteristics (e.g., age, performance status). For example, elderly or frail patients may receive hypofractionated radiation (e.g., 40 Gy in 15 fractions of 2.67 Gy over three weeks) to maintain effectiveness while reducing toxicity and delivering fewer but higher doses of radiation. Other approaches including stereotactic radiosurgery, reirradiation and proton therapy are still under investigation in clinical trials.[54] Unfortunately, radiotherapy efficacy in general remains poor due to the intervention of factors that lead to treatment resistance, including the persistence of resistant GSCs that fuel recurrence, a hypoxic and immunosuppressive TME, which accentuates

tumour aggressiveness, invasion, and immune escape, and upregulation of enzymes involved in DNA repair pathways in response to ionising radiation (e.g. MGMT).[55]

Chemotherapy

As part of standard care, radiotherapy treatment is delivered concurrently with **TMZ (75 mg/m²/day), then followed by adjuvant cycles of TMZ (150–200 mg/m²/day, 5/28 days)**.[49] As mentioned in section on molecular markers that enable diffuse gliomas classification, TMZ is a lipophilic therapeutic agent known for its alkylating properties on DNA, particularly efficient in patients with MGMT promoter methylation[39,54] and able to easily cross BBB. However, only 20% of the systemically administered dose remains in the brain, due to the existence of specific transporters at the BBB.[56] Overall, TMZ has few side effects, although it may cause patients to experience nausea, fatigue, vomiting, myelosuppression and in severe cases, hematologic disorders. While widely used for GBM and other solid tumours treatment, many patients face resistance to TMZ, especially duo to upregulation of MGMT. Even if no standard second-line treatment is recognised in case of recurrence, the use of other chemotherapeutic agents may be considered, such as lomustine (CCNU) and carmustine (BCNU) as well as a re-treatment with TMZ[57]. However, CCNU and BCNU are highly cytotoxic, with many side effects and did not demonstrate a significant improve of patients survival.[39,57] Another example is the monoclonal antibody (mAb) bevacizumab which specifically targets vascular endothelial growth factor-A (VEGF-A), to block new blood vessels formation (angiogenesis), which has already been used in the treatment of recurrent GBM. The combination of bevacizumab with TMZ and radiotherapy during clinical trials on newly diagnosed GBM cases has also been evaluated, with benefits on progression-free survival, but with modest effects on OS.[58,59,60]

Supportive care

Apart from treatments aimed at directly targeting tumour, supportive care is provided, addressing physical and psychological symptoms like gastrointestinal impairment, fatigue, venous thromboembolism (VTE), edema, seizures or neurocognitive disorders. In routine practice, clinicians may use corticosteroids such as Dexamethasone, which reduce vasogenic edema, but it has a double-edged effect, for example, by interfering with immunotherapy. In patient with seizures, Levetiracetam is often prescribed and has the advantage to not interact with chemotherapy and may improve GBM outcome. Furthermore, 20-30% of patients experience VTE especially during the first year of the disease course, due to activation of clotting factors, surgery, tumour size, age, etc. For managing this specific symptom, administration of heparin is recommended.[39,46,52]

2.4. The Main Mechanisms of Resistance and Recurrence in GBM

While multiple mechanisms (e.g., hypoxia, BBB, intratumoral heterogeneity, MGMT mutation, altered metabolism, transient tumour states) contribute to resistance and recurrence despite standard of care protocol, we specifically focus on two main actors: **(1) glioblastoma stem cells (GCSs)** which maintain

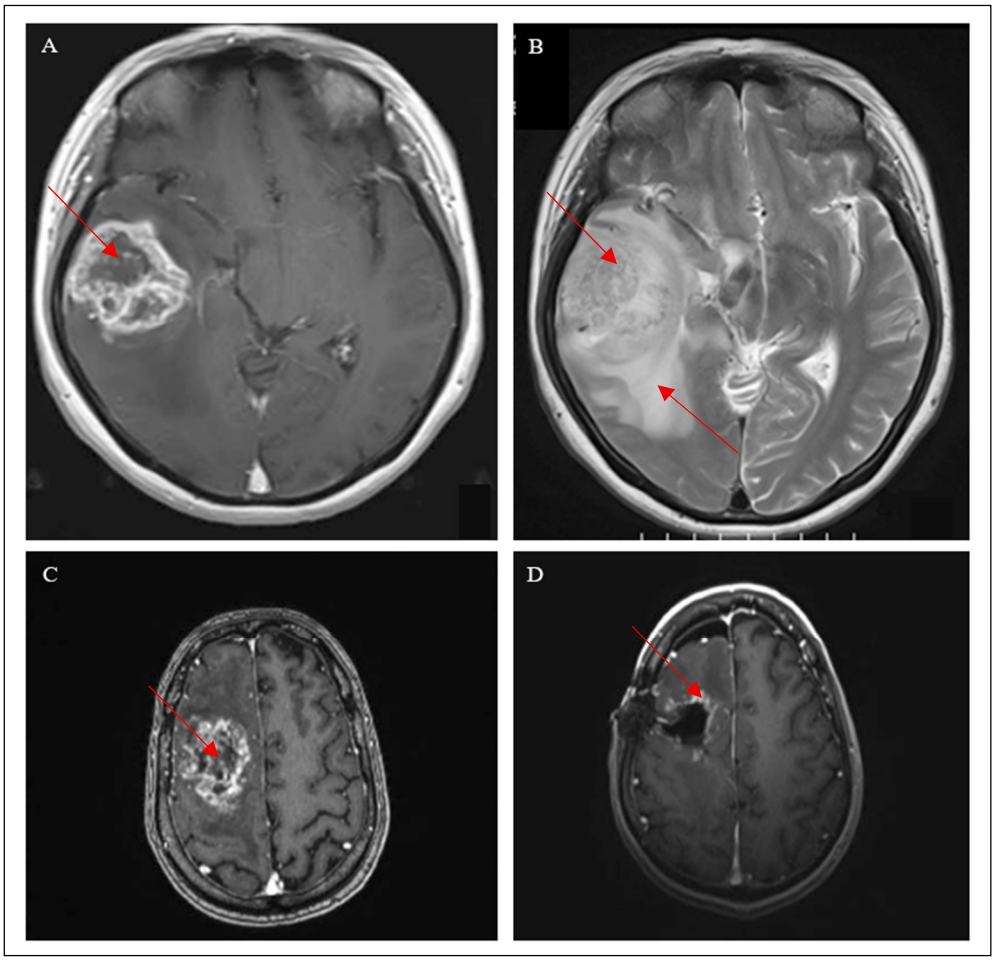

Figure 3. MRI Sequences of GBM. (**A**) contrast T1-weighted image showing necrotic core of the tumour; (**B**) T2-weighted image showing highly infiltrative tumour with peritumoral oedema; (**C**) Preoperative contrast T1-weighted image showing frontoparietal tumour mass with necrotic area; (**D**) Intraoperative contrast T1-weighted image with residual tumour tissue at the resection cavity. *Adapted from Ideguchi et al. (2015). and G. Kuzmik et al. (2017)* [ref 61: 62]

heterogeneity by demonstrating a high plasticity and adaptation to various environments, and (2) the tumour microenvironment (TME) which protects and dictates GSCs behaviour as well as the course of the disease. Both undertake crosstalk which means, broadly speaking, that GSCs allow remodelling of the TME to promote tumour growth, and in return, the different actors of the TME send signals, called "attractors", allowing GSCs to adapt to treatment and to environment conditions by directing them towards specific cellular states.[63,64]

2.4.1. Concept of Glioblastoma Stem Cells

In the context of GBM, cancer stem cells (CSCs), also called GSCs, are a small subpopulation of cells that can self-renew, generate non-stem tumour cells through differentiation, and recreate a complete heterogenous tumour resembling the primary tumour, after secondary transplantation. Those cells are at the apex of the tumour hierarchy.[63] In response to their environment and to treatments, GSCs have this capacity to change state reversibly and adaptably without requiring any mutation. This plasticity enables a rapid switch of states, resulting in high tumour heterogeneity and resistance, which highlights their importance in the development of new treatments.[64] Several surface markers, comprising CD133 (PROM-1), CD15, CD44, integrin α6, A2B5, L1CAM, and few transcription factors such as NANOG, SOX2, OLIG2, MYC, establish a connection between GSCs with their environment. However, no marker has currently been identified as a universal marker for GSCs.[63-65] A well-known example is the CD133 marker, since it has been shown that this surface protein can be expressed in normal stem cells and in certain differentiated cells, and that $CD133^-$ cells have already demonstrated tumour-inducing capabilities.[66]

2.4.2. The Tumour Microenvironment

The tumour microenvironment (TME) is a central driver of GBM behaviour. It comprises cellular elements, including glial cells, neurones and immune cells, as well as non-cellular components, such as the extracellular matrix (ECM), extracellular vesicles (exosomes) and signalling factors, which surround the tumour and foster invasion, proliferation and treatment resistance.[67] **(Figure 4A)**

First, the ECM, present in both normal brain and tumour tissues, is a key actor of tumour progression. It comprises a complex assembly of macromolecules which modulate tumour cells behaviour in terms of migration, maturation, differenciation and invasion. This tumoral ECM shares similarities with adult brain ECM, but with overexpression of several components like receptors, and activation of multiple signalling pathways which facilitate the adhesion and migration of cancer cells. In addition, tumour cells produce degradation enzymes that further remodel this TME.[68] Normal neural and glial cells actively 'feed' tumour growth via synaptic transmission, neurotransmitters, matrix-modifying enzymes (e.g. metalloproteases that degrade the ECM) and paracrine stimulation.[67] For example, neuronal electric activity leads to glutamate release, which binds to AMPAR receptors of the tumour, triggering calcium

currents in GBM cells, which stimulates invasion and proliferation. Likewise, neural cells produce various proteins able to stimulate tumour cells, namely Neuroligine-3 (NLGN3) which activates PI3K-mTOR pathway, promoting the survival and formation of new tumour microtubes, and BDNF which increases the number of synapses communicating between the neurons and the tumour.[67,69]

The GBM immune landscape is predominantly immunosuppressive, dominated by tumour-associated macrophages (TAMs)—resident microglia and periphery bone marrow-derived macrophages (BMDMs), polarised mostly toward an M2-like phenotype exhibiting pro-tumorigenic capabilities—with additional myeloid-derived suppressor cells (MDSCs), while neutrophils and tumour infiltrating lymphocytes (TILs) are comparatively rare.[3,67,70] A high myeloid cell burden in a GBM context aligns with poorer OS. These cells either arise from brain-resident lineages and undergo independent renewal (resident microglia) or are recruited from the peripheral circulation (BMDMs), particularly when the BBB is impaired. They support GSCs self-renewal via growth factor production, promote invasion, and angiogenesis (e.g., via VEGF). However, their spatial location in specific niches also shapes function: microglia cluster at invasive margins, whereas BMDMs accumulate in the tumour core.[70] Secondly, MDSCs are infiltrative immune cells which inactivate natural killer cells (NK) and effector $CD4^+$ and $CD8^+$ T lymphocytes, especially through a MIF-CD74 axis (MIF secreted by GBM cells, especially GSCs), activating the pERK proliferation pathway.[71] Finally, functional impairment of T cell can occur through several mechanisms, which leads to their dysfunction or exhaustion and immune evasion by the tumour : (1) overexpression of inhibitory checkpoint molecules (e.g. PD-1/PD-L1 and CTLA-4) by GBM cells and other immune cells[3], (2) expression of Fas ligand which binds to Fas receptors on CD4+ and CD8+ T cells, increasing their apoptosis, (3) secretion of immunosuppressive factors such as IL-10 and TGF-β by several cells of the TME[70,72], and (4) high acidosis and hypoxia of the TME due to metabolic reprogramming (e.g., Warburg effect)[67] among others.

Those interactions between normal and tumour cells are incorporated within specialised environment called ‘niches’, including perivascular, hypoxic/necrotic and invasive edge niches. These are particularly critical for the maintenance of GSCs through soluble factor secretion by endothelial cells, as well as a shift toward glycolytic metabolism and quiescence state in poor oxygenated regions, mainly through hypoxia-inductible factors (HIFs).[64,69]

2.5. Treatment Prospects based on Immunotherapy

Since the publication of the standard treatment protocol for GBM in 2005 by Stupp et al., several clinical trials have attempted to improve patient’ survival, as discussed previously (bevacizumab, lomustine, TTFields etc.), but without real success (*see section 2.3*). The unique profile of GBM directs therapeutic perspectives towards new approaches mainly based on immunotherapy and combinations. However, despite having demonstrated some success in other cancer types, those characteristics of GBM represent a significant challenge. Nevertheless, immunotherapy as well as combination approaches appear

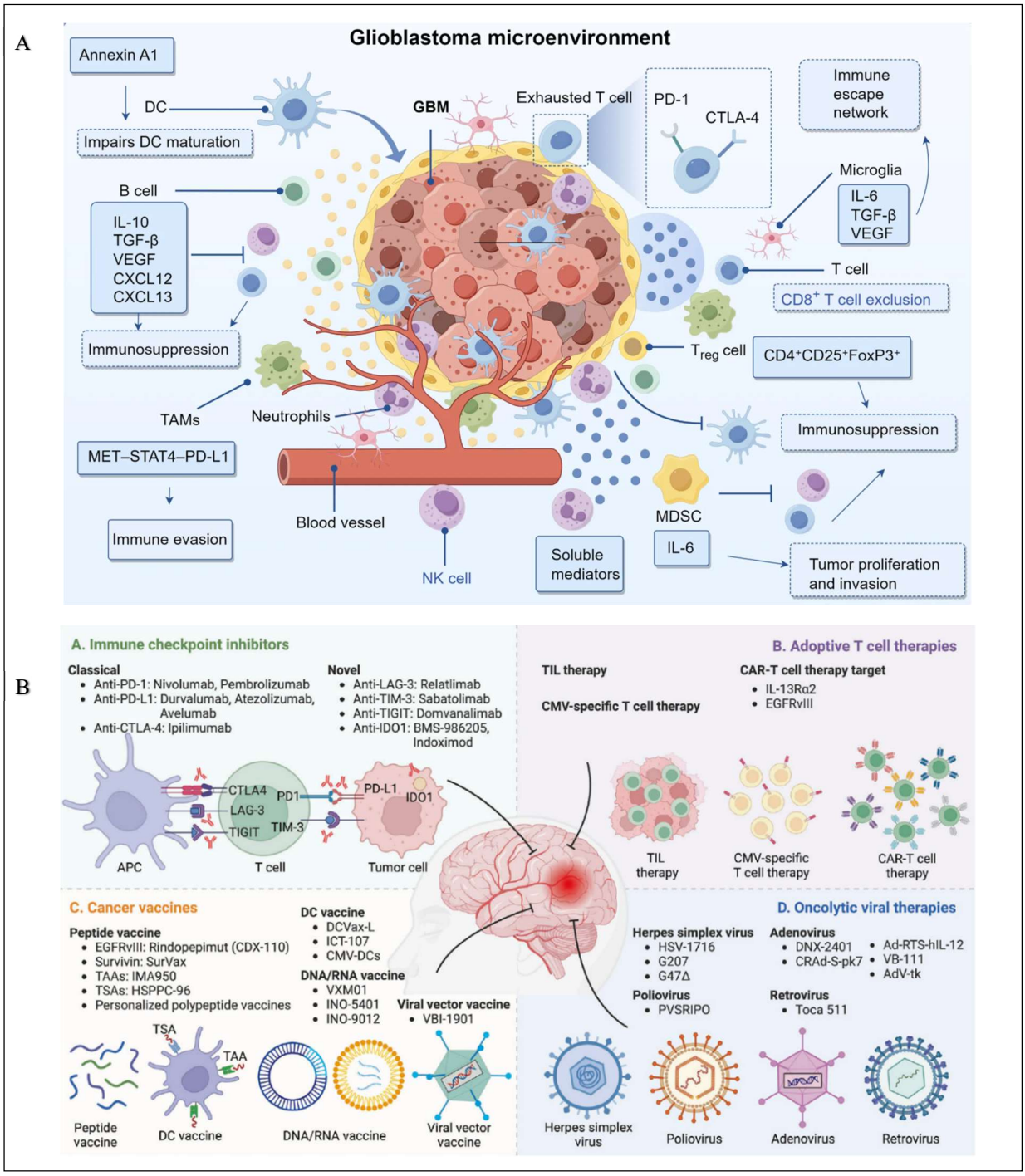

Figure 4. Schematic representation of the complexity of the TME and therapeutic strategies in GBM. (**A**) The TME is made of complex interactions between tumour cells, immune components, normal brain cells and surrounding elements such as chemicals, soluble factors etc. that contribute to GSC maintenance, immunosuppression, tumour progression and therapeutic failure.;(**B**) There are 4 main strategies based on immunotherapy for treating GBM. Immune checkpoint inhibitors (ICIs) are monoclonal antibodies (mAbs) which target immune checkpoint molecules and thus allow the immune system to recognize and target cancer cells. Adoptive T cells therapies use patients' autologous T lymphocytes to kill tumour cells. They can either be genetically engineered to express specific receptors, such as in chimeric antigen receptor (CAR) T-cell therapy or directly isolated from the tumour microenvironment (TME) as tumour-infiltrating lymphocytes (TILs) and expanded *ex vivo* before being re-implanted to the patient. Cancer vaccines use several tools such as nucleic acids (DNA or RNA), peptides or dendritic cells (DCs) to stimulate patient's immune system against cancer cells. Oncolytic viruses or viral particles are specifically directed against cancer cells, enabling the release of tumour antigens and molecules to promote immune activation and a switch from 'cold' to 'hot' tumour. *Image A is from Zhang et al. (2025). and Image B is from Y. Liu et al. (2024)* [ref 73: 74]

promising and numerous clinical trials are underway, mostly including immune checkpoint inhibitors, vaccines, CAR T-cell therapy, oncolytic viruses and nanocarrier-based delivery.[75,76,77] Representative approaches are described below to illustrate the main current strategies. **(Figure 4B).**

Immune checkpoint molecules are regulatory proteins mainly expressed at the surface of T lymphocytes among which are found PD-1 and CTLA-4 receptors. Those proteins allow regulation of immune response, preventing an excessive reaction against normal cells. Cancer cells take advantage of this strategy by overexpressing ligands such as PD-L1 which binds to PD-1, or B7 which binds to CTLA-4, causing exhaustion and even death by apoptosis of T lymphocytes, making them unable to trigger an immune response. Immune checkpoint inhibitors (ICIs) which target immune checkpoints are widely used in solid cancer treatments, particularly in melanoma and non-small-cell pulmonary carcinoma, and are actively tested in clinical trials for newly diagnosed and recurrent GBM.[75] Unfortunately, as GBM is described as a 'cold' tumour, harbouring immunosuppressive microenvironment, some of those advanced clinical trials failed to show a significant increase in OS and PFS, whatever alone or in combination with current treatments.[78,79] However, future studies are needed to test immune modulators in a GBM context.

Those immunotherapy strategies which consist of delivering external components like antibodies (Abs) are referred to as 'passive' therapies. On the contrary, active immunotherapies directly stimulate patient's immune system by involving tumour-specific Ag and could be a more interesting approach.[80] In GBM, one of the most studied candidates is EGFRvIII, an EGFR variant found in ~20-30% of GBM cases and other cancers, which undergoes a deletion of exons 2-7 of the extracellular domain, resulting in its constitutive activation.[81] A few clinical trials have been conducted, mainly testing peptide-based vaccine Rindopepimut (CDX-110) and CAR-T cell therapies. Despite disappointing results in phase III trial of Rindopepimut, the authors suggest multipeptide vaccines and combination therapies in the future, as the expression of this surface protein is highly heterogeneous and can diminish in cases of recurrence.[82] Beyond EGFRvIII targeting, other vaccine approaches are under investigation, including dendritic cell (DC), heatshot protein and personalised neoantigen vaccines. An advantage of DC vaccines is the direct stimulation and amplification *ex vivo* of those cells, which allows them to recognize specific Ag and thus boost T-cell response. Preliminary tests showed promising results when combined with standard treatments, but future investigations are needed.[80] However, antigenic recognition by the major histocompatibility complex (MHC), which triggers an adaptative immune response, represents a limitation in the effectiveness of vaccines, as GBM cells lack this surface protein. Therefore, even boosted T lymphocytes remain unable to recognize and kill tumour cells. This limitation is countered by Chimeric Antigen Receptor (CAR) T-cells. Those are patient-derived T lymphocytes genetically modified to express a chimeric Ag receptor, which binds to a specific Ag without having to resort to the presence of MHC. Already showing promising efficacy in haematological malignancies, this approach is currently being investigated in the GBM context by targeting tumour-associated Ag such as IL-13Rα2,

EGFR and HER2.[76,83] Oncolytic viruses (OVs) represent another promising approach, as they are designed to selectively infect certain cells and induce their lysis, releasing danger-associated molecular patterns (DAMPs), pathogen-associated molecular patterns (PAMPs) and tumour-associated antigens (TAAs). This process will thereby promote immune activation and may convert cold tumours into hot tumours. Several OVs are currently tested in clinical trials, including Herpes Simplex virus-1 (HSV), Adenoviruses, Polioviruses and Reovirus.[83,84]

Beyond therapeutic breakthroughs, access of drugs to the tumour site remains severely limited due to the BBB which is characterised by tight junctions and active efflux transporters. Accordingly, nanocarriers have been developed to facilitate drug path and decrease systemic toxicity. Those tiny, engineered vehicles encompass diverse formulations depending on therapeutic needs (e.g. lipids, polymers, micelles, silica, dendrimers) and can be coupled to targeting ligands. In GBM, several strategies seem promising and undergo extensive development specifically to target GSCs.[76,77] Some of those strategies will be reused in the subsequent section in the context of surface protein targeting.

3. Targeted Therapies

3.1. Surface Proteome in GBM

3.1.1. Diversity of Surface Proteins and Biological Implications

As discussed earlier, GBM exhibits a highly heterogeneous molecular landscape, characterised by the coexistence of multiple tumours subclones, displaying genetic and epigenetic alterations which are likely to influence responses to treatments. Advances in molecular profiling, by techniques such as NGS and transcriptomic analysis, have enabled improved patient's stratification. PD-L1 expression and MGMT promoter methylation illustrate the urgent need for new predictive and prognostic biomarkers in optimizing clinical trials and therapeutic decisions.[85] However, the spatial and temporal variability of these alterations highlight the need to identify biomarkers that better reflect the dynamic state of the tumour. In this context, surface proteins represent promising therapeutic targets in GBM, as they enable tumour cells to integrate signals from their microenvironment, but also their modulation thereby promoting migration, proliferation and communication with various cellular components.[86] Importantly, many surface proteins are aberrantly overexpressed in GBM cells compared with normal brain tissue, making them attractive candidates for both targeted therapies and diagnostic biomarkers.[87]

Surface proteins encompass several major functional categories. Receptor tyrosine kinases (RTKs) are frequently targeted by cancer therapies, among which growth factor receptors constitute the main components (e.g. EGFR, FGFR, PDGFR), and they play a central role in cellular processes including migration, proliferation, cell survival and immune tolerance by activating various intracellular phosphorylation signalling cascades (e.g. PI3K/Akt/mTOR, Ras/MAPK/ERK, JAK/STAT) after a

dimerization process.[86,88] Adhesion molecules, such as integrins, are essential components of communication between GBM cells and the ECM. For example, integrin α6 is highly expressed in GSCs and has been demonstrated to take part in radioresistance by modulating signalling mechanisms, leading to the maintenance of the expression of key transcription factors involved in self-renewal (e.g., OLIG2, SOX2).[89] A number of adhesion molecules belong to the cluster of differentiation (CD) family, such as CD133, CD44 and CD15, initially used to classify and identify mAbs. Nevertheless, they have also been shown to play an essential role in several cellular functions including cell-cell interactions, migration and proliferation.[63-66,86] Membrane transporter proteins, which include the superfamilies of solute carriers (SLC), ATP-binding cassette (ABC) transporters and ATP-dependent transporters, constitute another large family of surface proteins involved in cancer-related pathological processes. Some, such as ABCG2 (also known as BCRP1), act as efflux pumps for cytotoxic agents[86], while others, such as SLC16A1, respond to TGF-β signalling which contributes to tumour invasion and is associated with poor prognosis.[87] The diversity of surface proteins, together with their activation and deregulation, can therefore strongly influence downstream signalling pathways involved in tumour progression.

3.1.2. Brief Functional Role of Surface Proteins in GBM Signalling

Downstream of the surface receptors, intracellular signalling networks regulate the expression of genes involved in tumorigenesis. Among the most prominent pathways are PI3K/Akt/mTOR, Ras/MAPK/ERK, JAK/STAT, NFκB and Wnt/β-catenin, which control key cellular processes such as proliferation, survival, migration and angiogenesis. These signalling cascades are part of a complex interconnected network, where inhibition of a specific pathway leads to the subsequent activation of parallel pathways. This compensatory behaviour of tumour cells is strongly implicated in the limited efficacy of several therapies tested in clinical settings and underlines the need for new targets and development of combinatorial targeting strategies.[88,90]

3.1.3. GSCs as a key targeting issue

Consistent with previous observations, GSCs are highly aggressive tumour cells and represent major drivers of GBM recurrence. Those cells are found in specialised niches (hypoxic, perivascular), promoting the induction of a dormant state known as quiescence. GSCs ability to alternate between both proliferative and quiescent states allows them to acquire resistance to conventional treatments by chemotherapy and radiotherapy, and to fuel recurrences. Such plasticity is based on several key mechanisms. On the one hand, these cells express a wide variety of proteins on their surface, that are involved in interactions with the TME, although no marker is currently considered as specific. On the other hand, various molecular and epigenetic mechanisms—including DNA methylation, modification of DNA-associated proteins, and activation of signalling pathways and key factors—actively regulate the transition between cellular states. Those properties contribute significantly to the therapeutic resistance of GSCs. They can acquire new mutations during cell division, as well as under therapeutic

pressure, leading to the emergence of dormant tumour subclones that may respond differently to external conditions. In addition, central tumour necrosis induces signals that promote the emergence of dormant tumour cells, which are often located at the infiltrative tumour margins. Because tumour cells do not display the same sensitivity to treatments, it is crucial to distinguish between actively proliferating cells and those re-entering the cell cycle from a quiescent state. If those two cell populations are not clearly distinguished, therapeutic strategies cannot be effectively adapted. For example, TMZ and radiotherapy mainly target dividing cells, which are more vulnerable to DNA damage. However, GSCs exhibit highly efficient cell cycle checkpoints and frequently overexpress MGMT, particularly in hypoxic regions. In contrast, quiescent cells are not actively dividing and therefore tend to escape the effects of these conventional therapies.[63,64,91] According to several studies, GSCs even demonstrate multidrug resistance to therapies through the overexpression of ABC transporters such as ABCG2 or MDR1.[92,93]

3.1.4. Identification and Validation of Surface Targets

According to the WHO, a good biomarker can be defined as "a substance, structure, or process that can be measured in the body or its products to reliably predict or influence the incidence, outcome, or progression of a disease." In the context of GBM, the identification of relevant biomarkers involves different steps ranging from discovery to rigorous clinical validation. Although genomics and transcriptomics constitute powerful tools for biomarker identification, their clinical application remains limited, since they do not directly reflect the functional state of cells.[94] Consequently, identification of cell-surface proteins typically relies on high-throughput proteomic approaches. These strategies generally include enrichment of surface proteins (e.g., biotin-labelling), followed by MS analysis and bioinformatic filtering to select proteins of interest.[87,95]

The study of surface proteins in cancer provides valuable information on key cellular processes like cell-cell communication, adhesion, interactions with the ECM, metabolic activity or even cytoplasmic shift which consists of abnormal translocation of intracellular proteins to the cytoplasm.[95] Beyond identification, expression and location of those proteins must be confirmed in patients. As MS is the typical discovery technique, the selected reaction monitoring is a strong quantitative validation tool, as well as next-generation tissue microarrays. Furthermore, at the interface between identification and validation, the use of protein pathway arrays allows these proteins to be located within cellular signalling networks, to study how they interact with their environment. Thereby, overexpression and membrane location of proteins in a clinical situation can be validated. Importantly, many transmembrane proteins can undergo cleavage and be detected in biological fluids, highlighting their potential as circulating biomarkers and indicators of tumour state.[87,94]

3.2. Focus on PTK7 and Targeting Modalities

3.2.1. PTK7 functions in health and disease

In 1993, Lee et al. identified for the first time the protein tyrosine kinase 7 (PTK7) transcript while investigating TKs expressed in normal human melanocytes, enabling to identify a 220-bp sequence, although its cellular function and the complete gene sequence were still unknown at that time.[96] In 1995, Mossie et al. isolated the full-length PTK7 cDNA from a colorectal carcinoma and characterised the encoded protein as a 1,071 AA transmembrane glycoprotein, belonging to the RTK family, initially named colon carcinoma kinase 4 (CCK4).[97] One year later, Lee et al. reconstructed the complete PTK7 cDNA sequence, deduced the AA sequence, and identified several key structural features: (1) an extracellular domain (ECD) composed of seven immunoglobulin-like (Ig-like) loops, (2) a transmembrane helical domain, and (3) an intracellular kinase-like domain containing sequence alterations within the catalytic domain of TKs. **(Figure 5A)** At this stage, the function of PTK7 remained unknown.[98] It was not until the early 2000s that pioneering studies demonstrated the role of PTK7 in the regulation of planar cell polarity (PCP) and Wnt signalling during embryonic development, notably[99,100], which were later supplemented by numerous additional investigations. Although catalytically inactive, PTK7 acts as a signalling modulator and scaffolding protein for the recruitment of other proteins such as Dishevelled (Dsh), and contributes to cell-cell communication by interacting with the Scr kinase, activating actomyosin contractility.[101] In the canonical Wnt/β-catenin pathway, the role of PTK7 remains less clearly defined, acting as an activator or an inhibitor depending on the context. Furthermore, beyond Wnt signalling, PTK7 can also function as a co-receptor for other RTKs, including VEGFR.[102,103] **(Figure 5B)**

PTK7 expression in normal adult tissues is generally low, but is frequently dysregulated in many cancers, including both solid tumours and haematologic malignancies. This overexpression is generally associated with an unfavourable clinical course, together with increased invasiveness, high metastatic potential, and reduced response to conventional treatments.[102,104] Indeed, through its context-dependent expression, as well as its structural characteristics, and interactions with other cellular components PTK7 is a key regulator of tumour progression. Among the mechanisms involved, PTK7 may undergo proteolytic cleavages mediated by metalloproteinases (MMPs), enzymes responsible for ECM degradation, generating fragments implicated in the regulation of genes involved in tumour progression and migration.[102] Furthermore, PTK7 has already been shown to be involved in EMT regulation. For example, a study in ovarian cancer showed that PTK7 knockdown impairs Wnt/PCP signalling, leading to a shift from a mesenchymal to an epithelial phenotype through the regulation of key cytoskeletal proteins.[105] Finally, PTK7 also has the ability to act as a co-receptor by forming signalling complexes with other RTKs. A well-known example is its interaction with VEGR, which contributes to the promotion of angiogenesis.[106,107]

3.2.2. PTK7 Targeting Strategies

The strong involvement of PTK7 in tumour progression across various cancer types has driven the development of novel personalised and targeted therapeutic strategies, currently under investigation in preclinical and clinical studies, including antibody-drug conjugates (ADCs), CAR-T cells, aptamers and small molecule inhibitors.[104] **(Figure 5A)** The exploration of these therapeutic approaches is particularly relevant given that PTK7 expression is frequently associated with disease progression and that the existence of several PTK7 isoforms may contribute to its diverse functional roles.[103] Importantly, PTK7 has been reported to remain stably expressed in several tumour cell types after standard of care, an idea reinforced by its elevated expression in CSCs.[108,109]

Antibody-Drug Conjugates (ADCs)

ADCs are a class of targeted therapies consisting of a mAb conjugated to a cytotoxic payload via a linker. To date, 15 ADCs have received an approval by the U.S. Food and Drug Administration (FDA). While mAbs have been promising agents combining specificity and cytotoxic property, their targeted effect remains limitated when used as monotherapies (e.g. poor tumour penetrability, resistance mechanisms, etc.). Moreover, mAbs act by their own as therapeutic agents and have limited range of action due to tumour heterogeneity. In contrast, latest-generation ADCs can kill low- or non-target-expressing cells via bystander effects, through the diffusion of the cytotoxic agent. Some can also be designed to recognise two targets simultaneously[110,111] Among these, MTX-13 (Ab13-Val-Ala-T1000-exatecan) represents a promising example. The specificity of this drug for PTK7, including mice (mPTK7), provided by Ab13, symbolizes a major advantage for the elimination of metastatic cells and CSCs involved in recurrence, which strongly express PTK7, as well as for preclinical research. This specificity goes along with strong stability, ensured by a hydrophilic T1000 unit linking the Val-Ala linker to the exatecan payload. This exatecan molecule, a topoisomerase I inhibitor, is also able to induce the bystander effect, enabling killing of heterogeneous cell populations. Although MTX-13 has only been tested in *in vitro* models, its safety and encouraging preliminary results in terms of efficacy across various tumour types hold promise for further testing in preclinical and clinical trials.[112]

CAR T-cells

Since its development in the 1980s, CAR T-cell technology has continued to evolve by demonstrating a strong efficacy in the treatment of haematological malignancies such as large B-cell lymphomas and multiple myeloma. However, its application to solid tumours remains limited. This restriction can be attributed to several factors, including an immunosuppressive microenvironment, the difficulty in identifying tumour-specific antigenic targets—which is behind an “on-target, off-tumour” effect— as well as high intratumoral and interpatient heterogeneity.[113,108] To overcome these obstacles, targeting PTK7 using CAR T-cells approaches has recently demonstrated encouraging results across multiple cancer types in both *in vitro* and *in vivo* models. These studies have reported an important production of

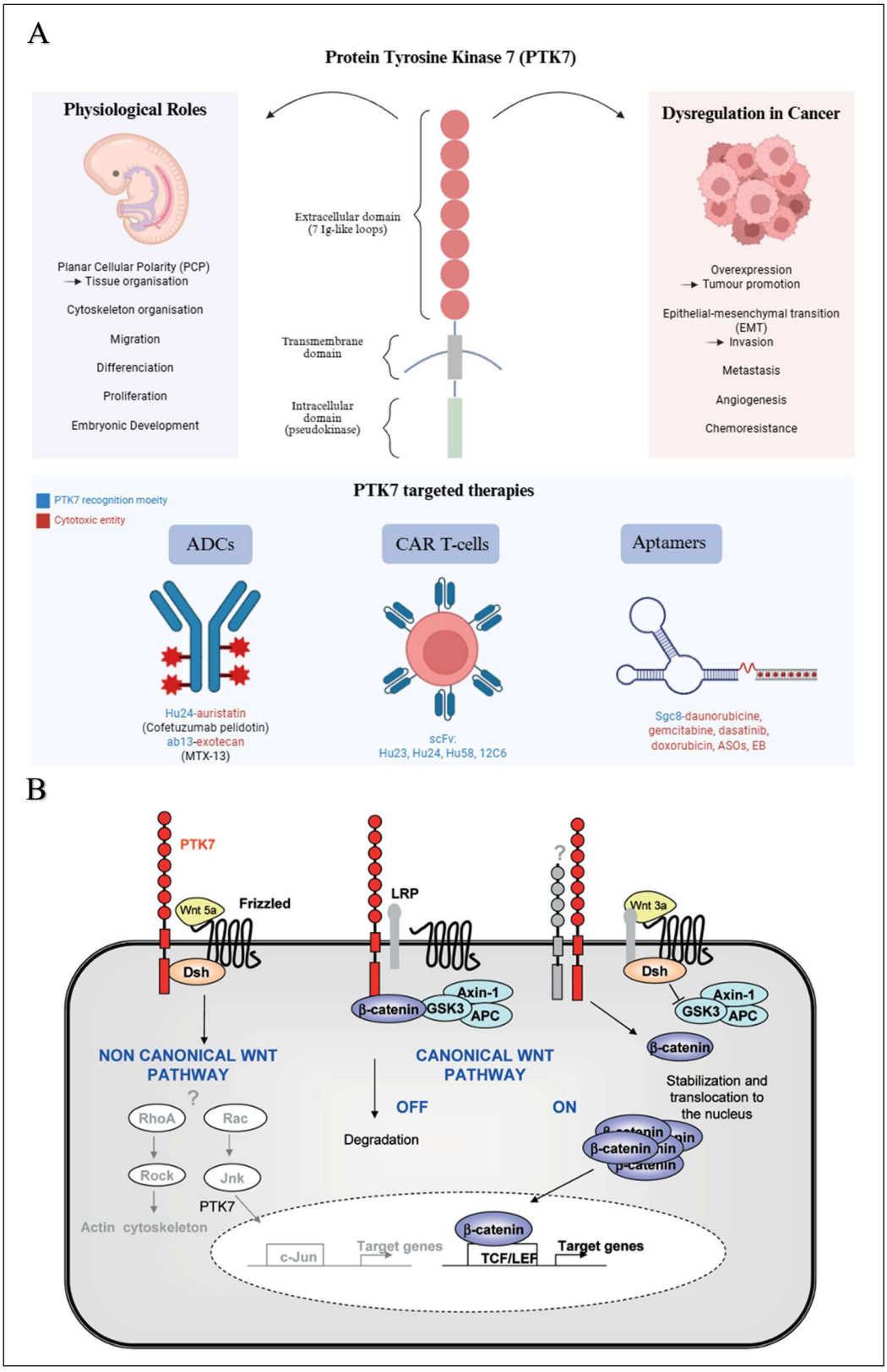

Figure 5. Structure, biological functions and targeted therapies developed against PTK7. (**A**) PTK7 is a receptor composed of an extracellular domain with seven Ig-like loops, a transmembrane domain, and an intracellular pseudokinase domain, involved in processes such as PCP, cell migration and embryonic development. In cancer, its dysregulation is associated with tumour progression, angiogenesis, invasion, metastasis, and chemoresistance. Several therapeutic approaches are currently under investigation, including ADCs, CAR T-cells and aptamer-based strategies. *Adapted from Mottard et al. (2025)*. [ref 104]; (**B**) It participates in non-canonical Wnt/PCP signalling and modulates Wnt signalling through regulation of β-catenin stabilisation and transcriptional activity. *From Lhoumeau et al. (2011).* [ref 114]

cytokines (IL-2, IFN-γ), concomitant with a high proliferation rate, as well as prolonged survival and tumour regression in preclinical models, accompanied by $CD3^+$ T cells infiltration. Notably, proliferation rate of CAR T-cells has been associated with PTK7 expression levels in cancer cells. In addition, none of those studies reported "on-target off-tumour" toxicity, despite low-level expression of PTK7 in certain normal tissues.[108,109,112-115] Furthermore, PTK7 expression is confirmed to be stable and even slightly increased following chemotherapy. For example, in neuroblastoma—primarily affecting children—chemotherapy seems to inhibit GD2 expression, the main Ag targeted by standard-of-care. Consequently, targeting GD2 using CAR T-cells in resistant patients could be ineffective, all the more reason to target proteins whose expression remains unchanged.[108] Finally, it is essential to keep in mind that the current success of CAR T-cell therapy relies on a preliminary lymphodepletion, which consists of reducing the number of own patients lymphocytes to prevent competition between both cell types.[113] In GBM, a work performed by Suryadevara et al. (2018) by administrating CAR T-cells targeting EGFRvIII failed in non-preconditioned host. However, after inducing lymphodepletion by administration of TMZ dose intensified (TMZ^{DI}), CAR T-cells expanded massively and persistently in the blood. This discovery led to a phase I clinical trial by combining TMZ^{DI} to CAR T-cells.[115] In conclusion, these challenges posed by CAR T-cell therapy necessitate the continuation of clinical trials for the treatment of solid tumours and further innovation in the development of other strategies for targeting PTK7.

Aptamer-Based Therapies

Aptamers are small molecules (~6-30 kDa), typically single-stranded DNA or RNA oligonucleotides, capable of specifically binding to a target. They are often compared to Abs due to several advantages. Indeed, their smaller size allows improved tissue penetration, which is particularly beneficial in the development of cancer therapies. Furthermore, unlike Abs, which are produced in cells or animals, aptamers are specifically generated and selected *in vitro*, notably through the Systematic Evolution of Ligands by EXponential Enrichment (SELEX) process. Briefly, this selection method involves a binding step where millions of random DNA or RNA sequences are put in contact with a specific target, followed by washing steps to remove non-specific binders, elution of bound sequences and amplification steps. As the selection cycles progress, the aptamer pool becomes increasingly enriched in sequences with high specificity and affinity for the target. Compared to Abs production, this process is cheaper, faster and more reproducible. In addition, aptamers can be easily chemically modified to improve their stability and specificity, or to deliver specific molecules. To date, only two aptamers have been approved by the FDA, both for the treatment of ocular diseases: (1) Pegaptanib (Macugen) approved in 2004 for the treatment of wet age-related macular degeneration (AMD), targeting the VEGF165 isoform and thus inhibiting angiogenesis, responsible for progressive macular cell destruction, and (2) Avacincaptad pegol (Izervay), approved in 2023 for the treatment of geographic atrophy (GA), an advanced and irreversible stage of dry AMD associated with complement system dysregulation and chronic

inflammation, by targeting complement component C5.[116,117] Although no aptamers have yet been approved for cancer treatment, numerous preclinical and clinical trials are currently investigating their potential to target molecules and cell surface proteins, including PTK7.[104] One of the most widely studied aptamers targeting PTK7 is Sgc8c, initially developed by Shangguan et al. (2009) to target PTK7 in T-cell acute lymphoblastic leukemia (T-ALL). Since then, it has been conjugated to various chemotherapeutic agents, including doxorubicin, daunorubicin, gemcitabine (GEM) etc., evaluated in multiple cancer models, demonstrating significant antitumour activity.[116,118] These examples illustrate the versatility of aptamers, which can function as neutralizing or blocking agents (antagonists), or agonists (stimulators), as cargo carriers, or as targeting moieties for nanocarriers.[104,116]

4. Adeno-Associated Viruses (AAVs) as Targeted Therapy Tools

4.1. Structure and Biological Characteristics of AAVs

The first identification of adeno-associated viruses (AAVs) was performed in 1965 by a group of three researchers in New York during studies on adenoviruses. They observed a contamination by tiny viral particles, later shown to be non-infectious agents, which require a helper virus for replication, leading to their designation as AAVs.[119] They are non-enveloped viruses from the Parvoviridae family, in which genome consists of a single-stranded DNA (ssDNA) of ~4.7 kb, enclosed within an icosahedral capsid. This genome comprises two inverted terminal repeat (ITR) regions that flank the Rep and Cap genes. The Rep genes (Rep78, Rep68, Rep52, Rep40) are essential for DNA replication and encapsulation, while the Cap genes (VP1, VP2, VP3) are necessary for capsid assembly during the formation of a new viral particle and determine tissue tropism.[120] **(Figure 6)**

Indeed, the AAV serotype, defined as a variant of an AAV based on its capsid surface proteins, determines the ability of the viral vector to infect specific tissues and cell types. To date, 13 common serotypes have been identified, which mainly differ by the variable regions of the VP3 protein, exposed at the capsid surface. As examples of tropism, AAV2 is the most studied serotype and can transduce a wide range of tissues across multiple species. In contrast, AAV9 has the unique ability to cross the BBB following systematic injection, enabling the targeting of neuronal cells such as astrocytes and neurons, and making it a promising candidate for the treatment of brain diseases. Beyond these differences in tropism, all AAV serotypes share major structural, genetic and functional similarities. Notably, the AAV receptor (AAVR) and the G protein-coupled receptor 108 (GPR108) are involved in the transduction of most serotypes. More specifically, it seems that both play a role in the stages following attachment, such as membrane penetration and intracellular trafficking.[121,122]

4.2. Recombinant AAVs and Therapeutic Applications

The ability of AAVs to transduce several cell and tissue types while exhibiting low pathogenicity has led to the development of recombinants AAV (rAAV) for gene therapy applications in various human

diseases. In a rAAV, Rep and Cap genes are substituted by a transgene, flanked by the two ITR regions, which are essential for the genome to be packaged and maintained within the targeted cell. As lacking replication and capsid genes, the rAAV can no longer replicate in the host cell, but will serve as a carrier for the gene of interest, strengthening their security profile.[123] The use of rAAVs as a gene therapy is particularly relevant in oncology, as most clinical trials in this field focus on cancer treatment. In the context of GBM, several AAVs have been tested *in vitro* and in mice to deliver different types of "payloads", such as suicide genes or immunomodulatory agents (e.g. AAV9-IFN-β). However, the transition from preclinical to clinical applications for the safe use of AAVs in the treatment of GBM depends heavily on the unique properties of AAVs and the biological constraints inherent to GBM. Indeed, AAVs are widely considered vectors of choice for treating CNS diseases, as they are not currently associated with pathologies in humans and allow for long-term transgene expression, which is crucial to treat persistent tumours.[120] Moreover, the AAV genome rarely integrates into the host cell genome, which reduces the risk of oncogene activation.[124] Nevertheless, like any therapy, AAVs present several limitations. First, their genome size (~4.7 kb), can only accommodate transgenes of limited size, thereby limiting the range of possible applications. Second, pre-existing neutralizing Abs against different serotypes may be present to varying degrees in the general population, which can reduce the efficacy of those vectors, particularly in cases of systematic administration.[121,122] Despite these limitations, AAVs remain highly promising vectors for gene therapy. Clinical approvals, such as Luxturna for inherited retinal dystrophy and Zolgensma for spinal muscular atrophy (SMA), demonstrate the potential of these vectors to significantly improve patient lives.[121]

5. Work Performed in The Host Laboratory

Altogether, these findings underscore the limited availability of therapies capable of effectively targeting and killing GBM cells within an extremely complex TME, as well as the description of the biological role that PTK7 plays in cancer progression and its potential as a therapeutic target. Based on these observations, the development of a new and innovative therapy targeting PTK7 emerged as a relevant approach, not only based on the existing literature but also to sustain therapeutic innovation. This therapy is based on four key elements: (1) an anti-PTK7 nanobody, (2) a recombinant AAV (rAAV), (3) a suicide gene (SG) encoding for Herpes Simplex Virus type 1 Thymidine Kinase (HSV1-TK), and (4) a prodrug, the ganciclovir (GCV).

5.1. Identification and Validation of PTK7 as a Candidate Target

Surface Proteomic Identification of PTK7 in GSCs

Within the Laboratory of Nervous System Disorders and Therapy at the GIGA Neurosciences, a series of GSCs cultures was established in collaboration with the Department of Neurosurgery at the University Hospital of Liège. To identify highly expressed surface proteins, the host laboratory performed surface protein enrichment on GSCs from six different patients, based on biotin-streptavidin purification and

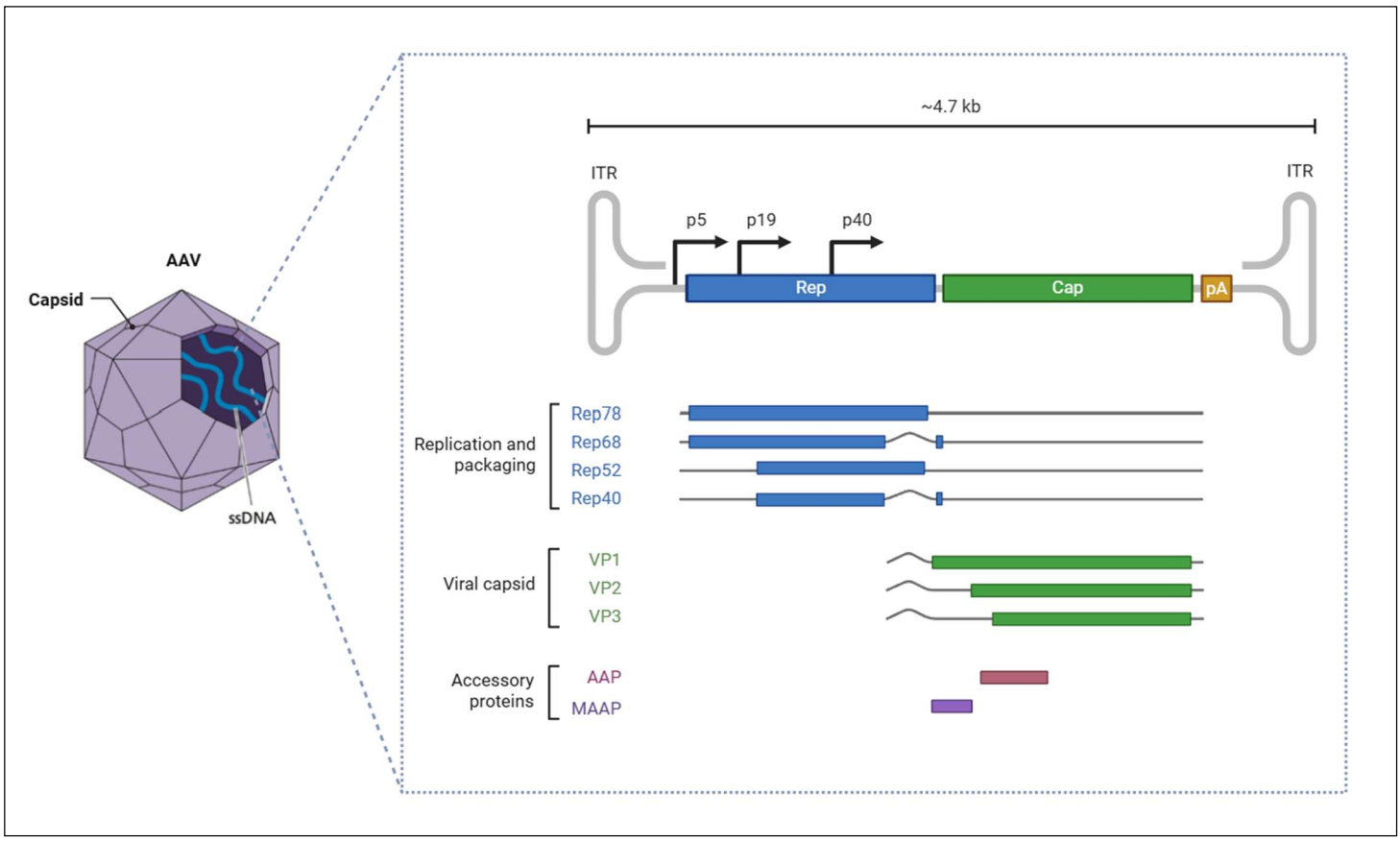

Figure 6. Structure and genome organization of adeno-associated virus (AAV). An AAV is a small, non-enveloped viral particle widely used in gene therapy. Its single-stranded DNA (ssDNA) genome comprises two inverted terminal repeats (ITRs) flanking two open-reading frames (ORFs); Rep encodes for replication and encapsulation proteins (Rep78, Rep68, Rep52, Rep40), and Cap encodes for the viral capsid proteins (VP1, VP2, VP3), as well as for accessory proteins, including the membrane-associated accessory protein (MAAP) and the assembly-activation protein (AAP). The expression of all those proteins is regulated by the 3 main promoters p5, p19 and p40. *AAV capsid image is adapted from Virology Blog (https://virology.ws/2021/09/30/gain-of-function-to-build-useful-viral-vectors/) and AAV genom representation comes from BioRender.*

analysis by mass spectrometry (MS). They identified a panel of cell surface proteins including PTK7. **(Figure 7A)** Not only PTK7 was found to be highly expressed by GSCs, but analysis of databases such as The Cancer Genome Atlas (TCGA) and the Chinese Glioma Genome Atlas (CGGA) also confirmed this overexpression of PTK7 compared to non-tumorous brain tissues. **(Figure 7B-C)** Afterwards, immunohistochemistry assays performed on normal brain tissue, GBM tissue and neurospheres, corroborated previous findings regarding PTK7 overexpression. **(Figures 7D-E)**

Biological Relevance of PTK7 in GBM treatment

Although PTK7 has been shown to be expressed by GBM cells, it is essential to determine whether its expression remains stable over time and under different conditions to identify a potential role in treatment resistance and to distinguish between targetable subpopulations. After treatment under TMZ or radiation, PTK7 expression was assessed by PTK7 staining and flow cytometry analysis. Overall, results highlighted that PTK7 was still expressed after the different treatment regimens, but this expression tends to vary from one GSC culture to another, which can result from the heterogeneity in GBM. Increased expression following standard therapies **(Figures 7F-G)** supports its relevance as a therapeutic target in resistant GSCs population.

5.2. Generation and Validation of Anti-PTK7 Nanobodies

Among the different targeted strategies developed to efficiently target PTK7, only the ADC cofetuzumab pelidotin has entered a phase I clinical trial.[125] However, despite their high specificity for their target and efficient tumour penetration, ADCs have a limited ability to cross the BBB, which remains a major obstacle in the treatment of brain tumours.[126] In this context, alternative strategies have been explored to improve both penetration and targeting specificity. Among them, nanobodies have emerged as particularly promising tools.

What is a Nanobody?

A nanobody (Nb) or Variable domain of the Heavy chain of Heavy-chain Abs (VHH) refers specifically to the variable region of heavy-chain Abs (HcAbs), most of which are derived from camelids and sharks. Unlike conventional mAb (~150 kDa), Nb are 10 times smaller (~12-15 kDa), which gives them high tissue and solid tumour penetration. Furthermore, the VHH domain consists of three hypervariable regions (CDR1-3) and four conserved regions (FR1-4). Notably, their CDR3 region is larger and more flexible, which allows them to bind to Ag in a highly specific manner and to recognize epitopes that are difficult to access for conventional Abs. **(Figures 8A-B)** In addition, small hydrophilic residues in the FR2 region increase their hydrophilicity, improving their solubility and stability. Those properties allow Nb to serve as targeting moiety for directing cytotoxic payloads towards specific cancer target—referring them to Nanobody-Drug conjugates (NDCs)—as well as to be coupled to radioisotopes, photosensitizers, or nanocarriers.[127,128]

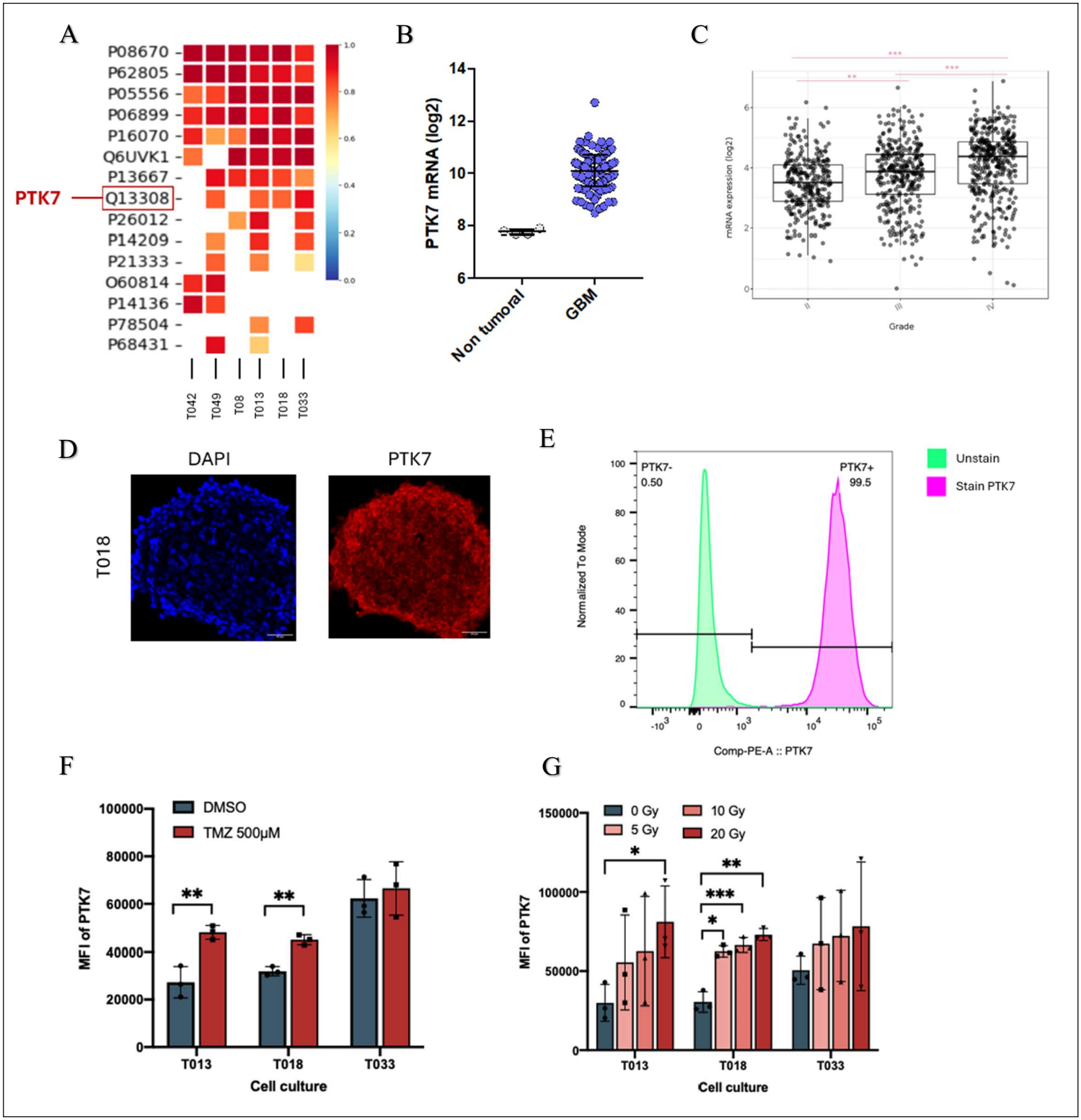

Figure 7. Identification of PTK7 as highly expressed at the surface of GBM cells. (**A**) Expression of PTK7 by MS analysis of patient-derived GSCs surface proteome; (**B**) PTK7 mRNA expression in GBM and normal brain tissues from TCGA dataset; (**C**) PTK7 mRNA expression comparison between glioma grades II, III and IV from CGGA dataset; (**D**) Surface expression of PTK7 in patient-derived GSCs assessed by immunohistochemistry assay, (**E**) Flow cytometry analysis confirming surface expression of PTK7; Verification of PTK7 stable and even increased expression upon therapy-like conditions, e.g. (**F**) TMZ and (**G**) ionizing radiations.

Production and validation of the anti-PTK7 Nb5

Sequences of four different anti-PTK7 VHHs were obtained from a chinese patent (WO2023020551A1). Each Nb sequence was integrated into a plasmid, then transformed into *E. coli* WK6. Each nanobody was then produced and purified individually. To characterise their specificity and binding properties for the PTK7-ECD, these candidates were subject to the Bio-Layer Interferometry (BLI) technology, which enables the measurement of protein-protein complex binding and dissociation in real time.[129] Overall, among the four previously selected VHHs, only one of them exhibited an affinity for PTK7 in the nanomolar (nm) range and was retained.

5.3. Concept of Suicide-Gene Therapy

Among gene therapies, suicide-gene therapy (SGT), also referred to as gene-directed enzyme/prodrug therapy (GDEPT), has been extensively investigated for its ability to selectively target tumour cells and localize the treatment, while limiting toxicity to healthy surrounding cells. This strategy involves the introduction, via a viral or non-viral vector, of a gene encoding an enzyme capable of converting a non-toxic prodrug into a toxic metabolite within the target cells. Following gene delivery, adding prodrug leads to localised cell death.

Among the various systems developed, the most extensively studied are HSV-TK/GCV and cytosine deaminase/5-fluorocytosine (CD/5-FC), which differ in their origin, their mechanism of action, and the way they mediate the therapeutic effect. In the HSV-TK/GCV system, viral TK phosphorylates GCV, leading to the formation of a toxic metabolite, GCV triphosphate, able to interfere with DNA synthesis. In the CD/5-FC system, CD converts the prodrug into 5-fluorouracil (5-FU), a cytotoxic compound, which is then metabolised into derivatives capable of disrupting nucleic acid synthesis or inhibiting thymidylate synthase. Interestingly, both systems are particularly investigated in the treatment of high-grade gliomas (HGGs). Due to the inability to eliminate all tumour cells, the efficacy of SGT also relies on the induction of a bystander effect, allowing for the elimination of adjacent cells. However, this effect depends on the enzyme-prodrug couple, as well as on cellular biology and the physicochemical characteristics of the tumour microenvironment. While 5-FU can diffuse across cell membranes and does not require cellular proximity, GCV triphosphate uses gap junctions, requiring proximity between cells. Overall, beyond bystander effect, SGT offers several advantages, including selective targeting of cancerous cells, the possibility to synergise with conventional therapies and potentially activating the immune system. Nevertheless, its efficacy remains limited by challenges related to vector delivery, transgene expression in targeted cells, physical barriers, and potential adverse immune response against viral vectors.[130,131]

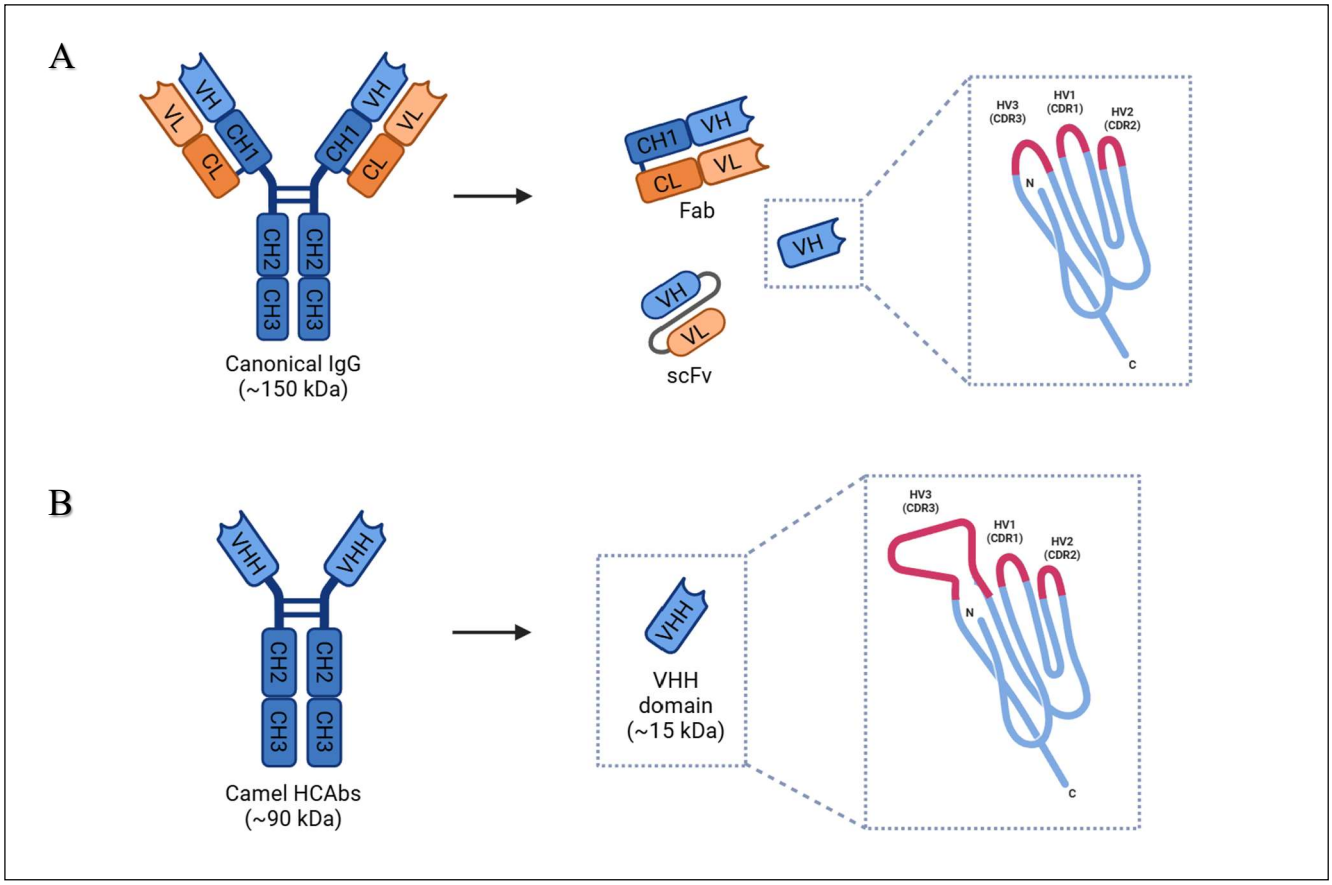

Figure 8. Structural comparison between conventional antibodies and nanobodies. (**A**) Conventional IgG antibodies of ~150 kDa, constituted of identical two light chains and two heavy chains, maintained by disulfide bonds and non-covalent interactions. The variable domain (VH) of the heavy chains comprises three hypervariable determining regions (CDR) in which CDR3 plays a critical role in Ab-Ag binding.; (**B**) Camelid HCAbs of ~90 kDa, lacking light chains and CH1 domains. The VHH domains of those Abs, of ~12-15 kDa, are highly stable, soluble and specific to a given Ag due to a CDR3 loop longer than that of conventional Abs. *Adapted from Liu et al. (2021).* [ref 121]

5.4. Assembly of AAV-Nanobody-TK Construct and Initial Validations

Construction of the rAAV

The aim of this project was to combine an AAV, a widely used vector in gene therapy, with a suicide gene strategy to specifically target PTK7 expressing cells. In this context, a rAAV was designed, consisting of a capsid enclosing a simplified genome containing the transgene encoding HSV1-TK, flanked by two ITR regions and lacking the viral Rep and Cap genes.

To achieve this rAAV, the capsid was first modified to abolish its natural tropism and prevent any nonspecific transduction. Subsequently, a Nb directed against PTK7 (Nb5) was conjugated to the capsid surface to specifically redirect viral transduction towards $PTK7^+$ cells. To validate the specificity of PTK7 targeting, a reporter transgene encoding green fluorescent protein (GFP) was used. Once the specificity was confirmed (**Figure 9A**), the reporter transgene was replaced with the therapeutic gene HSV1-TK. This final construction will allow AAV-Nb5-TK to bind to PTK7 at the surface of $PTK7^+$ GBM cells. After transduction, HSV1-TK gene will encode for the TK enzyme, capable of catalysing the phosphorylation of nucleoside analogues, such as GCV, into a toxic metabolite that is incorporated into DNA during replication, leading to cell death. As shown in Figure 9A, GFP expression was significantly increased in PTK7-expressing GSCs patient-derived cells transduced with the AAV-Nb5-GFP vector compared to both AAV-WT and AAV entry-defective vectors. Notably, cells transduced by the AAV-WT displayed an intermediate level of GFP expression, consistent with the ability of the vector to infect cells independently of PTK7 expression, whereas the entry-detective vector showed no detectable transduction. This absence of transduction confirms the loss of natural tropism and demonstrated that the transduction observed with the AAV-Nb5 vector is specifically mediated by PTK7 recognition. Consistently, treatment with AAV-Nb5-TK achieved a marked decrease in cell viability over time, as assessed by Syber Green fluorescence, compared to control conditions (**Figure 9B**), demonstrating the therapeutic potential of this SGT.

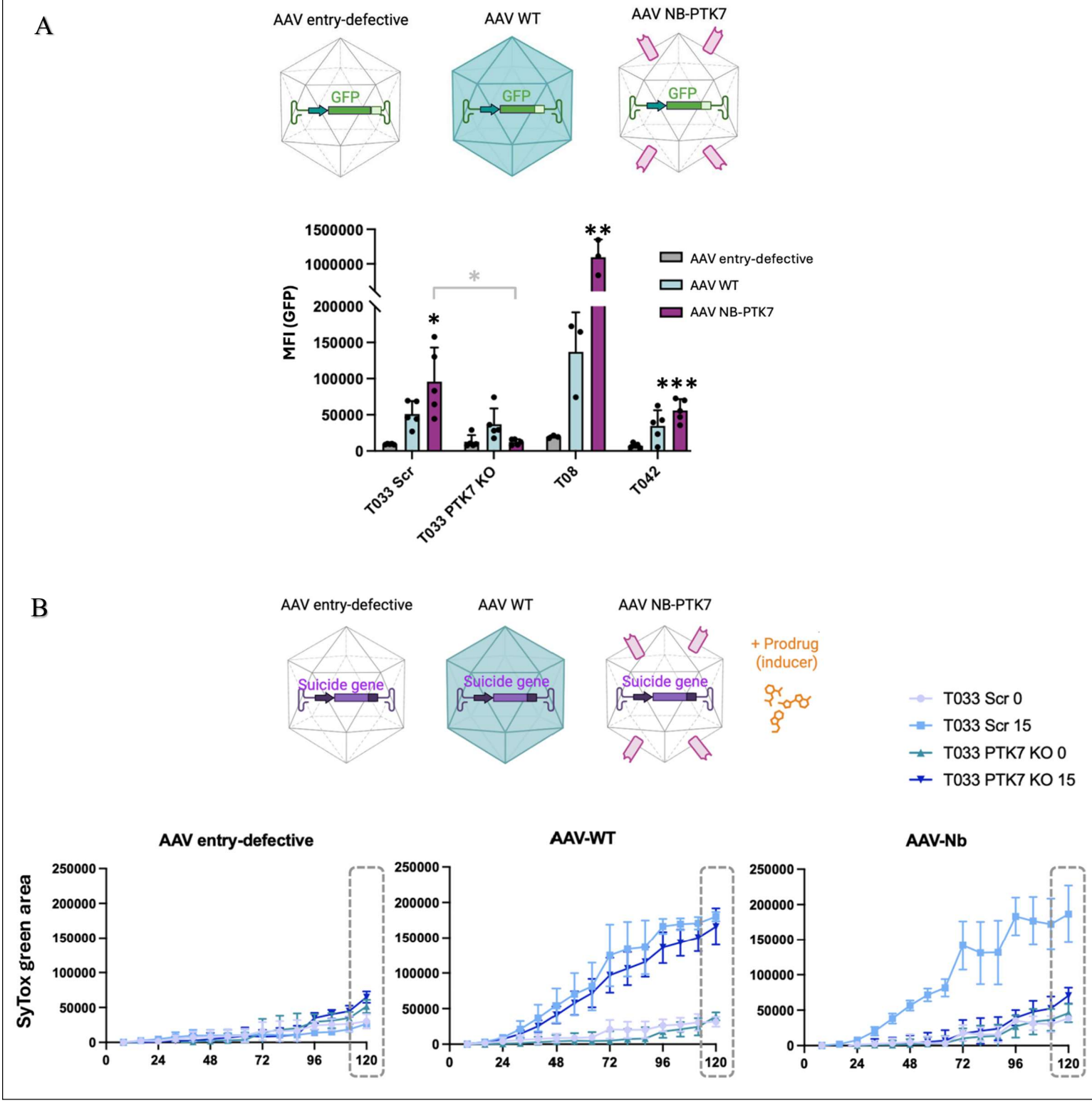

Figure 9. Preliminary results testing specificity and killing of the AAV-Nb-TK + GCV therapy. (**A**) The comparison of GFP expression between the three distinct constructs shows a specificity of the AAV-Nb of PTK7 compared to AAV-WT and AAV entry-defective vectors. (**B**) Treatment with the AAV-Nb-TK in the presence of ganciclovir (GCV) induced selective cell death in PTK7-expressing cells, while PTK7 knockout (KO) cells remained unaffected. In contrast, the AAV-WT-TK resulted in a non-specific cytotoxicity across all cell types in the presence of GCV, whereas the entry-defective AAV failed to induce cell death, confirming the specificity of the therapy for PTK7.

Chapter 2 - Objectives

Presented by Sarah Grodent

1. Hypotheses and Objectives

Despite the current standard of care, median survival for patients with GBM remains short, with near-universal recurrence. This reflects intra- and inter-tumour heterogeneity, persistence of GSCs, the BBB limiting treatment access to the tumour site, and the vulnerability of the brain tissue, where non-specific therapies may cause irreversible damage—etc. These considerations support the development of targeted therapies capable of delivering a cytotoxic payload to tumour cells while sparing non-tumour tissue. The aim of this master's thesis is to evaluate a targeted therapy, directed against PTK7, which is highly expressed in human GBM cells relative to non-tumour nervous tissue. This therapy consists of an anti-PTK7 AAV-nanobody (Nb) vector encoding HSV-1 thymidine kinase (HSV1-TK), activated by ganciclovir (GCV). We formulate the following objectives and linked hypotheses:

- **Demonstrate and characterise cell death in PTK7$^+$ cell lines *in vitro*.** *Hypothesis*: The anti-PTK7 AAV-Nb-TK induced specific cytotoxicity of PTK7$^+$ GBM cells upon GCV exposure.
- **Establish target specificity in PTK7$^+$/PTK7$^-$ co-culture.** *Hypothesis*: cytotoxicity spares PTK7$^-$ cells, with assessment of any bystander component and selectivity of the effect.
- **Validate efficacy and specificity in translational models.** *Hypothesis*: Efficacy and specificity are maintained in models of increasing complexity, including *in vivo* (orthotopic human xenograft), and in a murine GSC context to extend evaluation of the therapy in an immunocompetent murine model.

2. Experimental Strategy

To address these objectives, we will implement a **four-stage strategy**:

1. *In vitro* analysis of suicide-gene therapy (SGT) cell death in GBM cells: We will transduce PTK7$^+$ GBM cells with the AAV-Nb-TK and expose them to GCV. We will then quantify viability and characterise the mode of cell death using Annexin V/DAPI alongside death-pathway protein markers (e.g., cleaved-caspase-3 and PARP cleavage).

2. *In vitro* analysis of the SGT bystander effect: We will mix PTK7$^+$/PTK7$^-$ cells in a co-culture with different labelling to: (i) first, evaluate the expression of PTK7 and binding of the AAV-Nb5; (ii) second, compare survival of each subpopulation with therapy by assessment of potential bystander effect.

3. SGT efficacy in human GSC xenograft model: We will test the therapy in an orthotopic xenograft model, derived from human PTK7$^+$ GBM cells, performing immunostaining for PTK7 to specifically delineate the tumour and for cell death markers to assess therapy response.

4. Development of a PTK7$^+$ murine GSC culture: We will develop a PTK7$^+$ murine GSC model and check for PTK7 expression. This cell model will allow the extend of the therapy to an immunocompetent murine model to evaluate antitumour efficacy and specificity in this context.

Chapter 3 - Materials & Methods

Presented by Sarah Grodent

1. Cell cultures

To perform a systemic evaluation of whether AAV-Nb5-TK+GCV therapy effectively kills PTK7^{+} GBM cells, spares or impacts PTK7^{-} cells, and is transposable to immunocompetent settings, we relied on the use of several cell models: (1) patient derived GSCs, (2) commercial GBM cells, and (3) murine GBM cells derived from genetically-driven brain tumours in C57BL/6 background mice.

1.1. Patients-derived GSCs cultures

A collaboration with the Neurosurgery department of the University Hospital of Liège (CHU) and the University Hospital Biobank (BHUL, Liège, Belgium), allowed the establishment of in-house patient-derived GSC cultures within the laboratory. The ethical aspects of the research carried out at the GIGA Neurosciences (Laboratory of Nervous System Disorders and Therapies) have already been approved by the Ethics Committee of the CHU (accepted on July 12, 2016). Those cells are cultured as neurospheres in serum-free medium, comprising DMEM/F-12 (1:1) (1X) + GlutaMAX™-I, supplemented in B27 NeuroCultTM SM1 without Vitamin A (STEMCELL Technologies, 05731), 2 µg/mL of heparin (LEO, 030710), 100 µg/mL of Normocin (InvivoGen, ant-nr-05), 1% Penicillin-Streptomycin Solution 100X (biowest, L0022), as well as 20 ng/mL of recombinant human epidermal growth factor, and recombinant human fibroblast growth factor 2 (BioLegend). For this master thesis, we used T033 cells, which are GSCs originating from a recurrent GBM tumour.

1.2. U87MG cell line

U87 MG is a cell line with epithelial morphology, derived from a GBM from a 44-year-old female patient. Those cells are deposited in the American Type Culture Collection (ATCC) repository and are currently available. Those cells were cultured as adherent monolayers in DMEM High Glucose medium (biowest), supplemented with 10% of filtered fetal bovine serum (Lonza) and 1% of Penicillin-Streptomycin Solution 100X (biowest, L0022).

1.3. m005 cell line

Originally, m005 are glioma stem cells, which were generated by Marumoto et al. through the transduction of a lentivirus HrasV12-LoxP in the subventricular zone of TP53 -/+ GFAP-Cre mice. Thus, the p53 inactivation and the Ras activation via recombinase Cre allowed the development of aggressive gliomas in immunocompetent mice, which mimic human condition.[132] Those cells were later isolated from murine tumours and cultured as neurospheres, in the same conditions as patient-derived GSCs (see above).

All cells were maintained at 37°C in a humidified incubator containing 5% CO_2. During cell passages, 2D (adherent) and 3D (neurospheres) cells were respectively dissociated with 0.05% Trypsin-EDTA (1X) (gibco, 25300-054) or Accutase™ (STEMCELL Technologies, 07922).

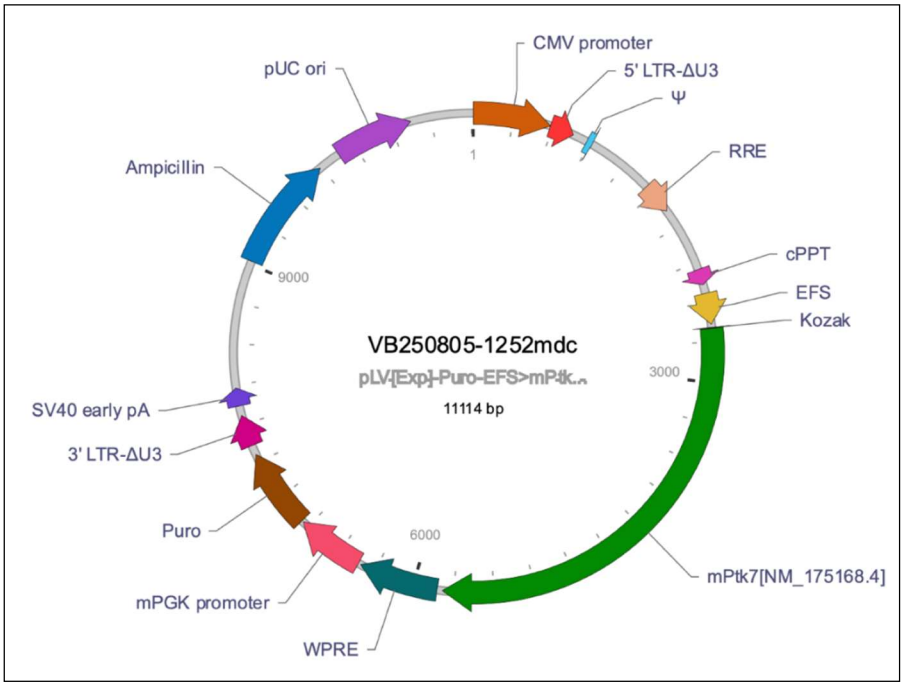

Figure 10. Vector map of the lentiviral construct used for mPTK7 overexpression in m005 cells. Schematic representation of the pLV[Exp]-Puro-EFS>mPtk7 vector expressing murine PTK7 under the control of the EFS promoter. The construct contains a puromycin resistance cassette driven by the mPGK promoter.

Table 1. *Overview of AAV vectors used for 'suicide-gene therapy' in vitro*

Vector ID	Transgene	Target	Experimental purpose	Batch used and concentrations
AAV-Nb5 CMV HSV1 TK	HSV1-TK	PTK7	Evaluation of therapeutic specificity and cell killing in monoculture and coculture models (+-GCV)	**VV-25.0219**: 2.75E+13 TU/mL **VV-25.0294**: 2.75E+13 TU/mL **VV-25.0355**: 2.75E+13 TU/mL **VV-25.0375**: 2.75E+13 TU/mL
AAV-Nb5 CMV GFP	GFP	PTK7	Assessment of selective binding to $PTK7^+$ cells in co-culture with $PTK7^-$ cells	**VV-25.0112**: 1.28+13 TU/mL **VV-25.0356**: 4.45E+12 TU/mL
AAV-2 CMV GFP	GFP	None	Control AAV to evaluate non-specific transduction in co-culture	**VV-25.0113**: 2.34E+13 TU/mL

1.4. Generation of modified cell lines by lentiviral transduction

Prior to this study, the lab performed a CRISPR-Cas9 KO of PTK7 in T033 cells (initially $PTK7^+$) using guide RNA (gRNA) targeting. On the other hand, PTK7 was overexpressed in U87 (initially $PTK7^-$) by lentiviral transduction. During this master's thesis, m005 cells were transduced by lentiviral vector (VB250805 encoding for murine PTK7 (mPTK7, NM_175168.4)), under the control of the EFS promoter (pLV[Exp]-Puro-EFS>mPtk7; VB250805-1252mdc), with a multiplicity of infection (MOI) of 100. The vector also contained a puromycin resistance cassette driven by the mPGK promoter **(Figure 10)**. After 3 changes of culture medium, a Replication-Competent Lentivirus (RCL) detection test was applied for warranting a return in BSL1 culture settings. At each passage and cell medium change, m005 PTK7 OE cells were treated with 1 µg/mL of Puromycin (10 mg/mL solution, InvivoGen). m005 PTK7 OE were compared to other previously established cultures based on PTK7 status, together with (T033 PTK7 KO, U87 PTK7 OE).

2. Immunoblotting

2.1. Preparation of protein samples

Suicide-gene therapy in vitro, using U87 and T033

After dissociation in single cells of 3D (T033 scr, T033 PTK7 KO) and 2D (U87 WT, U87 PTK7 OE) cell cultures, 500,000 cells were seeded in a final medium volume of 4 mL in a 6-well plate. In corresponding conditions, cells were transduced with the AAV-Nb5-TK. As AAV preparations from different batches were used for transduction, the viral input was normalised across batches based on their functional titers in transducing units per millilitre (TU/mL). A reference batch of 3.21×10^{13} TU/mL was used to define the viral dose (1 µL per 100,000 cells). Volumes of other viral preparations were adjusted proportionally to ensure equivalent numbers of transducing units were applied per 100,000 cells. The plate was then incubated at 37°C under 5% CO_2. After 3 days, Ganciclovir (Cayla/Invivogen #sud-gvc) (GCV) was added in corresponding wells at 15 µg/mL and the plate was re-placed in the incubator for 48h. Cells were dissociated into single cells using Accutase (3D) or Trypsin-EDTA (2D), rinsed respectively with Dulbecco's Phosphate Buffered Saline (PBS) (biowest, L0615) or DMEM High Glucose, centrifuged at 300g for 3 minutes. Finally, dry cell pellets were collected for protein extraction.

Validation of PTK7 expression in m005

m005 WT and m005 PTK7 OE cells were harvested directly from culture, dissociated with Accutase in single cells, rinsed with PBS, centrifuged at 300g for 3 minutes and dry cell pellets were collected for protein extraction.

Protein extraction and quantification

Cell pellets were resuspended in 100 µL of lysis buffer containing Tris-HCl 50 mM, NaCl 450 mM, Triton 1% (100x), to which protease and phosphatase inhibitors were added (Thermo Scientific™, 78440), then left to incubate for 10 minutes on ice. Each sample was sonicated 10x/sample and centrifuged for 10 minutes at 12,000 rpm at 4°C. The supernatant containing the proteins was then collected and the protein concentration was determined by Bradford assay, using Ascent Software.

2.2. SDS-PAGE and immunodetection

For the immunoblotting, proteins were denatured at 95°C for 5 minutes, in the presence of Loading buffer containing Tris HCl 62.50 mM (pH 6.8), glycerol 20%, SDS 2%, bromophenol blue 0.01% and β-mercaptoethanol 5%. For each condition, 18 µg of proteins were loaded as well as a molecular weight marker PageRuler™ Prestained Protein Ladder (ThermoFisher Scientific, 26616). Proteins were resolved on 12% polyacrylamide gel (cleaved-CASP3, HMGB1), and 6% polyacrylamide gels (PARP, cleaved-PARP and PTK7). Migration was applied at 80 V until a clear migration front was formed, increased to 100 V, then proteins were transferred on a PVDF western blotting membrane for 1h at 100V. All membranes were blocked with a 5% dry milk in TBST (TBS with 0.1% Tween20) for 1h under stirring, then incubated with respective antibodies at 4°C overnight. After 3 washes of 5 minutes, membranes were incubated with secondary antibody anti-Rabbit IgG HRP conjugated (Cell Signalling, 7074S) for 1h at room temperature (RT), before undergoing three more 5-minute washes. The Ag-Ab interactions were revealed using HRP-based chemiluminescence with SuperSignal™ West Pico PLUS Chemiluminescent Substrate (Thermo Scientific, 34577) or SuperSignal™ West Femto Maximum Sensitivity Substrate (Thermo Scientific, 34096) kits and the chemiluminescent blots were imaged with the Amersham ImageQuant 800 (Cytiva). For all proteins, β-actin is used as a normalizing control, revealed with the Pierce® ECL Western Blotting Substrate kit.

All Antibodies used for immunoblotting are summarised in ***Table 2***.

3. Flow Cytometry analysis

Expression of PTK7 and GFP, as well as cell death assessment by Annexin V and DAPI staining were analysed by flow cytometry. Neurospheres (T033 scr, T033 PTK7 KO, m005) were dissociated into single cells using Accutase at 37°C for approximately 10 minutes, washed with PBS and centrifuged at 300g for 3 minutes. Adherent cells (U87 WT, U87 PTK7 OE) were dissociated using Trypsin-EDTA, neutralised with DMEM-High Glucose medium, and subsequently processed under the same centrifugation conditions. Cell counting was carried out using Countess II FL (Life Technologies), and the average viability was 90%. Calculation of the required AAV volumes were performed using the same logic as described in section 2.1.

3.1. PTK7 membrane expression in m005 cells

After dissociation of neurospheres, 100,000 cells were seeded in 1 mL of NPC medium, followed by incubation for 72h. Afterwards, m005 cells were transferred into Eppendorf tube, then centrifuged at 4,000 rpm for 4 minutes. After removal of supernatant, cells were dissociated by Accutase for approximately 10 minutes at 37°C, then diluted in PBS and centrifuged in same conditions as previously. Respective conditions were incubated into primary antibody anti-PTK7 PE-Vio 770 1/100 (Miltenyi, 130-112-679) and Nb5 500 nM, at 4°C for 30 minutes. Cells were then rinsed with PBS, and respective conditions were incubated with secondary antibody anti-VHH APC conjugated 1/500 (Jackson ImmunoResearch, 128-605-232) at RT for 30 minutes. Finally, cells were centrifuged at 4°C and 300g for 5 minutes, rinsed with PBS, and resuspended in 200 µL of PBS for FACSCanto II analysis.

3.2. Annexin V/DAPI apoptosis assay in cells upon SGT *in vitro*

Then, cells were resuspended in 100 µL of Annexin V Binding Buffer 1x diluted in water (stock 10x, BioLegend, 422201). In respective conditions, we added DAPI 1/5000 (Invitrogen, D1306) as well as Annexin V FITC (SONY, 3804530) in T033 conditions, or Annexin V PE (BioLegend, 640908) in U87 conditions, and let incubate at 4°C for 15 minutes. Finally, cells were rinsed with PBS, centrifuged and resuspended in 300 µL of PBS for FACS CytoFlex (V-B-R laser line) analysis.

3.3. Co-culture assays

After dissociation, 100,000 cells were seeded in 1 mL of NPC medium, including 50,000 cells of each type for co-culture condition, adequate volume of AAV2-GFP, AAV-Nb5-GFP and AAV-Nb5-TK were added in respective conditions, then followed by incubation at 37°C for 72h. After steps of dissociation and incubation with respective antibodies, analyses were performed on FACS CytoFlex (V-B-R laser line).

Evaluation of PTK7 expression and AAV-Nb5 specific binding upon co-culture

Respective conditions were incubated into primary antibody anti-PTK7 PE-Vio 770 1/100 (Miltenyi, 130-112-679), at 4°C for 30 minutes. Finally, cells were rinsed with PBS, centrifuged and resuspended in 300 µL of PBS.

Evaluation of viability for assessment of the "bystander effect"

After 3 days of incubation with respective AAVs, 15 µg/mL of GCV were added and the plate was re-placed in the incubator for 48h more. After dissociation steps, cells were incubated with respective antibodies anti-PTK7 and Annexin V FITC diluted in Annexin V Binding Buffer 1x, at 4°C for 20 minutes. Then, cells were rinsed and resuspended in 250 µL of Annexin V Binding Buffer 1x.

All Antibodies used for flow cytometry are summarised in ***Table 3***.

4. Immunostainings

4.1. Brain tissue processing

Adult 6-week-old female nude mice (Crl:NU-Foxn1nu) (Charles River Laboratories, Brussels, Belgium) were housed in sterilised, filter-topped cages at the Animal Facility at the University of Liège, and all experiments were performed as previously approved by the Animal Ethical Committee of the University of Liège, in accordance with the Declaration of Helsinki and following the guidelines of the Belgium Ministry of Agriculture agreement with European Commission Laboratory Animal Care and Use Regulation. Briefly, U87 PTK7 OE cells (50,000 cells) resuspended in 2µL of PBS were transplanted in the right striatum of the mice, according to stereotaxic coordinates (+0.5mm A/P, -2mm M/L, 2.5mm D/V) under anaesthesia with 2.5% isoflurane gas (Isoflutek, Alivira). Two weeks later, 2µL of AAV-anti-PTK7-Nb-TK (1AAV:1PBS) was transplanted intratumorally, following the same coordinates as before. Three days after the AAV injection, mice received an intraperitoneal injection (IP) of GCV (75mg/kg/day) or PBS as control for 7 consecutive days. Health status was evaluated daily, and mice were weighed regularly.

4.2. Immunofluorescence on cryosections

Tissue cryosections obtained were first washed with PBS for 5 minutes. All the slides were then blocked with Normal Donkey Serum 10% (Jackson ImmunoResearch, 017-000-121) diluted in PBS-T 0.01% and incubated for 1h at RT. Afterwards, slides were incubated with the appropriate primary antibody at 4°C overnight. After 3 sessions of PBS washes for 5 minutes, slides were incubated with the secondary antibody conjugated to Rhodamine Red™-X (RRX) for 1h at RT. Following 3 more sessions of washing with PBS, all slides were co-stained with DAPI for 10 more minutes, then rinsed with water. After they were completely dry, slides were coverslipped using EZ-Mount (epredia). Images were acquired on Zeiss Imager Z1 microscope, using 5x and 10x objectives for PTK7 detection, and 20x objective for cleaved CASP-3 detection. All antibodies used for immunostaining are summarised in ***Table 4***.

5. Quantification and Statistical analysis

Concerning immunoblotting, quantification was performed with Fiji (ImageJ) program, which enabled background subtraction, to determine band intensity and to normalize data using β-actin control. All statistical analyses were performed using GraphPad Prism 8 and all data were displayed as mean +/- SEM. The error bars (SEM) shown for all results were derived from biological replicates. When comparing means between two groups, an unpaired t-test was applied, but when comparing means between more than two groups for a single variable, an ANOVA 1 was applied, with Tukey's multiple comparisons. Differences between values were considered statistically significant when p-value < 0.05. All experiments were performed at least three times unless otherwise stated.

Table 2. *Western blotting:* Antibodies

Antibody	Host	Firm	Reference	Dilution
Anti-Cleaved Caspase-3	Rabbit	Cell Signaling	9661S	1/1000
Anti-PARP	Rabbit	Cell Signaling	9542S	1/1000
Anti-PTK7	Rabbit	Atlas Antibodies AB	HPA003222	1/1000
Anti-HMGB1	Rabbit	Cell Signaling	3935S	1/1000
Anti-β-Actin, HRP-linked	Mouse mAb	Sigma	A3854	1/10 000
Anti-Rabbit IgG, HRP-linked	Goat	Cell Signaling	7074S	1/4000

Table 3. *Flow cytometry*: Antibodies and fluorescent molecules

Antibody	Conjugate	Host	Firm	Reference	Dilution
Anti-PTK7	PE-Vio770	Human	Miltenyi	130-112-679	1/100
Anti-Annexin V	FITC	/	SONY	3804530	1/20
Anti-Annexin V	PE	/	BioLegend	640908	1/20
DAPI	DAPI	/	Invitrogen	D1306	1/5000
Anti-VHH	APC	/	Jackson ImmunoResearch	128-605-232	1/500

Table 4. *Immunofluorescence*: Antibodies

Antibody	Conjugate	Host	Firm	Reference	Dilution
Anti-Cleaved Caspase-3	/	Rabbit	Cell Signaling	9661S	1/100
Anti-PTK7	/	Rabbit	Cell Signaling	25618	1/100
Anti-Rabbit	Rhodamine Red™-X (RRX)	Donkey	Jackson ImmunoResearch	711-296-152	1/500

Chapter 4 - Results

Presented by Sarah Grodent, as obtained from the laboratory work performed from September 2025 to February 2026

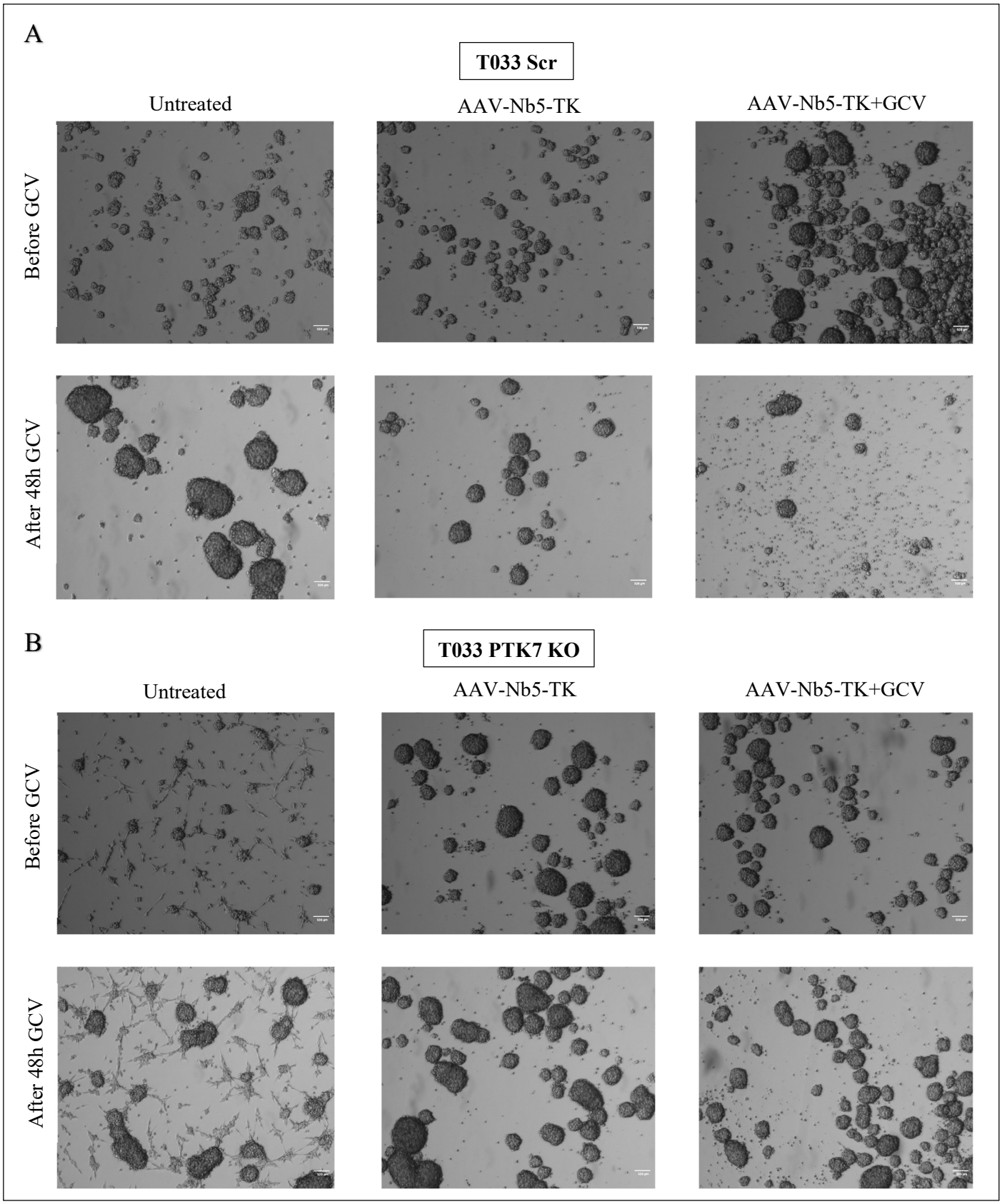
A
T033 Scr
Untreated
AAV-Nb5-TK
AAV-Nb5-TK+GCV
Before GCV
After 48h GCV
B
T033 PTK7 KO
Untreated
AAV-Nb5-TK
AAV-Nb5-TK+GCV
Before GCV
After 48h GCV

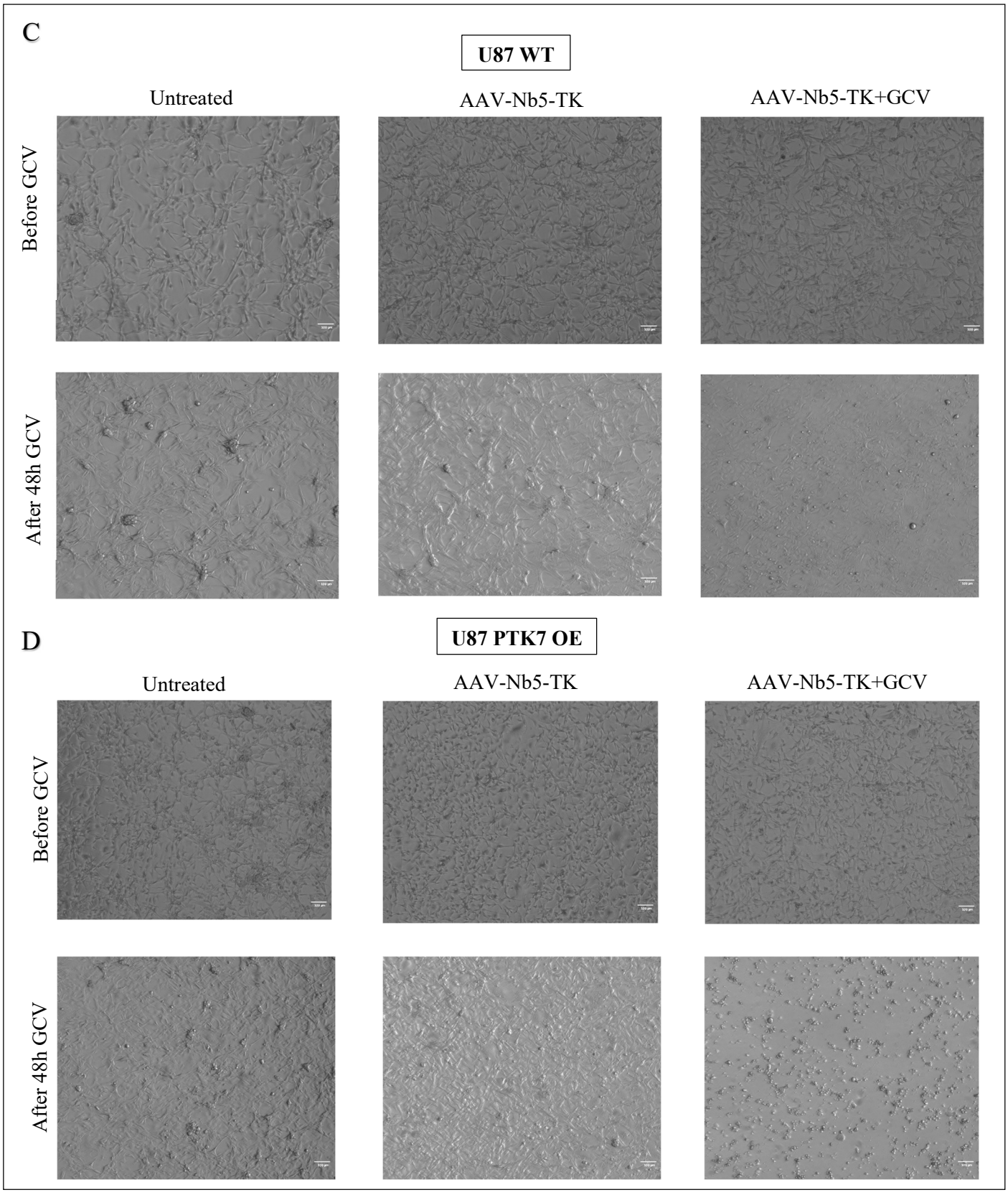

Figure 11. Visual evidence of PTK7-dependent cytotoxicity induced by the AAV-Nb5-TK in the presence of GCV. Genetically modified patient-derived GSCs (**A**) T033 Scr and (**B**) T033 PTK7 KO, and commercial GBM cell-lines (**C**) U87 WT and (**D**) U87 PTK7 OE after treatment with the AAV-Nb5-TK in the presence of GCV. Representative images illustrate specific cell death in PTK7 expressing cells, while PTK7-deficient cells remain largely unaffected. This effect is associated with marked morphological changes, including the dissociation of neurospheres into single cells in T033 Scr culture and the loss of adherence in U87 PTK7 OE culture.

1. Evaluation of SGT-induced cytotoxicity in GBM cells

Previous studies performed by the laboratory demonstrated that PTK7-targeted AAV-based SGT therapy (AAV-Nb5-TK + GCV) induces cell death in GBM cells. The first aim of this study was to further characterise cell death mechanisms induced by this SGT therapy. For this purpose, we analysed the expression of specific cell death-associated markers by western blot (WB), followed by a quantitative assessment of cell death using Annexin V/DAPI staining.

1.1. Characterisation of cell death marker expression

First, therapy-induced expression of several cell death markers was analysed by WB in two GBM models: patient-derived T033 cells and commercial U87 cells. To assess the effect of the treatment according to PTK7 status, $PTK7^+$ cells (T033 Scr and U87 PTK7 OE) were compared with $PTK7^-$ cells (T033 PTK7 KO and U87 WT), which served as negative controls for targeting specificity. Cells were submitted to three culture conditions: untreated, treated with AAV-Nb5-TK alone, or treated with the combined (AAV-Nb5-TK + GCV) therapy.

Alongside molecular analysis, the impact of the treatment on cell morphology was assessed by microscopy. T033 cells, cultured under 3D conditions, form neurospheres. In T033 Scr cells treated with the combined treatment, neurospheres appeared less compact, with increased dissociation and a high number of single cells (**Figure 11A**). Much less single cells were observed in the T033 PTK7 KO cells exposed to the same treatment (**Figure 11B**). Notably, T033 PTK7 KO cells displayed partial adherence under untreated conditions, whereas this adherence was reduced upon exposure to AAV-Nb5-TK, both in the presence and absence of subsequent GCV addition. U87 PTK7 OE cells, cultured under adherent 2D conditions, showed a marked loss of adhesion and an increase in the number of cells in suspension following the combined treatment (**Figure 11D**). Following the same trend as $PTK7^-$ cells in the 3D culture condition, U87 WT cells also exhibited morphological alterations, including partial reduced adhesion and altered cell protrusions in the presence of the combined treatment (**Figure 11C**).

The expression of cleaved caspase-3 (CASP-3) was investigated as a marker of apoptosis activation. A signal corresponding to this protein was detected at approximately 15 kDa in $PTK7^+$ cells exposed to the combined treatment, in both T033 and U87 models. However, the two closely spaced signals corresponding to the cleaved subunits were more clearly resolved in the U87 cells. Notably, CASP-3 expression showed variability across biological replicates and was weak or undetectable depending on detection conditions (**Figure S1**). In contrast, this signal was absent in control conditions, including untreated cells, cells transduced with AAV-Nb5-TK alone, as well as $PTK7^-$ cells exposed to the combined treatment. This observation suggests that the expression of cleaved CASP-3 is associated with cells expressing PTK7 and exposed to all components of the therapy. The expression of the cell repair enzyme Poly(ADP-ribose) polymerase (PARP) was also assessed in its cleaved (inactive) and uncleaved

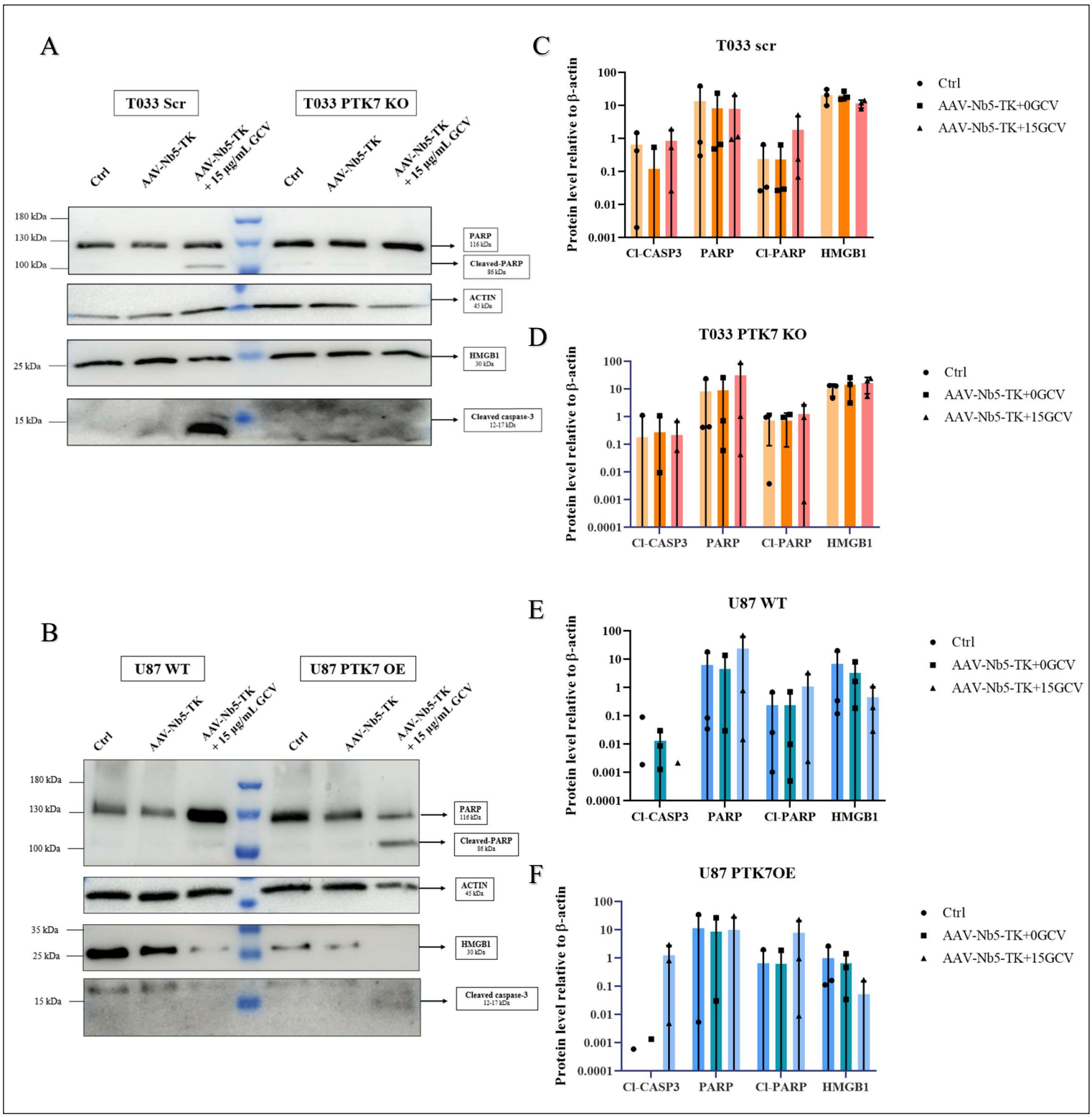

Figure 12. Immunoblot analysis of cell death-related proteins following the AAV-based SGT. Western blot analysis of cleaved-CASP-3, PARP and HMGB1, as cell death indicators in (**A**) T033 patient-derived cells and (**B**) U87 cells under different treatment conditions, including untreated, AAV-Nb5-TK alone, and combined AAV-Nb5-TK + GCV treatment. PTK7^{+} cells were compared with PTK7^{-} controls. Cleaved CASP-3 and PARP cleavage were predominantly detected in PTK7^{+} cells exposed to the combined treatment. (**C-F**) Corresponding quantifications of protein levels normalised to β-actin are shown.

(active) forms. In PTK7$^+$ cells treated with the combined treatment, a signal corresponding to the cleaved PARP was detected, while the uncleaved form was observed at similar levels across all conditions. These observations are consistent with activation of a cell death process (**Figures 12A-B**). The expression of the nuclear High mobility group box 1 (HMGB1) protein was also analysed as additional indicator of cell death. Depending on biological replicates and treatment conditions, variations in signal intensity were observed under certain treatment conditions, although it was not statistically significant after normalization to β-actin. These results should therefore be interpreted with caution.

WB signals were subsequently quantified after background correction and normalisation to β-actin. This quantification did not reveal any statistically significant differences between the conditions analysed in PTK7$^+$ cells (**Figures 12C, 12F**) or PTK7$^-$ cells (**Figures 12D-E**) due to high signal variability between experiments. However, a trend towards increased levels of cleaved CASP-3 and cleaved PARP was observed in PTK7$^+$ cells treated with SGT.

1.2. Quantitative analysis of cell death using Annexin V/DAPI staining

To further characterise therapy-induced cell death, we performed a quantitative analysis using Annexin V/DAPI staining in the same experimental conditions as previously described. For clarity, comparisons were made between T033 Scr and T033 PTK7 KO, and between U87 PTK7 OE and U87 WT cells (PTK7$^+$ vs PTK7$^-$). Representative images were acquired before and after adding GCV (at 24 and 48 hours), demonstrating morphological changes consistent with those described before. This approach allowed us to discriminate between living cells (Annexin V$^-$/DAPI$^-$), early apoptotic cells (Annexin V$^+$/DAPI$^-$), late apoptotic cells (Annexin V$^+$/DAPI$^+$), and necrotic or dead cells (Annexin V$^-$/DAPI$^+$). The flow cytometry plots shown (**Figures 13A-B**) are representative of a single biological replicate, while the quantifications (**Figures 13C-D**) combine the data of three independent experiments. Detailed quantifications for each cell population are provided in the appendix (**Figure S2**).

Under untreated conditions, comparable proportions of living cells were found between PTK7$^+$ and PTK7$^-$ cells, in both T033 (72.77% in Scr vs 83.96% in KO) and U87 (84.67% in OE vs 81.77% in WT) models, indicating a similar baseline viability between the cell lines. Notably, a higher proportion of late apoptosis cells were detected in T033 Scr cells compared to T033 PTK7 KO cells. Following treatment with combined therapy, a significant reduction in the proportion of living cells occurred in PTK7$^+$ cells compared to PTK7$^-$ cells (T033: 28.04% in Scr vs 63.97% in KO, $p = 0.0440$; U87: 35.43% in OE vs 70.03% in WT, $p = 0.0088$). This decrease in viability was accompanied by an increase in apoptotic populations. In T033 cells, a significant increase in the number of late apoptosis cells was observed in PTK7$^+$ cells (27.48% in Scr vs 7.63% in KO, $p = 0.0015$). In contrast, early apoptosis populations remained relatively similar between the two cellular conditions, with no statistically significant difference (15.57% in Scr vs 22.33% in KO, $p > 0.05$). In U87 cells, the combined treatment led to a

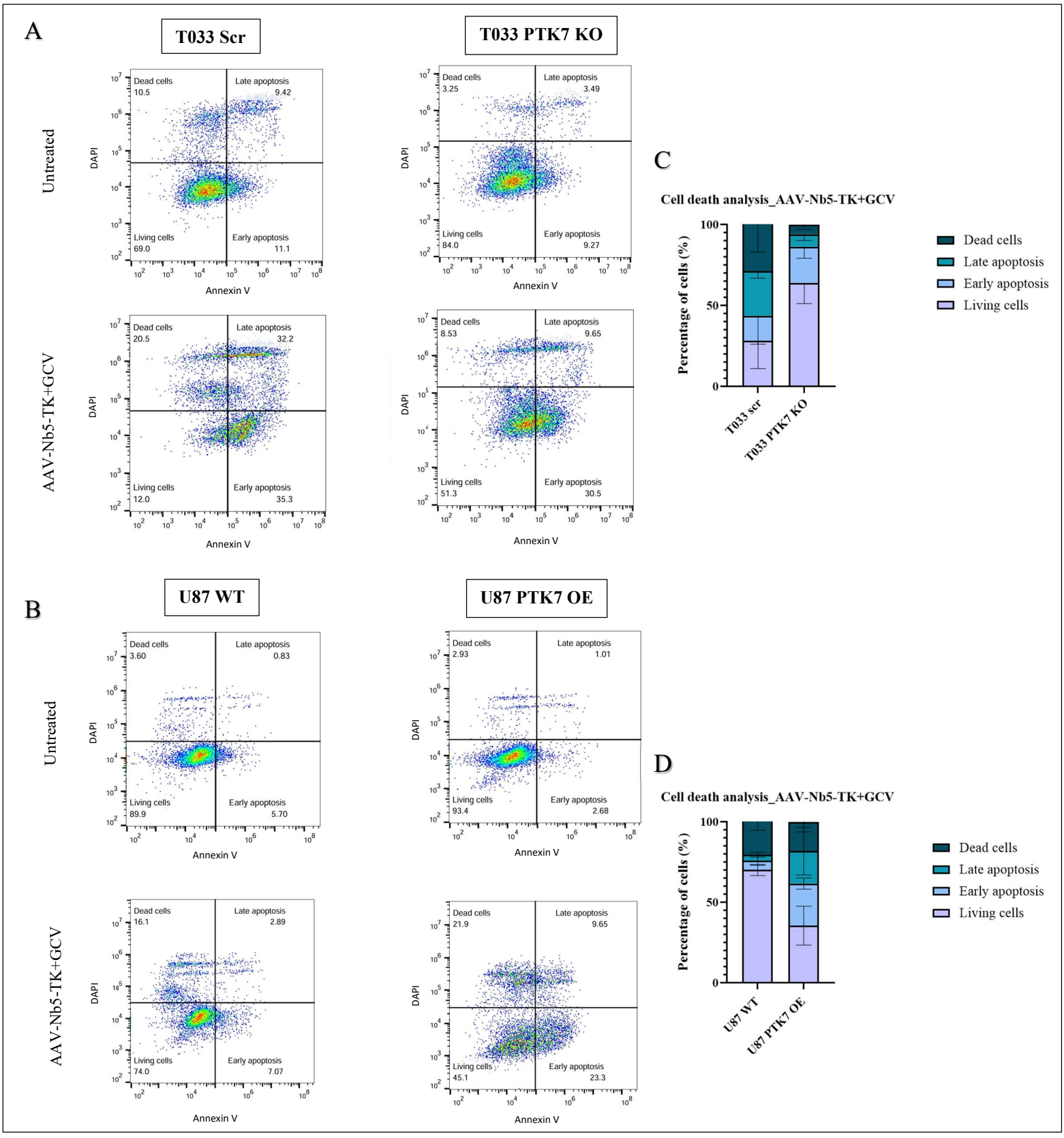

Figure 13. Quantification of cell death by Annexin V/DAPI staining following AAV-based SGT. Representative flow cytometry plots of Annexin V and DAPI staining in (**A**) T033 and (**B**) U87 cells under untreated conditions and following combined treatment. (**C-D**) Quantification of living (Annexin V^-/$DAPI^-$), early apoptotic (Annexin V^+/$DAPI^-$), late apoptotic (Annexin V^+/$DAPI^+$) and necrotic/dead (Annexin V^-/$DAPI^+$) cell populations.

significant increase in early apoptotic cells compared to PTK7$^-$ cells (26.17% in OE vs 5.84% in WT) (**Figure 13D**), as well as an increase in late apoptotic cells, although it was not statistically significant (3.98% in OE vs 2.41% in WT, $p > 0.05$). An increase in the number of dead cells was also observed in PTK7$^+$ cells, particularly in T033 cells (28.93% in Scr vs 6.05% in KO, $p = 0.0833$) despite not being statistically significant. Although the overall trend remained consistent across replicates, inter-experimental variability was observed. These preliminary results indicate that the combined treatment preferentially induces cell death in PTK7$^+$ cells, primarily through apoptotic mechanisms.

2. Evaluation of therapeutic specificity in PTK7$^+$/PTK7$^-$ co-culture

2.1. Evaluation of PTK7 expression and AAV-Nb5 specific binding

To evaluate the specificity of AAV-Nb5-mediated targeting under monoculture and co-culture conditions of PTK7$^+$ and PTK7$^-$ cells, PTK7 expression and the vector suitability for targeted transduction were first studied. This step allowed reliable discrimination of cell populations based on their PTK7 status and enabled assessment of whether AAV-Nb5 mediated transduction is specific to PTK7$^+$ cells or not.

First, PTK7 expression was assessed in monocultures of T033 Scr and T033 PTK7 KO cells. PTK7 expression was maintained in T033 Scr cells under all treatment conditions (**Figure 14A**), whereas T033 PTK7 KO cells showed no detectable signal compared to the unstained control (**Figure 14C**), confirming their respective PTK7$^+$ and PTK7$^-$ status. These results indicate that PTK7 expression can be used as a reliable marker to distinguish between PTK7$^+$ and PTK7$^-$ populations in subsequent co-culture experiments.

Next, transduction efficiency was evaluated using AAV-Nb5-GFP and AAV2-GFP, the latter serving as a non-targeted transduction control. The corresponding GFP fluorescence profiles are shown (**Figures 14B, 14D**). Following transduction with AAV-Nb5-GFP, T033 Scr cell population exhibited a significantly higher proportion of GFP$^+$ cells compared to T033 PTK7 KO cells (71.4% vs 26.3%, $p=0.012$) (**Figure 14E**). A difference between the two cell populations was also observed in terms of GFP fluorescence intensity, with a significantly higher mean fluorescent intensity (MFI) in T033 Scr cells compared to T033 PTK7 KO (468,137 vs 1449, $p = 0.0001$). Although a fraction of T033 PTK7 KO cells was classified as GFP$^+$, the MFI measured in this population remained very low compared to that observed in T033 Scr cells (**Figure 14F**). Concurrently, AAV2-GFP transduction resulted in comparable proportions of GFP$^+$ cells between T033 Scr and T033 PTK7 KO cells (48.9% vs 35%, $p > 0.05$), with no statistically significant difference (**Figure 14G**). Similarly, GFP MFI values remained of the same order of magnitude between the two cell populations (93,000 vs 63,790, $p > 0.05$) (**Figure 14H**). However, preferential targeting of AAV2-GFP towards T033 Scr cells was still observed. Overall, these results show that AAV-Nb5-GFP transduction differs between PTK7$^+$ and PTK7$^-$ cells, whereas AAV2-GFP transduction appears comparable between the two populations.

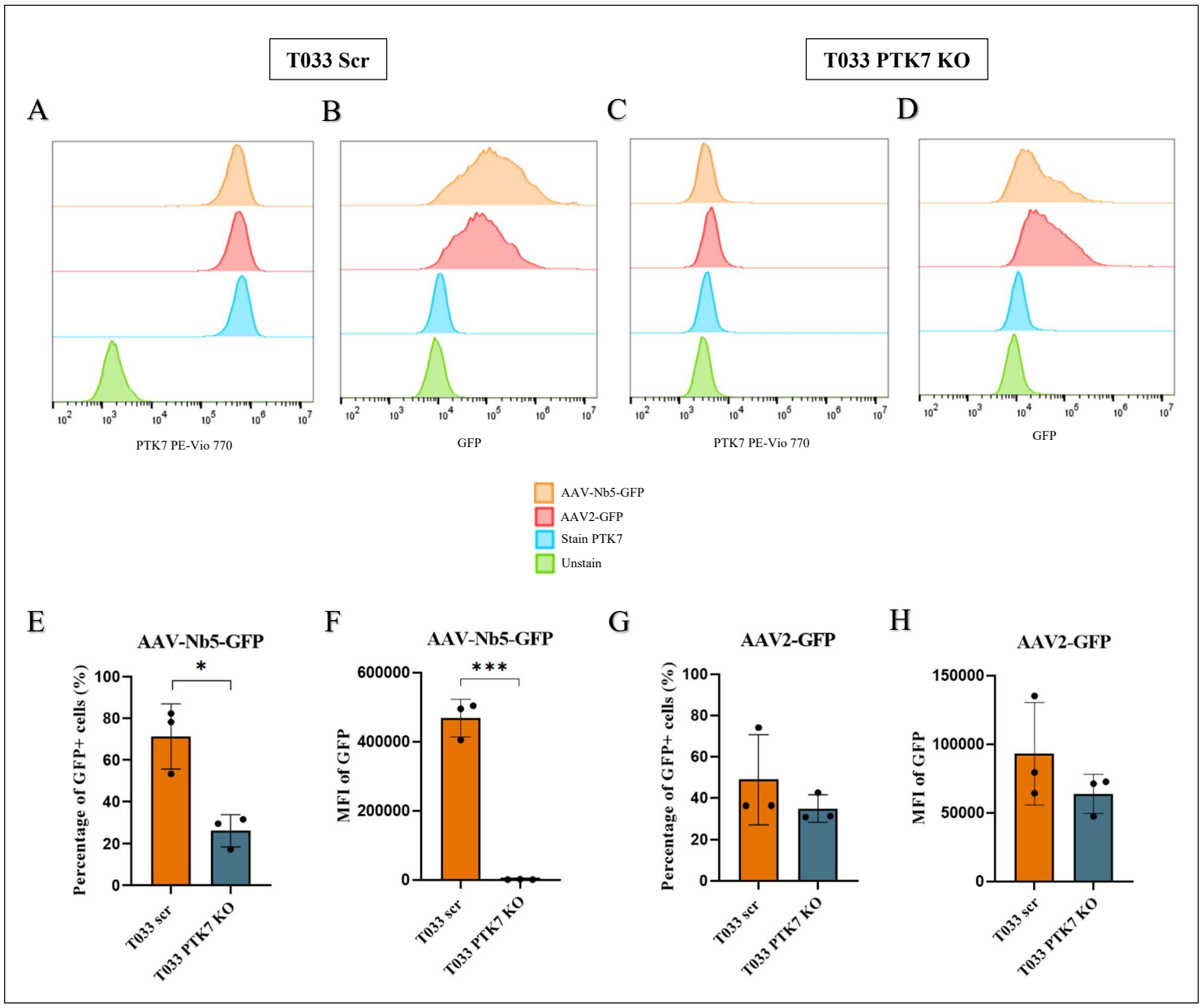

Figure 14. Assessment of PTK7 expression and AAV-Nb5 binding in a GBM monoculture model. Representative flow cytometry histograms showing PTK7 and GFP expression in (**A-B**) T033 Scr and (**C-D**) T033 PTK7 KO cells under different treatment conditions, including unstained control, PTK7 staining, AAV-Nb5-GFP and AAV2-GFP transduction. Quantification of (**E**) the percentage of GFP^+ cells and (**F**) mean fluorescent intensity (MFI) following AAV-Nb5-GFP transduction, showing higher values in T033 Scr compared to T033 PTK7 KO cells. Quantification of (**G**) the percentage of GFP^+ cells and (**H**) MFI following AAV2-GFP transduction, showing comparable values between both cell populations.

Under co-culture conditions, flow cytometry analysis of the PTK7 signal revealed three distinct cell populations: a $PTK7^+$ population, a $PTK7^-$ population, and a population exhibiting an intermediate level of fluorescence and thus an intermediate level of PTK7 expression, referred to as PTK7 intermediate. This distribution was visible in the histogram, which displayed a positive peak and a negative peak broadened towards higher fluorescence intensities (**Figure 15A**). Analysis using a dot plot representing cell size (FSC-A) as a function of PTK7 fluorescence intensity further allowed visualisation of the distribution of cells across these three subpopulations (**Figure 15B**). The overall cell distribution showed a majority of $PTK7^+$ cells (50.43%), followed by $PTK7^-$ cells (27.9%) and PTK7 intermediate cells (20.7%), notably with variability between replicates, including an enrichment in $PTK7^+$ cells in one replicate (**Figure 15C**). The presence of an intermediate PTK7 population, together with the broadening of the negative peak towards higher fluorescence intensities, indicates a continuum of PTK7 expression levels between the clearly negative and positive populations.

Following transduction with AAV-Nb5-GFP, the proportion of GFP^+ cells differed according to PTK7 status, with higher values in $PTK7^+$ cells compared to $PTK7^-$ cells (73.9% vs 26.3%, $p = 0.0181$), whereas the PTK7 intermediate population displayed an intermediate proportion of GFP^+ cells (45.4%), with no statistically significant difference compared to the other groups (**Figure 15D**). A similar distribution was observed for GFP fluorescence intensity, with higher MFI values in $PTK7^+$ cells, intermediate values in the PTK7 intermediate cells, and lower values in the $PTK7^-$ cells (327,882 vs 160,996 vs 72,650). Statistically significant differences were observed between $PTK7^+$ and $PTK7^-$ cells ($p = 0.005$), as well as between $PTK7^+$ and PTK7 intermediate cells ($p = 0.0341$), while no significant difference was observed between $PTK7^-$ and PTK7 intermediate cells (**Figure 15E**).

In contrast, AAV2-GFP transduction resulted in comparable proportions of GFP^+ cells across the three subpopulations, with no statistically significant differences (51.4% vs 36.9% vs 26.3%, $p > 0.05$) (**Figure 15F**). Similarly, GFP MFI values remained within the same order of magnitude between the populations, following a comparable distribution (206,894 vs 131,532 vs 90,449, $p > 0.05$) (**Figure 15G**).

Overall, both the proportion of GFP^+ cells and MFI values observed in co-culture thus followed a gradient consistent with the level of PTK7 expression, in agreement with observations made under monoculture conditions.

2.2. Evaluation of viability for assessment of the “bystander effect”

Previously, Annexin V/DAPI staining analysis showed that, following combined treatment, $PTK7^+$ cells exhibited a higher proportion of apoptotic cells than $PTK7^-$ cells. Notably, in the T033 model, a significant increase in late apoptotic cells was observed. In parallel, transduction experiments demonstrated preferential targeting of $PTK7^+$ cells by AAV-Nb5 in both monoculture and co-culture conditions. Based on these findings, we sought to evaluate the impact of the combined treatment on cell

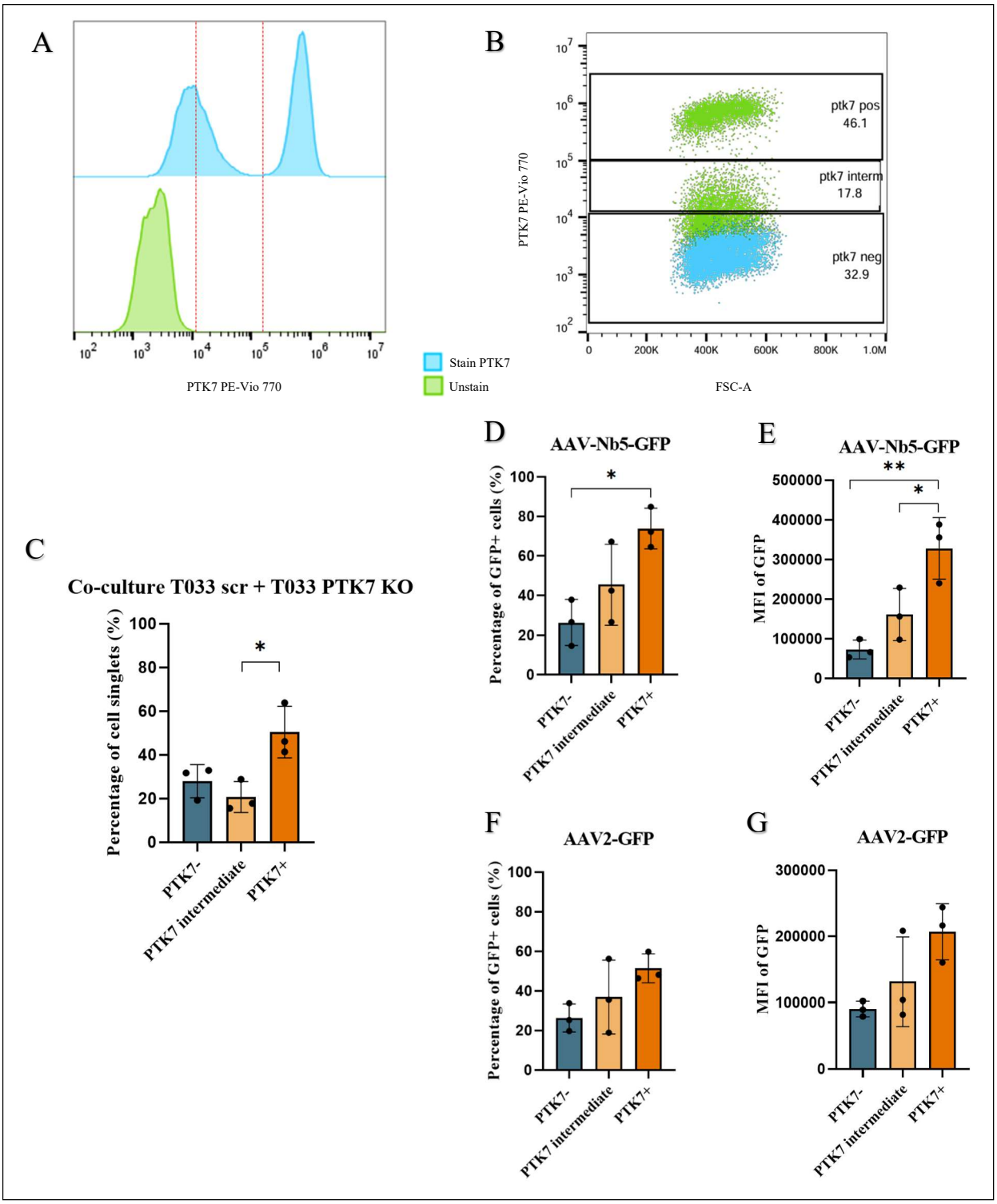

Figure 15. Assessment of PTK7 expression and AAV-Nb5 binding in a GBM co-culture model. Representative (**A**) flow cytometry histogram and (**B**) dot plot, showing PTK7 expression gradient, which allow to distinguish between PTK7^{+}, PTK7 intermediate and PTK7^{-} cell populations. (**C**) Distribution of cell populations according to PTK7 expression in co-culture conditions. PTK7^{+} cells represent most of the population. Quantification of (**D**) the percentage of GFP^{+} cells and (**E**) mean fluorescent intensity (MFI) following AAV-Nb5-GFP transduction, showing higher values in PTK7^{+} cells compared to other subpopulations. Quantification of (**F**) the percentage of GFP^{+} cells and (**G**) MFI following AAV2-GFP transduction, showing comparable values between the three cell subpopulations.

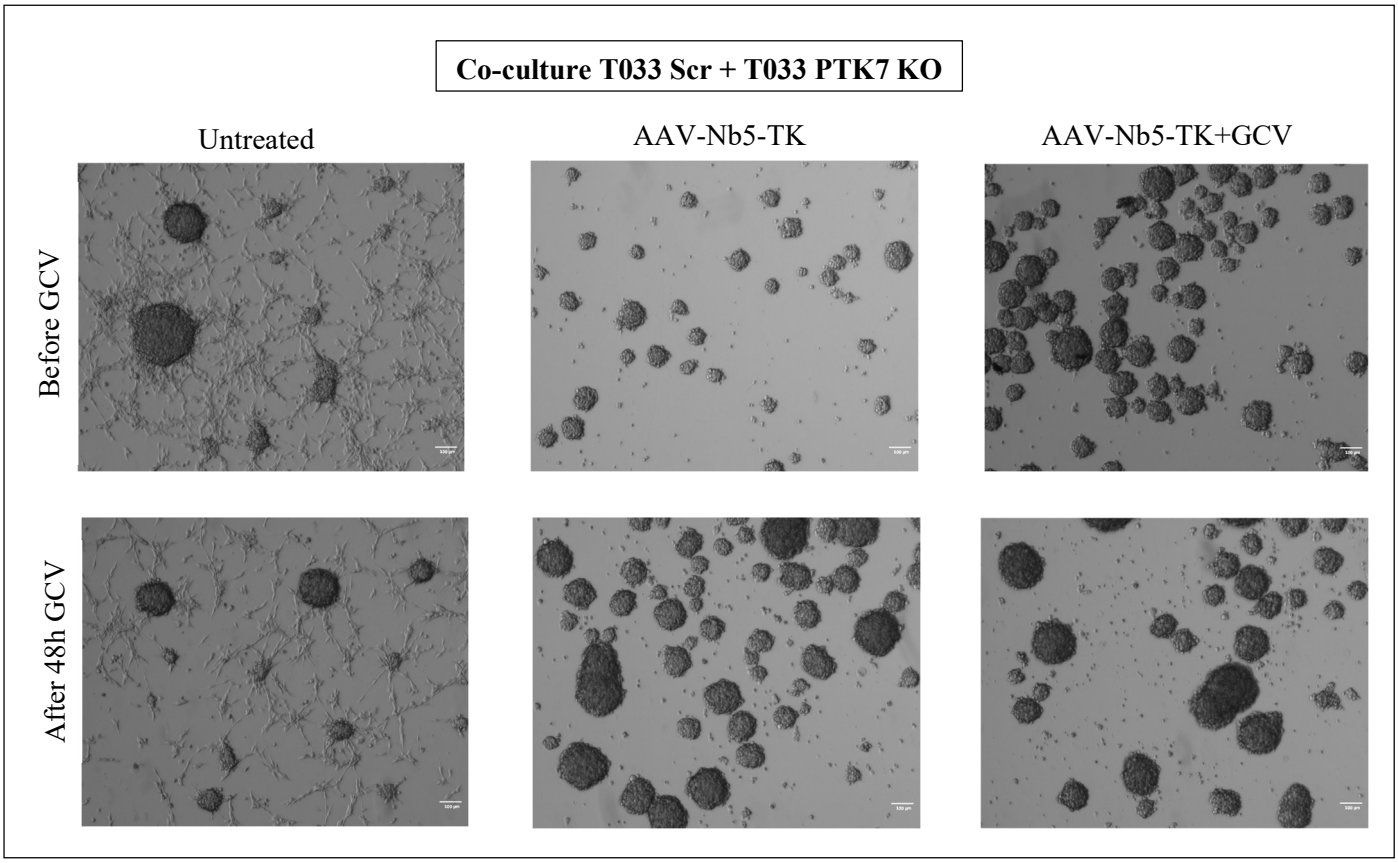

Figure 16. Morphological evidence of PTK7-dependent cytotoxicity induced by the AAV-based SGT in a GBM cells co-culture. Representative microscopy images of T033 cells co-culture following treatment with combined therapy AAV-Nb5-TK + GCV. Images illustrate morphological alterations including increased dissociation into single cells and some neurospheres which appear denser and darker, with reduced visibility of individual cell boundaries, suggesting alterations in structural organisation.

viability under monoculture and co-culture conditions using Annexin V staining alone. As this experiment was performed only once, results are presented descriptively without statistical analysis.

Under monoculture conditions, the morphological effects of the treatment were consistent with previous observations and are therefore not shown. However, to illustrate treatment effects in co-culture, microscopy images were acquired. These images revealed morphological alterations, including increased cell dissociation, and changes in neurospheres appearance, with structures appearing denser and darker, and showing reduced visibility of individual cell contours (**Figure 16**).

First, PTK7 expression was reassessed to confirm the specificity of the observed cell death. As expected, T033 Scr cells remained PTK7$^+$, whereas T033 PTK7 KO cells remained PTK7$^-$ (**Figures 17A, 17C**). Under combined treatment, a slight dispersion of the populations was observed, with a broadening of the fluorescence peak towards lower intensities in T033 Scr cells and towards higher intensities in T033 PTK7 KO cells. Analysis of Annexin V labelling revealed a progressive increase in the proportion of Annexin V$^+$ cells in T033 Scr cells across treatment conditions (**Figure 17B**). In untreated conditions, 42.8% of cells were Annexin V$^+$. This proportion increased to 55.1% following treatment with AAV-Nb5-TK alone and reached 73.8% after combined treatment. In contrast, T033 PTK7 KO cells showed a more moderate increase in the proportion of Annexin V$^+$ cells, rising from 21.1% in untreated condition to 29.2% after AAV-Nb5-TK treatment, and 32.8% after combined therapy (**Figure 17D**).

Under untreated conditions, T033 Scr and T033 PTK7 KO cells already displayed distinct levels of Annexin V staining, with 42.8% and 21.1% of Annexin V$^+$ cells, respectively (**Figure 17E**). Consistently, Annexin V MFI was higher in T033 Scr cells compared with T033 PTK7 KO cells (7,057 vs 5,459) (**Figure 17F**). Quantification of the percentage of Annexin V$^+$ cells following AAV-Nb5-TK treatment alone confirmed a higher proportion in T033 Scr cells compared to T033 PTK7 KO cells (**Figure 17G**), along with increased fluorescence intensity (**Figure 17H**). After combined treatment, this difference became more pronounced, with a higher proportion of Annexin V$^+$ cells in T033 Scr compared to T033 PTK7 KO (73.8% vs 32.8%) (**Figure 17I**). Annexin V fluorescence intensity followed a similar pattern, with a marked increase in MFI in T033 Scr cells between treated and untreated conditions (26,638 vs 7,057), while remaining relatively stable in T033 PTK7 KO cells (4,959 vs 5,459) (**Figure 17J**).

Under coculture conditions, flow cytometry analysis revealed an overall balanced distribution between PTK7$^+$ and PTK7$^-$ populations (46.3% vs 47.2%), while a small proportion of PTK7 intermediate cells remained detectable (5.49%). This distribution was visible both on the PTK7 fluorescence histogram (**Figure 18A**) and on the dot plot representing cellular distribution according to PTK7 status in co-culture (**Figure 18B**). Quantification of the different cell subpopulations confirmed this distribution, with neither of the two main populations predominating over the other (**Figure 18C**). Due to its low representation, PTK7 intermediate population was not included in the main analysis. Indeed, with a

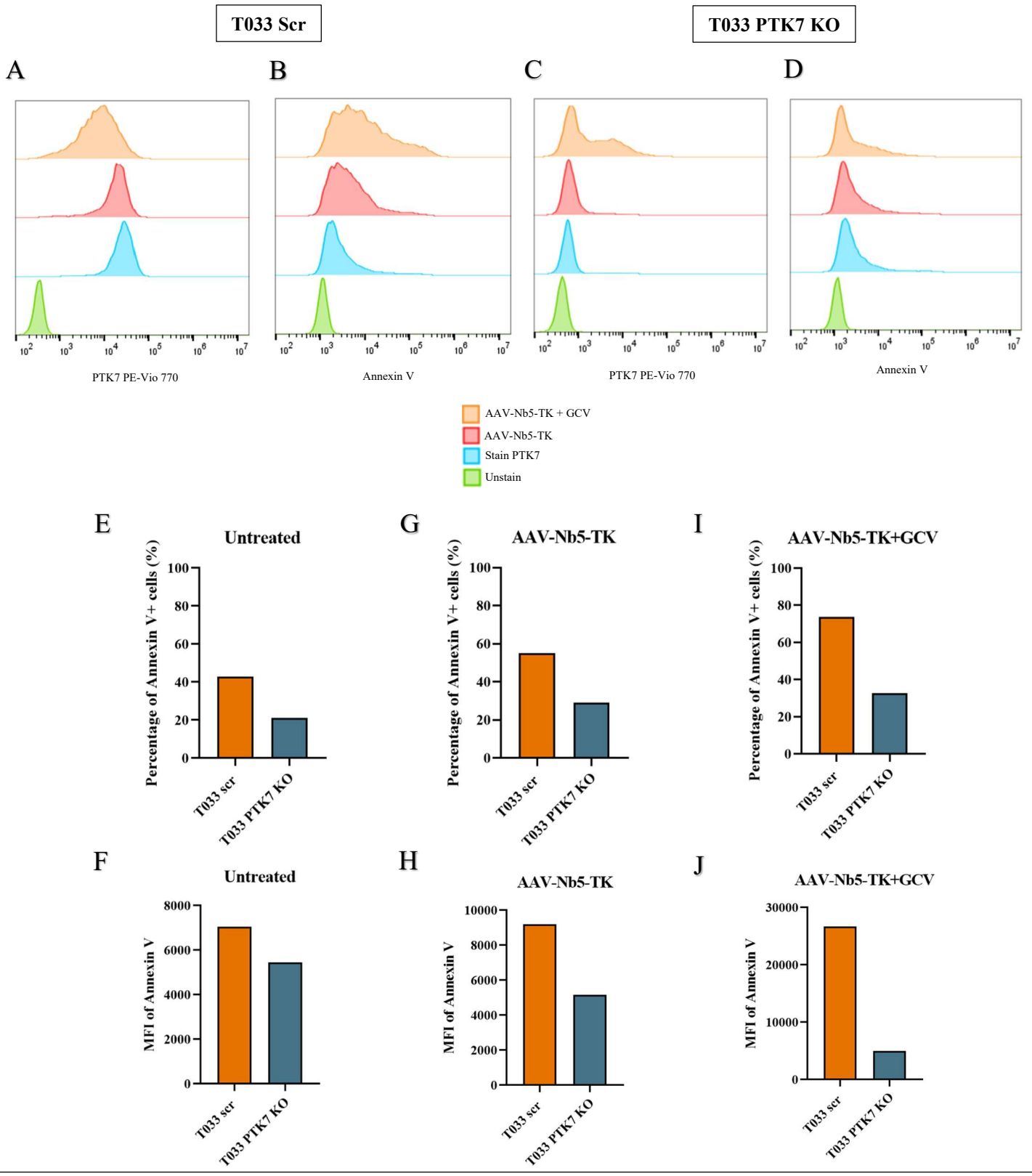

Figure 17. Assessment of AAV-Nb5-TK and GCV-induced cytotoxicity in a GBM monoculture. Representative flow cytometry histograms of PTK7 and Annexin V expression in (**A-B**) T033 Scr and (**C-D**) T033 PTK7 KO cells across unstained control, untreated PTK7 staining, AAV-Nb5-TK, and AAV-Nb5-TK+GCV. Under untreated condition, T033 Scr displayed higher levels of (**E**) Annexin V+ cells and of (**F**) fluorescence intensity. Quantification of (**G**) the percentage of Annexin V^+ cells and (**H**) mean fluorescent intensity (MFI) following AAV-Nb5-TK transduction, showing moderate difference of values between T033 Scr and T033 PTK7 KO cells. Quantification of (**I**) the percentage of Annexin V^+ cells and (**J**) MFI following AAV-Nb5-TK+GCV treatment, showing higher values in T033 Scr cells. Results are shown from a single biological replicate.

limited number of cellular events, only a few positive events are generated to cause proportionally significant variations in the percentage of Annexin V^+ cells and MFI. This may artificially increase the apparent contribution of this subpopulation to the analysis and complicate comparisons between populations. Results including the PTK7 intermediate population are therefore presented in the appendix (**Figure S3**).

Under untreated conditions, comparable proportions of Annexin V^+ cells were observed between $PTK7^+$ and PTK7- populations (16.4% vs 15.4%) (**Figure 18D**). In contrast, Annexin V fluorescence intensity appeared higher in $PTK7^+$ cells than in $PTK7^-$ cells (23,117 vs. 4,521). Following treatment with AAV-NB5-TK alone, a moderate increase in the proportion of Annexin V^+ cells was shown in both cell populations, reaching 30.2% in $PTK7^+$ cells and 22.5% in $PTK7^-$ cells, respectively (**Figure 18F**). However, Annexin V fluorescence intensity remains broadly comparable to untreated conditions in both populations, with MFI values of 21,530 and 4,295 in $PTK7^+$ and $PTK7^-$ cells (**Figure 18G**). Under combined treatment, a markedly greater divergence between the two populations was observed. While the proportion of Annexin V^+ cells in $PTK7^-$ cells remained relatively limited (28%), accompanied by only a slight increase in MFI (5,721), $PTK7^+$cells exhibited a pronounced increase in Annexin V^+ cells, reaching 83.6%. Consistent with this trend, Annexin V fluorescence intensity also increased substantially in $PTK7^+$ cells, with an MFI reaching 39,829 (**Figures 18H-I**).

Overall, these observations support preferential induction of treatment-associated cell death in $PTK7^+$ cells under co-culture conditions.

3. Validation of AAV-based SGT efficacy in xenograft tissues

In vitro results demonstrated that AAV-Nb5-TK targeting appear to preferentially target $PTK7^+$ cells and that the administration of the combined treatment was associated with a significant increase in Annexin V staining in these cells. These observations suggest a preferential induction of cell death in PTK7 expressing cells. To assess whether this association between PTK7 expression and therapy-induced cell death can also be observed in a more complex setting, immunostaining analyses were performed on brain sections from nude mice previously grafted with U87 PTK7 OE cells. Two weeks after intracerebral tumour graft, all mice received an injection of AAV-Nb5-TK. After three days, each mouse received an IP injection of GCV or PBS (control) for seven consecutive days, followed by euthanasia and brain collection for histological analysis. Coronal cryosections were then prepared and subjected to anti-PTK7 and anti-cleaved CASP-3 immunostainings. Analyses were performed on sections from the same four mice, including two mice that received the combined treatment regimen and two control mice that received PBS injections. Controls without primary antibody were also performed to verify the specificity of the staining. Anti-PTK7 staining revealed apparent differences between treatment conditions (**Figure 19A**). In tissues from control-treated mice (AAV-Nb5-TK + PBS), large $PTK7^+$ tumour regions were observed, characterised by dense and relatively homogeneous staining. DAPI

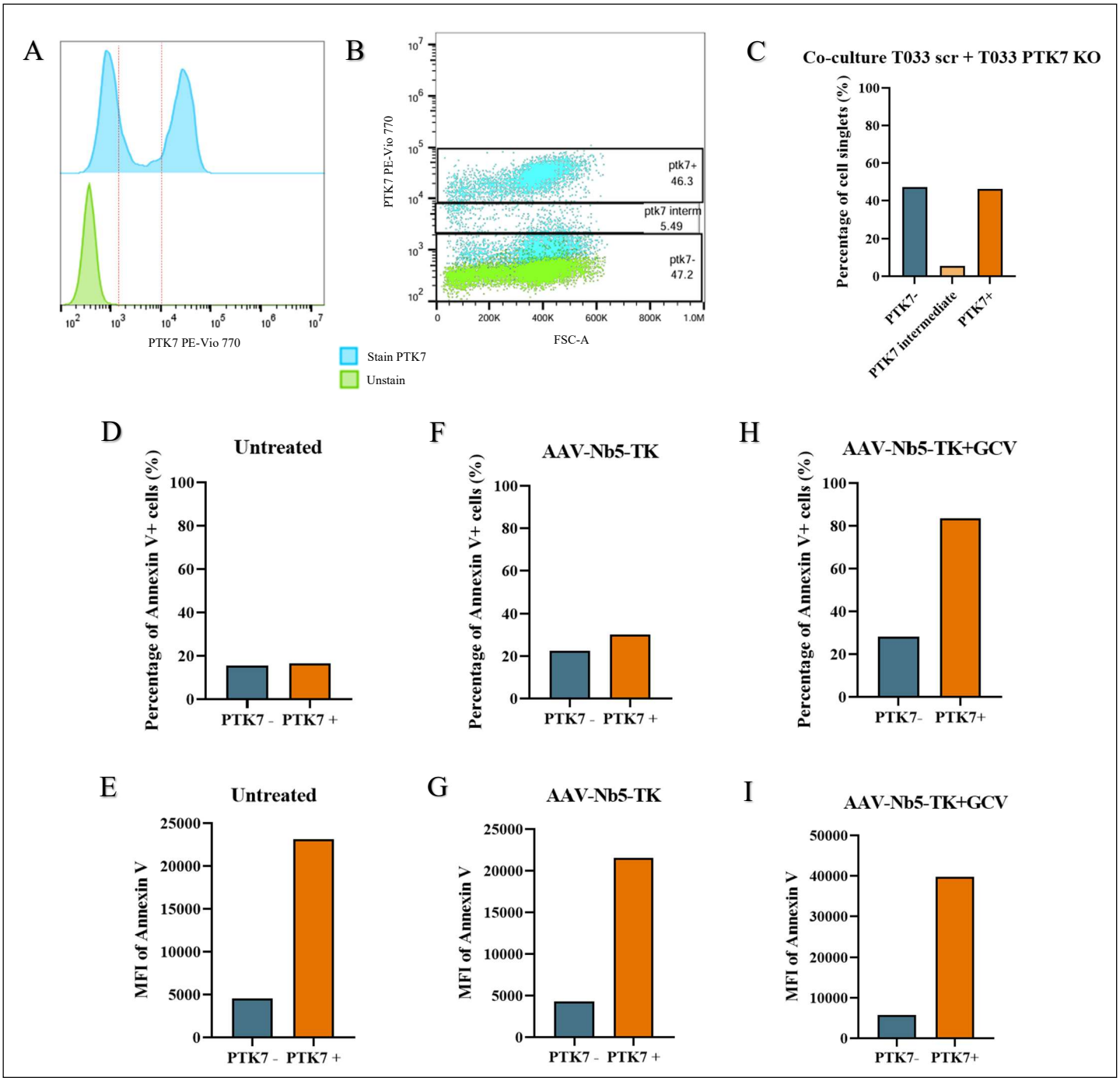

Figure 18. Assessment of AAV-Nb5-TK and GCV-induced cytotoxicity in a GBM co-culture. Representative (**A**) flow cytometry histogram and (**B**) dot plot illustrating PTK7 expression in co-culture condition, which allow to discriminate between PTK7^{+}, PTK7 intermediate and PTK7^{-} cell populations. (**C**) Distribution of cell populations according to PTK7 expression in co-culture conditions, showing similar proportions of PTK7^{+} and PTK7^{-} cells. Due to poor contribution of PTK7 intermediate population, subsequent analyses focused on the two major populations. Quantification of (**D**) the percentage of Annexin V^{+} cells and (**E**) MFI under untreated conditions, showing comparable proportions of Annexin V^{+} cells between PTK7^{+} and PTK7^{-} populations but higher fluorescence intensity in PTK7^{+} cells. Quantification of (**F**) the percentage of Annexin V^{+} cells and (**G**) MFI following AAV-Nb5-TK transduction, showing a moderate increase in Annexin V staining in both populations. Quantification of (**H**) the percentage of Annexin V^{+} cells and (**I**) MFI following AAV-Nb5-TK +GCV treatment, showing a marked increase in Annexin V staining preferentially in PTK7^{+} cells.

staining further revealed high tumour density associated with a compact tissue organisation, while tumour borders appeared relatively well-defined. In contrast, tissues from mice treated with the combined treatment (AAV-Nb5-TK + GCV) displayed more restricted $PTK7^+$ regions, associated with a visually less dense and more heterogeneous staining pattern. Tumour borders also appeared less defined, whereas DAPI staining suggested a looser cellular organisation, with nuclei appearing less densely packed. In both treatment conditions, PTK7 signal was predominantly detected surrounding the nuclei in merged images, consistent with the expected localisation of this transmembrane protein. No signal was observed in sections processed without primary Ab, while DAPI staining confirmed tissue preservation, supporting specific anti-PTK7 immunolabelling.

Anti-cleaved CASP-3 staining showed greater heterogeneity between mice and treatment conditions (**Figure 19B**). In tissues from mice treated with the combined treatment, staining remained relatively weak but reproducible between the two mice, appearing as scattered focal signals distributed throughout the tumour tissue and corresponding to localised areas enriched in cleaved CASP-3 positive cells. In contrast, significant inter-animal variability was observed in control-treated mice. While one mouse exhibited only sparse stained focal signal, the other displayed abundant cleaved CASP-3 signal exclusively concentrated within the tumour core. Across all conditions, DAPI staining revealed differences in tissue organisation consistent with those observed following anti-PTK7 staining. Thus, tissues from the combined treatment appeared globally less compact and composed of less densely packed nuclei compared to those from control-treated mice. Similarly, no signal was detected in sections processed without primary Ab.

4. Establishment and validation of a PTK7-expressing murine model for Nb5-VHH targeting

Although xenograft models established in immunodeficient Nude mice provide initial insights into the therapy efficacy, they do not allow for an assessment of its impact on the immune system. In this context, a complementary approach was initiated to develop an immunocompetent mouse model. Mouse GBM stem-like cells (005mGSCs), initially PTK7-negative, underwent lentiviral transduction to induce PTK7 expression. The expression of this protein, as well as the binding capacity of Nb5-VHH, was then validated in these transduced cells. This model, derived from tumours formed in immunocompetent C57BL/6 mice, serves as a model for future *in vivo* studies. Initially, PTK7 expression in the modified murine cells was assessed using Western blot (WB) and flow cytometry techniques, respectively. This assessment was performed in comparison with WT murine cells (m005 WT), used as a negative control, and T033 Scr cells, known to express PTK7 and used as a positive control. WB analysis revealed a 160kDa signal, corresponding to the expected molecular weight of PTK7, in the transduced cells (m005 PTK7 OE), as well as in patient-derived T033 Scr cells. These initial observations appear to confirm the

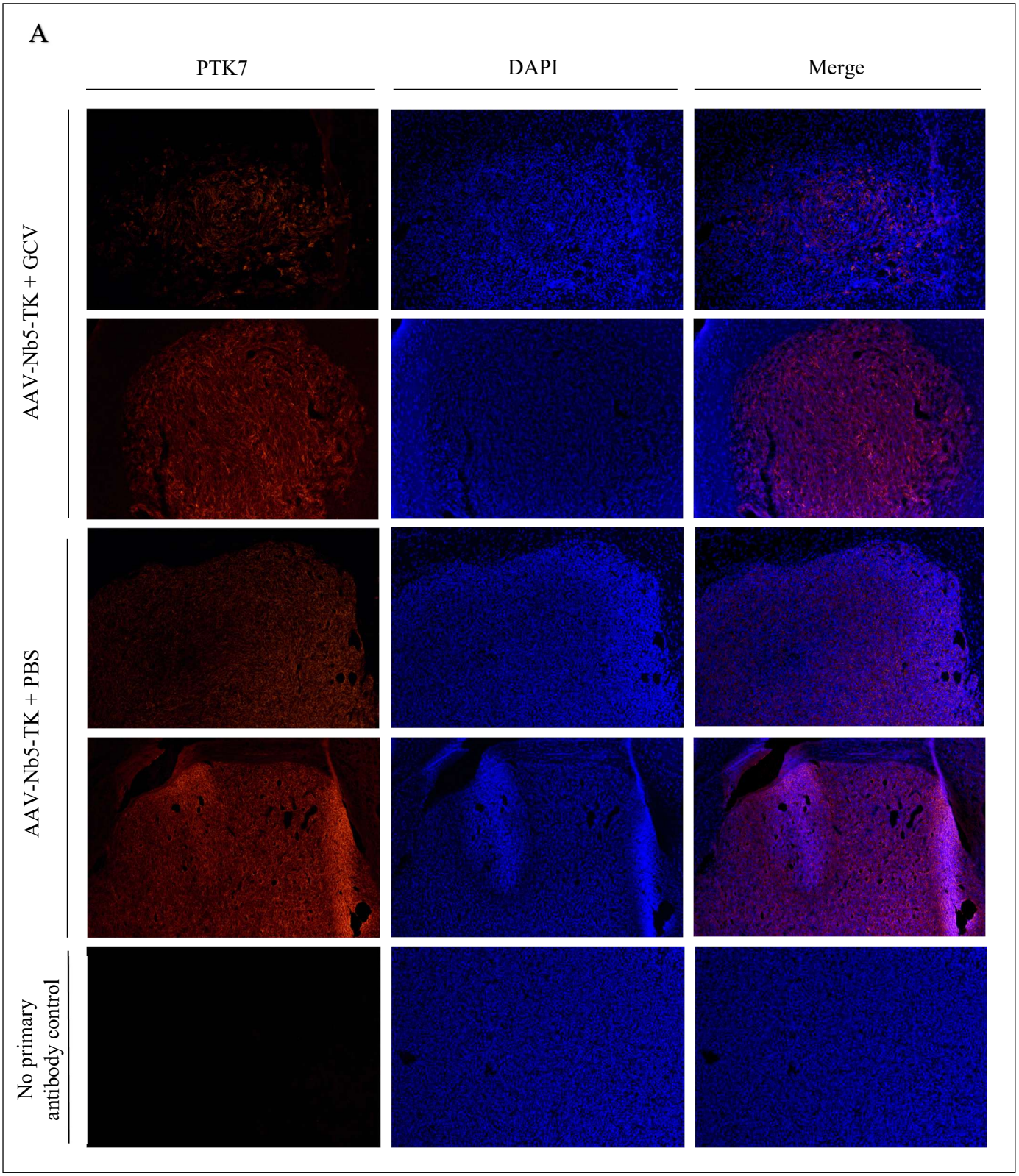
A
PTK7
DAPI
Merge
AAV-Nb5-TK + GCV
AAV-Nb5-TK + PBS
No primary antibody control

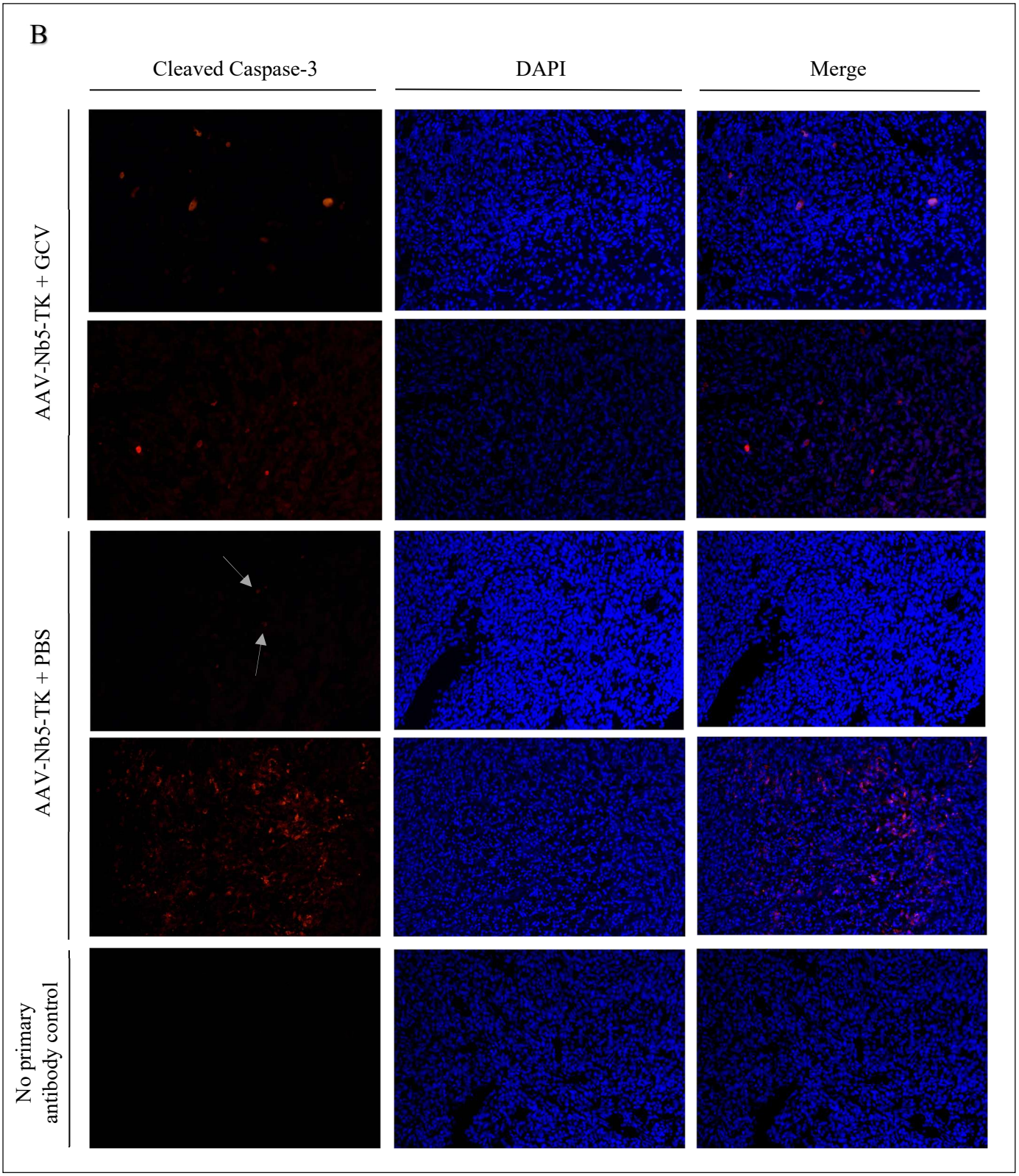

Figure 19. Expression of PTK7 and cleaved CASP-3 on GBM xenograft tissues. Optical images of immunolabelling using (**A**) anti-PTK7 and (**B**) anti-cleaved CASP-3 antibodies. DAPI is a marker used for nuclear labelling. A no primary antibody control was used to assess specificity of the signals.

expression of the PTK7 protein in murine cells following lentiviral transduction, whereas no signal was detected in m005 WT cells (**Figure 20A**). These WB results were consistently observed across independent experiments. To confirm these results, we performed a flow cytometry analysis for the same cell conditions, using an Ab directed against human PTK7 (**Table 3**). As expected, no signal corresponding to PTK7 expression was detected in m005 WT cells (**Figure 20B**). However, contrary to the results obtained by WB, no PTK7 expression was detected in the transduced cells (**Figure 20C**), whereas a signal was still observed in the T033 cell line (**Figure 20D**).

Simultaneously with the determination of PTK7 expression in these mouse cells, we also performed an assay where Nb5-VHH specific binding was assessed by using an Ab against VHH domain and coupled to APC (**Table 3**). Again, Nb5-VHH did not bind to m005 WT (**Figure 20E**), while labelling was confirmed in T033 Scr and m005 PTK7 OE cells (**Figures 20F-G**). However, the labelling profile of Nb5-VHH appears to vary depending on the cell line. Indeed, in T033 Scr cells, a narrow fluorescence peak is observed, that is clearly distinct from the unlabelled control, indicating a homogeneous population of positive cells. In contrast, in m005 PTK7 OE cells, the fluorescence profile appears more diffuse, with a broader distribution of the signal. Thus, a fraction of the cells exhibits a signal comparable to that of cells not labelled with Nb, suggesting the presence of subpopulations of cells that bind strongly to Nb5-VHH.

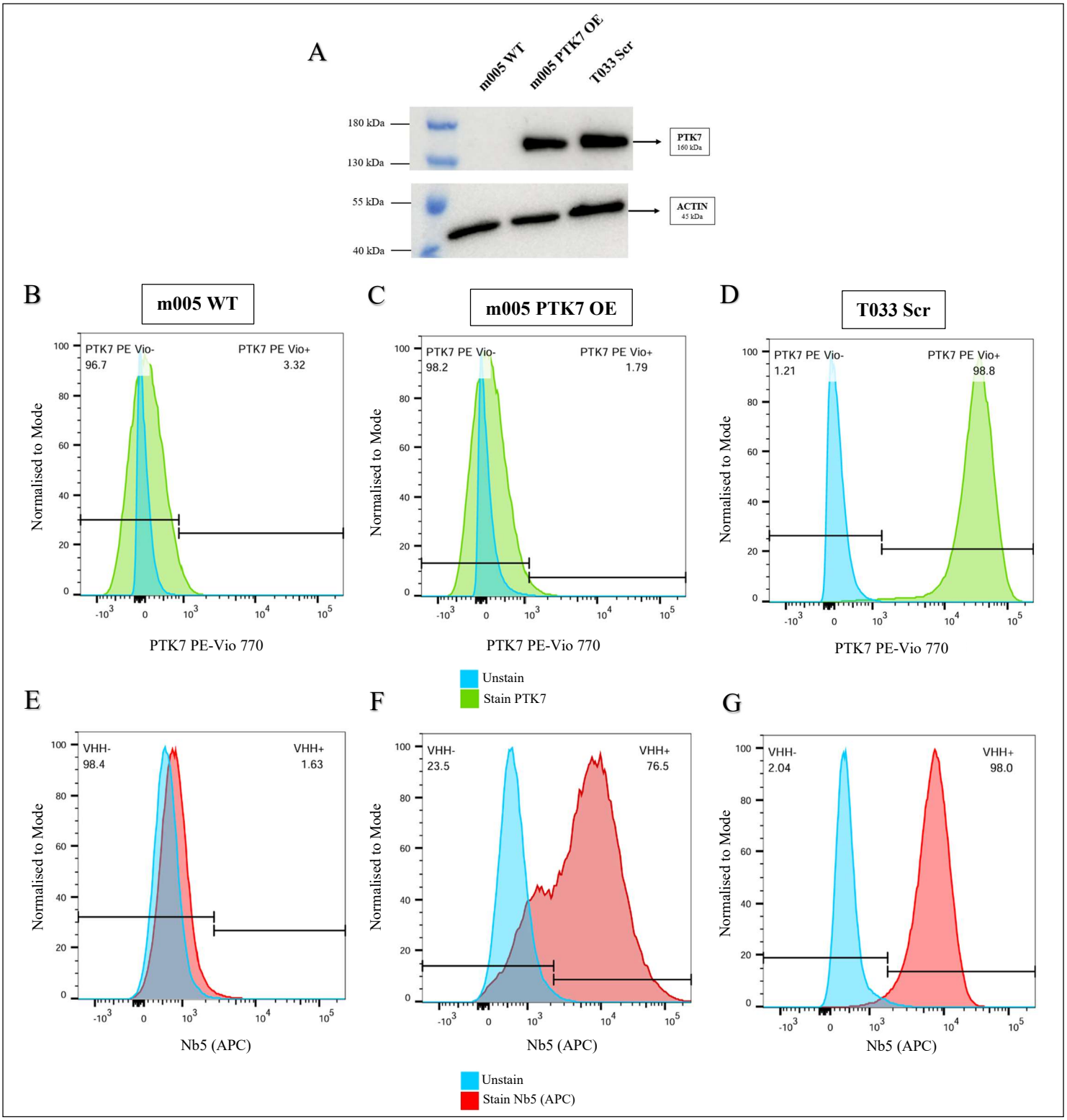

Figure 20. PTK7 expression and Nb5-VHH linking on PTK7-expressing m005 GSCs. Following lentiviral transduction to induce PTK7 expression in murine GBM stem-like cells (m005 GSCs), PTK7 expression was assessed by (**A**) western blot analysis, revealing a signal at the respected molecular weight in PTK7-expressing cells, and by flow cytometry. (**B**) No signal was detected in m005 WT cells, used as negative control. (**C**) Similarly, no positive signal was observed in m005 PTK7 OE cells when using an anti-human PTK7 Ab, whereas (**D**) a positive signal was detected in the PTK7 positive control cell line T033 Scr control. To evaluate Nb5-VHH binding, flow cytometry was performed, showing (**E**) no binding in m005 WT cells, while specific binding was observed in (**F**) m005 PTK7 OE and (**G**) T033 Scr cells.

Chapter 5 - Discussion

Presented by Sarah Grodent, based on the results presented in Chapter 4

GBM is a highly aggressive brain tumour with low survival rates despite current standard treatments.[38] This therapeutic failure can be attributed to numerous cellular and environmental factors, including, among others, the persistence of GSCs, able to self-renew and switch between different cellular states, thereby enhancing their resistance to treatments.[64] Furthermore, GSCs express a wide variety of proteins involved in resistance mechanisms, although no specific markers have yet been identified.[91] Therapeutic approaches, particularly immunotherapies, have been developed but have not yet demonstrated a major therapeutic effect, due to the immunosuppressive TME and the presence of physical barriers.[78-84] In this context, PTK7 has been identified as a promising target, as it is overexpressed by GSCs and its expression remains stable, or even increases, following exposure to TMZ and radiotherapy regimens. The main objective of this master thesis was to assess the specificity of a PTK7-targeting SGT via the HSV-TK/GCV system, using AAV vector coupled to an anti-PTK7 Nb. The efficacy of gene therapy using viral vectors has already been demonstrated. In 1996, AAV-HSV-TK injections combined with the interleukine-2 (IL-2) gene demonstrated significant tumour regression in mice injected with malignant gliomas.[133] In a subsequent experiment, repeated injections of AAV-HSV-TK coupled with GCV exposure demonstrated complete tumour regression and prolonged survival in the majority of treated mice.[134] These initial results offer a promising outlook for this approach. By limiting the transduction of our targeted therapy to PTK7-expressing cells, we evaluated whether this strategy was both effective and specific, focusing on cell death mechanisms and the selectivity of the AAV-Nb5-TK vector. Finally, we addressed the translational potential of this approach in a xenograft mouse model, and we developed a syngeneic immunocompetent cell model.

SGT strategy induces selective apoptotic cell death in PTK7$^+$ cells

First, marked morphological alterations were observed following combined treatment, including neurosphere dissociation into a more single-cell-like suspension in T033 Scr cells and loss of adherence in U87 PTK7 OE cells. These changes may reflect a disruption of cell-cell cohesion and cell-matrix interactions. Although these observations support the induction of cell death in PTK7$^+$ cells, they cannot, by themselves, identify the molecular pathways responsible for the observed phenotype.

The nature of cell death was further investigated by WB and Annexin V/DAPI staining. These analyses revealed an increased proportion of apoptotic cells in PTK7$^+$ populations following combined treatment, consistent with the detection of cleaved CASP-3 and cleaved PARP. The induction of apoptosis following HSV-TK/GCV SGT has been widely reported in several experimental models. In this system, GCV is converted into GCV triphosphate, which can be incorporated into DNA, promoting DNA damage, replication stress and cell cycle arrest in S or G2/M phases, thereby triggering apoptotic signalling pathways. These pathways lead to the activation of initiator caspases, such as caspase-9, followed by activation of effector caspases, including caspases-3 and -7.[130] These effector caspases are known to be involved in cytoskeleton dysregulation and PARP cleavage, impairing DNA repair.[135] Previous studies investigating HSV-TK/GCV system-induced cytotoxicity provided support for our

observations. For example, an induction of cell apoptosis in an ovarian cell model after HSV-TK/GCV treatment induced PARP cleavage as early as 14h of GCV exposure and caspase-3 activation after 24h. As caspase-9 activation preceded both caspase-3 activation and PARP cleavage, and as pharmacological inhibition of caspase-9 prevented PARP cleavage more efficiently than caspase-3 inhibition, the authors proposed caspase-9 as the main mediator in this GCV-induced apoptotic model.[136] Similarly, a study performed on a human neuroblastoma cell line demonstrated an early cleavage of PARP into an 85 kDa fragment, which became almost complete after 96-120h.[137] These observations may help explain the concomitant detection of cleaved and uncleaved PARP forms in our model, where GBM cells were exposed to GCV for only 48 hours. HMGB1 was also analysed as an additional cell death-associated marker. This DNA-binding protein is implicated in various cancer-related processes, including CSC self-renewal. However, these results were difficult to interpret, as HMGB1 levels remained stable between treatment and cellular conditions in some replicates but also varied markedly in others. Moreover, HMGB1 subcellular location varies in response to cellular stress or treatment regimens. In some cases, HMGB1 can also be released into the extracellular space, where it may act as a DAMP and contribute to immune modulation.[138] Therefore, its biological relevance appears to depend more strongly on its localisation and extracellular release than on total protein abundance. In this context, WB on total protein extracts does not appear to be the most suitable method to link HMGB1 expression to a treatment-associated cell death mechanism. Thus, it was not considered sufficient to draw conclusions regarding the modality of cell death induced by the therapy.

Taken together, these results suggest that apoptotic processes may be associated with the morphological alterations previously described. During apoptosis, caspases cascade activation leads to major structural changes, including nuclear condensation, cell fragmentation, altered adhesion, and detachment from the ECM. These morphological changes may result, at least in part, from proteolytic cleavage of proteins involved in cytoskeletal organisation and cell adhesion, including cadherins, laminins, keratins, kinase regulators and integrins.[139] Although the exact mechanisms underlying morphological changes were not directly investigated in this study, apoptosis-associated cellular disorganisation could explain the morphological alterations observed in $PTK7^+$ cells following combined treatment.

AAV-Nb5 vector mediates PTK7-dependent targeting

After establishing that combined treatment preferentially induced apoptosis in $PTK7^+$ cells, it was essential to assess whether this selectivity could be attributed to PTK7-dependent targeting by AAV-Nb5. Across both monoculture and co-culture conditions, AAV-Nb5-GFP transduction was higher in $PTK7^+$ cells, both in terms of GFP^+ cells proportion and MFI of GFP. In contrast, the non-targeted AAV2-GFP vector did not show significant PTK7-dependent differences between cell populations, supporting the specificity of AAV-Nb5-mediated targeting. However, this targeting appeared to be preferential rather than absolute, as a small proportion of $PTK7^-$ cells showed GFP expression, although MFI of GFP remained low and close to basal levels. This suggests that a weak residual transduction may

still occur in PTK7$^-$ cells, possibly through limited non-specific internalisation or residual interactions of the AAV-Nb5 with other cell-surface molecules. Importantly, this low-level transduction did not appear to significantly affect PTK7$^-$ cells viability after AAV-Nb5-TK transduction and GCV exposure. Although a slight increase in Annexin V$^+$ PTK7$^-$ cells was observed compared with the untreated condition, the MFI of Annexin V remained relatively unchanged, suggesting that this limited increase may reflect culture-related stress or residual transduction rather than efficient therapeutic cytotoxicity. Since this experiment was conducted only once, these observations and hypotheses should be interpreted with caution and require further investigations.

In co-culture, AAV-Nb5-GFP transduction followed a gradient according to PTK7 expression, with the highest GFP signal detected in PTK7$^+$ cells, intermediate levels in the PTK7-intermediate population and the lowest signal in PTK7$^-$ cells. This suggests that AAV-Nb5 transduction is not strictly binary but could depend on the level of PTK7 expression at the surface of target cells. The emergence of a PTK7-intermediate population may also reflect potential intercellular transfer of membrane-associated material. The release of extracellular vesicles for intercellular transfer of membrane-associated proteins could contribute to the emergence of these populations. For example, tiny vesicles of 30-100 nm called exosomes can be released in extracellular space, carrying nucleic acids, protein and other biomolecules for cell-cell communication. Interestingly, PTK7 has already been reported in exosomal extracts of cancer cells, suggesting it may be transferred from a cell to another by this mechanism.[140] However, similar experiments previously performed in the laboratory using U87 cells did not reveal PTK7 expression in the isolated exosomes. Therefore, the intervention of these mechanisms in our study should remain speculative. Nevertheless, it could be interesting to repeat this approach using PTK7$^+$ cells monoculture and PTK7$^+$/PTK7$^-$ co-cultures to further isolate exosomes and determine whether PTK7 can be detected in extracellular vesicles.

Finally, given the highly infiltrative and heterogeneous nature of GBM, achieving complete targeting of all tumour cells remains a major challenge. In this context, the bystander effect represents an important feature of the HSV-TK/GCV system, as toxic phosphorylated GCV metabolites can be transferred from transduced cells to neighbouring non-transduced cells, notably through gap junctions. This mechanism was illustrated in a recent study on lung cancer brain metastases using stem cells as vehicles for HSV-TK delivery. In co-culture with H1299 carcinoma cells, therapeutic cells induced significant cytotoxicity even at low ratios of tumour-to-therapeutic cells, with time-lapse imaging showing that cell-death continued 72 hours after the start of co-culture.[141] In our model, however, treatment-associated toxicity was limited to PTK7$^+$ cells, suggesting that a marked bystander effect was not demonstrated under the tested conditions. This might be partly explained by the loss of cellular cohesion observed under the microscope after treatment, which could limit cell-cell contacts, thereby reducing metabolite transfer. The absence of a strong bystander effect may support the selectivity of the strategy but could also limit

its efficacy against heterogeneous tumours. Further studies are needed to determine whether optimizing vector or combined therapies could overcome this limitation.

SGT reduces tumour volume *in vivo* and alters tissue organization and integrity

As a support of the *in vitro* observations supporting a preferential apoptosis cell-death mechanism, the xenograft analysis provided additional information on the histological alterations occurring *in vivo*. In brain sections from mice treated with AAV-Nb5-TK/PBS, PTK7-positive regions appeared dense and well delimited, with compact DAPI staining. In contrast, sections from mice receiving the combined AAV-Nb5-TK/GCV treatment displayed more restricted PTK7-positive regions, associated with a marked apparent reduction in tumour area, less compact cellular organisation, and lower cellular density. This phenotype is consistent with the previous *in vitro* findings, where combined treatment was associated with marked morphological changes, loss of adherence, and increased detection of apoptotic cell death markers in $PTK7^{+}$ cells. Apoptosis-associated cytoskeletal reorganisation, nuclear condensation and loss of cell cohesion may therefore contribute to the structural alterations observed in treated tumour tissue. These changes can result, at least in part, from caspase-mediated cleavage of proteins involved in cytoskeletal organisation and cell adhesion. Accordingly, the altered tissue architecture and looser nuclear organisation observed after AAV-Nb5-TK/GCV treatment may reflect apoptosis-associated remodelling of the tumour tissue. However, this interpretation should remain cautious, as these histological observations were only descriptive and were not supported by quantitative measurements of tumour area and nucleus density.

The presence of focal cleaved CASP-3 expression may also reflect the transient and dynamic nature of apoptosis. Indeed, at the time of tissue collection, only a subset of cells may have been captured at a cleaved CASP-3-positive stage, while other cells may already have progressed towards later stages of cell death or, on the contrary, have not already undergone cell death process. It is also necessary to consider the three-dimensional organisation of solid tumours and the complexity of the TME, which could limit access of the therapy to targeted cells and influence the heterogeneity of the treatment response. In one non-treated tumour, a stronger cleaved CASP-3 signal was observed near the tumour core. Since this mouse did not receive GCV, this signal cannot be attributed to treatment-induced apoptosis. However, solid tumours are frequently characterised by highly hypoxic regions, mainly located in the tumour core, the region furthest from blood vessels. It has been demonstrated that hypovascular tumour regions can display a “dormant” state, resulting either from a limited proliferation or from a balance between proliferation and apoptosis.[142,143] This could partly explain the observed staining pattern on our sections.

Finally, although the use of U87 cell lines represents a first proof-of-concept to assess treatment-associated efficacy, this model remains insufficient to accurately recapitulate the GBM microenvironment and to predict treatment consequences in a clinical GBM context. U87 cells are easy

to manipulate, but U87-derived tumours are relatively well-delimited and form a rather homogeneous cell population, lacking the infiltrative behaviour and cellular heterogeneity that characterise GBM. Moreover, due to multiple cell passages and genetic manipulation to induce PTK7 expression in the whole cell population, this model may not reproduce the genetic and phenotypic features observed in patient tumours.[144] Therefore, complementary investigations using patient-derived GBM cells are required to assess the efficacy of this therapy.

PTK7 expression and specific recognition by Nb5-VHH are confirmed in the m005 tumour model

One of the major limitations to SGT efficacy and clinical translation remains the limited ability of preclinical models to accurately recapitulate GBM pathophysiological characteristics.[131] To date, a few murine models of GBM have been investigated in preclinical studies. Particularly, xenograft models including those established in Nude mice struggle to recapitulate the immunological properties of GBM and do not allow the evaluation of treatment-associated immune recruitment.[144] To overcome this limitation, we developed an immunocompetent syngeneic mice model expressing PTK7, based on 005 murine GBM stem-like cells, for future investigations. The objectives were to demonstrate PTK7 expression in a m005 cell line after lentiviral transduction and to confirme the specificity of Nb5-VHH binding for PTK7.

PTK7 expression analyses revealed a discrepancy between WB and flow cytometry. A PTK7-compatible signal was detected by WB in m005 PTK7 OE and T033 Scr cells, whereas no signal was detected at the surface of m005 PTK7 OE cells by flow cytometry. This discrepancy may be explained by both species-related sequence differences and by specific detection conditions. Human and murine PTK7 share 92.6% sequence identity[145], indicating high global conservation but also local amino acid (AA) variations that may influence Ab recognition. Moreover, WB detects denatured proteins and may therefore reveal conserved linear epitopes between human and murine PTK7, whereas flow cytometry requires the recognition of a surface-native epitope of PTK7. Thus, the Ab used in WB could recognise a conserved epitope accessible after denaturation, while the Ab used in flow cytometry may depend on an epitope not conserved, not accessible, or not presented by murine PTK7 protein. Importantly, Nb5-VHH binding in m005 PTK7 OE cells was confirmed, showing that the epitope recognised by this Nb is accessible at the cell surface, which could not be demonstrated by WB alone. This supports the hypothesis that the absence of PTK7 detection by flow cytometry results from a compatibility limitation of the Ab used, rather than a lack of PTK7 expression. However, Nb5-VHH binding profiles differed between the two PTK7$^+$ populations. While T033 Scr cells displayed a more homogeneous fluorescence profile, likely reflecting stable and endogenous PTK7 expression, m005 PTK7 OE showed a broader fluorescence profile, possibly due to heterogeneous PTK7 expression following lentiviral transduction. Although such heterogeneity may limit the standardisation of this murine model, it could also partially mimic, to some extent, the variability in PTK7 expression in human GBM. Overall, Nb5-VHH

recognition of m005 PTK7 OE cells supports the accessibility of the function Nb target in this mouse model and opens the way for future investigations on the efficacy of the SGT strategy in an immunocompetent setting.

Perspectives for the AAV-Nb5-TK/GCV strategy

Although these preliminary results support the therapeutic potential of this SGT strategy, several factors must be considered, with a view to future clinical application. First, this approach should be positioned within the current clinical management of GBM. Maximal safe resection does not allow complete resection of the tumour mass due to the highly invasive nature of GBM and the persistence of residual tumour cells.[53] In this context, local administration of AAV-Nb5-TK into the resection cavity could be considered to eliminate residual PTK7-expressing cells located at the tumour margins. It would also allow to bypass the BBB without relying on systemic circulation. However, a single injection of AAV solution could be insufficient to ensure sustained and homogeneous therapeutic distribution. Since AAV transgene is expressed via an episomal process, i.e., without integrating into the host cells genome, it could be progressively diluted, as GBM cells are highly proliferative, potentially reducing HSV-TK expression over time.[120] Therefore, the use of an implantable system such as an "Ommaya reservoir" could represent a promising delivery strategy. This system comprises an implantable port placed under the patient's scalp, connected to a catheter positioned in the cerebral ventricles or in the tumour resection cavity. Such system could represent a promising local delivery route for the therapy, while avoiding repeated surgeries and bypassing BBB.[146] In a phase I clinical trial, two ICIs, nivolumab (NIVO) and ipilimumab (IPI), respectively targeting PD-1 and CTLA-4, were administered to patients with recurrent high-grade glioma (rHGG), using this reservoir system. Results from two cohorts were then compared. Both received NIVO 24h before surgery and intraoperative intracerebral (iCer) administration of both agents. The difference lay in the postoperative intracavitary (iCav) treatment, where one cohort received NIVO alone at escalating doses, whereas the other cohort received a combination of a fixed dose of NIVO and escalating doses of IPI. Overall, this study demonstrated the feasibility of this technique; however, the authors suggest that repeated injections using this system did not result in overall or progression-free survival benefits compared to cohorts of patients treated without reservoir-based delivery, which requires further investigation.[147] Finally, PTK7 has shown to be expressed at low levels in normal brain tissues, which could be a supplementary argument for local delivery, limiting the risk of on-target/off-tumour effect.

Beyond delivery, another limitation of GBM treatment remains its high heterogeneity. While PTK7 is overexpressed in GBM and has been associated with tumorigenesis, its expression varies between patients and according to treatment regimen, as shown by the screening of GSC cultures performed in the laboratory (see Figure 7). Under therapeutic pressure, tumour cells may also adapt and develop resistance mechanisms through clonal selection and the activation of alternative signalling pathways, leading to the emergence of cellular subclones.[64,90] Thus, a monovalent strategy targeting PTK7 alone

may not be sufficient to eliminate all tumour cell populations. However, an additional target should ideally be accessible at the cell surface, exhibit low expression in normal tissues and remain stable following therapeutic pressure from standard treatments. Previous investigations carried out in the laboratory identified B7-H3 as a promising candidate that fulfils these criteria. B7-H3 acts as an immune checkpoint molecule and has been associated with a poor clinical outcome in HGGs. In this field, B7-H3-targeted CAR-T cells have already been developed and showed enhanced cytotoxic activity *in vitro* and in orthotopic xenograft models. Interestingly, B7-H3 has also been reported to be expressed at the surface of tumour-associated blood vessels, raising the possibility that targeting this protein could also contribute to vascular disruption.[148,149]

Altogether, these perspectives provide further insight into the promising future of SGT. This therapeutic approach, when combined with a targeting module such as the AAV-Nb5 platform developed by the laboratory, paves the way for future investigations, as it could help overcome some of the limitations encountered in the context of GBM. The use of more representative models and the testing of combinations with other targeting strategies will be essential to determine the safety and efficacy of this therapy before considering its future clinical application.

Bibliography

1. Filho, A. M. *et al.* Cancers of the brain and central nervous system: global patterns and trends in incidence. *J. Neurooncol.* **172**, 567–578 (2025).
2. Aldape, K. *et al.* Challenges to curing primary brain tumours. *Nat. Rev. Clin. Oncol.* **16**, 509–520 (2019).
3. Perus, L. J. M. & Walsh, L. A. Microenvironmental Heterogeneity in Brain Malignancies. *Front. Immunol.* **10**, 2294 (2019).
4. Byun, Y. H. & Park, C.-K. Classification and Diagnosis of Adult Glioma: A Scoping Review. *Brain NeuroRehabilitation* **15**, e23 (2022).
5. Ferris, S. P., Hofmann, J. W., Solomon, D. A. & Perry, A. Characterization of gliomas: from morphology to molecules. *Virchows Arch. Int. J. Pathol.* **471**, 257–269 (2017).
6. Alcantara Llaguno, S. R. & Parada, L. F. Cell of origin of glioma: biological and clinical implications. *Br. J. Cancer* **115**, 1445–1450 (2016).
7. Chen, R., Smith-Cohn, M., Cohen, A. L. & Colman, H. Glioma Subclassifications and Their Clinical Significance. *Neurother. J. Am. Soc. Exp. Neurother.* **14**, 284–297 (2017).
8. Modrek, A. S., Bayin, N. S. & Placantonakis, D. G. Brain stem cells as the cell of origin in glioma. *World J. Stem Cells* **6**, 43–52 (2014).
9. Silvani, A. *et al.* Malignant gliomas: early diagnosis and clinical aspects. *Neurol. Sci. Off. J. Ital. Neurol. Soc. Ital. Soc. Clin. Neurophysiol.* **32 Suppl 2**, S207-208 (2011).
10. Louis, D. N. *et al.* The 2016 World Health Organization Classification of Tumors of the Central Nervous System: a summary. *Acta Neuropathol. (Berl.)* **131**, 803–820 (2016).
11. Kros, J. M. Grading of gliomas: the road from eminence to evidence. *J. Neuropathol. Exp. Neurol.* **70**, 101–109 (2011).
12. Sturm, D. *et al.* New Brain Tumor Entities Emerge from Molecular Classification of CNS-PNETs. *Cell* **164**, 1060–1072 (2016).
13. Ray, A., Swain, M. & Lath, R. Gliomas: The history of diagnosis and classification: Part 1. *Int. J. Neurooncology* **3**, 63–67 (2020).
14. Louis, D. N. *et al.* The 2007 WHO classification of tumours of the central nervous system. *Acta Neuropathol. (Berl.)* **114**, 97–109 (2007).
15. Ray, A., Meenakshi, S. & Rahul, L. Gliomas: History of diagnosis and classification: Part 2. *Int. J. Neurooncology* **3**, 68–74 (2020).
16. Perry, A. & Wesseling, P. Histologic classification of gliomas. *Handb. Clin. Neurol.* **134**, 71–95 (2016).
17. Penkova, A. *et al.* Comprehensive clinical assays for molecular diagnostics of gliomas: the current state and future prospects. *Front. Mol. Biosci.* **10**, 1216102 (2023).
18. Louis, D. N. *et al.* The 2021 WHO Classification of Tumors of the Central Nervous System: a summary. *Neuro-Oncol.* **23**, 1231–1251 (2021).
19. Antonelli, M. & Poliani, P. L. Adult type diffuse gliomas in the new 2021 WHO Classification. *Pathologica* **114**, 397–409 (2022).
20. Rubiano, E. G. O. *et al.* Understanding the molecular profiling of diffuse gliomas classification: A brief overview. *Surg. Neurol. Int.* **14**, 225 (2023).
21. Zuo, M. *et al.* Weakly supervised deep learning-based classification for histopathology of gliomas: a single center experience. *Sci. Rep.* **15**, 265 (2025).
22. Thenuwara, G., Curtin, J. & Tian, F. Advances in Diagnostic Tools and Therapeutic Approaches for Gliomas: A Comprehensive Review. *Sensors* **23**, 9842 (2023).
23. Appay, R. *et al.* IDH2 mutations are commonly associated with 1p/19q codeletion in diffuse adult gliomas. *Neuro-Oncol.* **20**, 716–718 (2018).
24. Kang, K. M. *et al.* MRI Scoring Systems for Predicting Isocitrate Dehydrogenase Mutation and Chromosome 1p/19q Codeletion in Adult-type Diffuse Glioma Lacking Contrast Enhancement. *Radiology* **311**, e233120 (2024).
25. Valvi, S., Fouladi, M., Fisher, M. J. & Gottardo, N. G. IDH mutant high-grade gliomas. *Front. Mol. Neurosci.* **18**, 1662414 (2025).
26. Dang, L., Yen, K. & Attar, E. C. IDH mutations in cancer and progress toward development of targeted therapeutics. *Ann. Oncol.* **27**, 599–608 (2016).
27. Clark, O., Yen, K. & Mellinghoff, I. K. Molecular Pathways: Isocitrate Dehydrogenase Mutations in Cancer. *Clin. Cancer Res. Off. J. Am. Assoc. Cancer Res.* **22**, 1837–1842 (2016).
28. Cohen, A. L., Holmen, S. L. & Colman, H. IDH1 and IDH2 mutations in gliomas. *Curr. Neurol. Neurosci. Rep.* **13**, 345 (2013).
29. Santosh, V. & Rao, S. A review of adult-type diffuse gliomas in the WHO CNS5 classification with special reference to Astrocytoma, IDH-mutant and Oligodendroglioma, IDH-mutant and 1p/19q codeleted. *Indian J. Pathol. Microbiol.* **65**, S14–S23 (2022).
30. Tauziède-Espariat, A. *et al.* ATRX loss in adult gliomas lacking H3 alterations or IDH mutations, an exceptional situation for exceptional diagnoses: the experience of Sainte-Anne hospital. *Acta Neuropathol. Commun.* **13**, 131 (2025).
31. Noor, H., Briggs, N. E., McDonald, K. L., Holst, J. & Vittorio, O. TP53 Mutation Is a Prognostic Factor in Lower Grade Glioma and May Influence Chemotherapy Efficacy. *Cancers* **13**, 5362 (2021).

32. Stichel, D. *et al.* Distribution of EGFR amplification, combined chromosome 7 gain and chromosome 10 loss, and TERT promoter mutation in brain tumors and their potential for the reclassification of IDHwt astrocytoma to glioblastoma. https://doi.org/10.5167/UZH-153711 (2018) doi:10.5167/UZH-153711.
33. Wang, H. *et al.* Clinical roles of EGFR amplification in diffuse gliomas: a real-world study using the 2021 WHO classification of CNS tumors. *Front. Neurosci.* **18**, 1308627 (2024).
34. Chen, Y. *et al.* Tumor-associated monocytes promote mesenchymal transformation through EGFR signalling in glioma. *Cell Rep. Med.* **4**, 101177 (2023).
35. Nair, N. U. *et al.* Chromosome 7 Gain Compensates for Chromosome 10 Loss in Glioma. *Cancer Res.* **84**, 3464–3477 (2024).
36. Yuile, A. *et al.* CDKN2A/B Homozygous Deletions in Astrocytomas: A Literature Review. *Curr. Issues Mol. Biol.* **45**, 5276–5292 (2023).
37. Komori, T. Grading of adult diffuse gliomas according to the 2021 WHO Classification of Tumors of the Central Nervous System. *Lab. Investig. J. Tech. Methods Pathol.* **102**, 126–133 (2022).
38. Madour, J. *et al.* Glioblastoma: Epidemiology and Imaging-Based Review. *R. I. Med. J. 2013* **108**, 50–56 (2025).
39. Hanif, F., Muzaffar, K., Perveen, K., Malhi, S. M. & Simjee, S. U. Glioblastoma Multiforme: A Review of its Epidemiology and Pathogenesis through Clinical Presentation and Treatment. *Asian Pac. J. Cancer Prev. APJCP* **18**, 3–9 (2017).
40. Rivera, M., Sukhdeo, K. & Yu, J. Ionizing radiation in glioblastoma initiating cells. *Front. Oncol.* **3**, 74 (2013).
41. Mrowczynski, O. D., Yang, A. L., Liao, J. & Rizk, E. The Potential of Glioblastoma Patient Symptoms to Diagnose and Predict Survival. *Cureus* **13**, e16675 (2021).
42. Bernstock, J. D. *et al.* Standard clinical approaches and emerging modalities for glioblastoma imaging. *Neuro-Oncol. Adv.* **4**, vdac080 (2022).
43. Ohgaki, H. & Kleihues, P. The definition of primary and secondary glioblastoma. *Clin. Cancer Res. Off. J. Am. Assoc. Cancer Res.* **19**, 764–772 (2013).
44. Wang, Q. *et al.* Tumor Evolution of Glioma-Intrinsic Gene Expression Subtypes Associates with Immunological Changes in the Microenvironment. *Cancer Cell* **32**, 42-56.e6 (2017).
45. Xu, C. *et al.* Comprehensive understanding of glioblastoma molecular phenotypes: classification, characteristics, and transition. *Cancer Biol. Med.* **21**, 363–381 (2024).
46. Wen, P. Y. *et al.* Glioblastoma in adults: a Society for Neuro-Oncology (SNO) and European Society of Neuro-Oncology (EANO) consensus review on current management and future directions. *Neuro-Oncol.* **22**, 1073–1113 (2020).
47. Neftel, C. *et al.* An Integrative Model of Cellular States, Plasticity, and Genetics for Glioblastoma. *Cell* **178**, 835-849.e21 (2019).
48. Nomura, M. *et al.* The multilayered transcriptional architecture of glioblastoma ecosystems. *Nat. Genet.* **57**, 1155–1167 (2025).
49. Stupp, R. *et al.* Radiotherapy plus Concomitant and Adjuvant Temozolomide for Glioblastoma. *N. Engl. J. Med.* **352**, 987–996 (2005).
50. Nabors, L. B. *et al.* Central nervous system cancers. *J. Natl. Compr. Cancer Netw. JNCCN* **11**, 1114–1151 (2013).
51. Watts, C. & Sanai, N. Surgical approaches for the gliomas. *Handb. Clin. Neurol.* **134**, 51–69 (2016).
52. Tan, A. C. *et al.* Management of glioblastoma: State of the art and future directions. *CA. Cancer J. Clin.* **70**, 299–312 (2020).
53. Price, S. J. *et al.* Precision Surgery for Glioblastomas. *J. Pers. Med.* **15**, 96 (2025).
54. Fernández, C., Ciérvide, R., Díaz, A., Garrido, I. & Couñago, F. Radiotherapy in Glioblastoma Multiforme: Evolution, Limitations, and Molecularly Guided Future. *Biomedicines* **13**, 2136 (2025).
55. Aiyappa-Maudsley, R., Chalmers, A. J. & Parsons, J. L. Factors affecting the radiation response in glioblastoma. *Neuro-Oncol. Adv.* **4**, vdac156 (2022).
56. Ter Linden, E., Abels, E. R., Van Solinge, T. S., Neefjes, J. & Broekman, M. L. D. Overcoming Barriers in Glioblastoma—Advances in Drug Delivery Strategies. *Cells* **13**, 998 (2024).
57. Jezierzański, M. *et al.* Temozolomide (TMZ) in the Treatment of Glioblastoma Multiforme-A Literature Review and Clinical Outcomes. *Curr. Oncol. Tor. Ont* **31**, 3994–4002 (2024).
58. Habibi, M. A. *et al.* Is add-on Bevacizumab therapy to Temozolomide and radiotherapy associated with clinical utility for newly diagnosed Glioblastoma? A systematic review and meta-analysis. *Neurosurg. Rev.* **47**, 445 (2024).
59. Vredenburgh, J. J. *et al.* Bevacizumab plus irinotecan in recurrent glioblastoma multiforme. *J. Clin. Oncol. Off. J. Am. Soc. Clin. Oncol.* **25**, 4722–4729 (2007).
60. Reardon, D. A. *et al.* Phase II study of metronomic chemotherapy with bevacizumab for recurrent glioblastoma after progression on bevacizumab therapy. *J. Neurooncol.* **103**, 371–379 (2011).
61. Ideguchi, M. *et al.* MRI findings and pathological features in early-stage glioblastoma. *J. Neurooncol.* **123**, 289–297 (2015).

62. *Malignant Brain Tumors*. (Springer International Publishing, Cham, 2017). doi:10.1007/978-3-319-49864-5.
63. Lathia, J. D., Mack, S. C., Mulkearns-Hubert, E. E., Valentim, C. L. L. & Rich, J. N. Cancer stem cells in glioblastoma. *Genes Dev.* **29**, 1203–1217 (2015).
64. Prager, B. C., Bhargava, S., Mahadev, V., Hubert, C. G. & Rich, J. N. Glioblastoma Stem Cells: Driving Resilience through Chaos. *Trends Cancer* **6**, 223–235 (2020).
65. Eckerdt, F. & Platanias, L. C. Emerging Role of Glioma Stem Cells in Mechanisms of Therapy Resistance. *Cancers* **15**, 3458 (2023).
66. Holmberg Olausson, K. *et al.* Prominin-1 (CD133) defines both stem and non-stem cell populations in CNS development and gliomas. *PloS One* **9**, e106694 (2014).
67. Sharma, P., Aaroe, A., Liang, J. & Puduvalli, V. K. Tumor microenvironment in glioblastoma: Current and emerging concepts. *Neuro-Oncol. Adv.* **5**, vdad009 (2023).
68. Mohiuddin, E. & Wakimoto, H. Extracellular matrix in glioblastoma: opportunities for emerging therapeutic approaches. *Am. J. Cancer Res.* **11**, 3742–3754 (2021).
69. De Fazio, E. *et al.* Intrinsic and Microenvironmental Drivers of Glioblastoma Invasion. *Int. J. Mol. Sci.* **25**, 2563 (2024).
70. Solomou, G., Young, A. M. H. & Bulstrode, H. J. C. J. Microglia and macrophages in glioblastoma: landscapes and treatment directions. *Mol. Oncol.* **18**, 2906–2926 (2024).
71. Alban, T. J. *et al.* Glioblastoma Myeloid-Derived Suppressor Cell Subsets Express Differential Macrophage Migration Inhibitory Factor Receptor Profiles That Can Be Targeted to Reduce Immune Suppression. *Front. Immunol.* **11**, 1191 (2020).
72. Woroniecka, K. I., Rhodin, K. E., Chongsathidkiet, P., Keith, K. A. & Fecci, P. E. T-cell Dysfunction in Glioblastoma: Applying a New Framework. *Clin. Cancer Res. Off. J. Am. Assoc. Cancer Res.* **24**, 3792–3802 (2018).
73. Zhang, W., Zhang, W., Wu, H. & Han, X. Harnessing innate immunity against glioblastoma microenvironment. *Front. Immunol.* **16**, 1648601 (2025).
74. Liu, Y., Zhou, F., Ali, H., Lathia, J. D. & Chen, P. Immunotherapy for glioblastoma: current state, challenges, and future perspectives. *Cell. Mol. Immunol.* **21**, 1354–1375 (2024).
75. Rodríguez-Camacho, A. *et al.* Glioblastoma Treatment: State-of-the-Art and Future Perspectives. *Int. J. Mol. Sci.* **23**, 7207 (2022).
76. Angom, R. S., Nakka, N. M. R. & Bhattacharya, S. Advances in Glioblastoma Therapy: An Update on Current Approaches. *Brain Sci.* **13**, 1536 (2023).
77. Kim, S.-S., Harford, J. B., Pirollo, K. F. & Chang, E. H. Effective treatment of glioblastoma requires crossing the blood-brain barrier and targeting tumors including cancer stem cells: The promise of nanomedicine. *Biochem. Biophys. Res. Commun.* **468**, 485–489 (2015).
78. de Melo, S. M. *et al.* Anti-PD-1 and anti-PD-L1 antibodies for glioma. *Cochrane Database Syst. Rev.* **1**, CD012532 (2025).
79. Omuro, A. *et al.* Radiotherapy combined with nivolumab or temozolomide for newly diagnosed glioblastoma with unmethylated MGMT promoter: An international randomized phase III trial. *Neuro-Oncol.* **25**, 123–134 (2023).
80. Thomas, A. A., Fisher, J. L., Ernstoff, M. S. & Fadul, C. E. Vaccine-based immunotherapy for glioblastoma. *CNS Oncol.* **2**, 331–349 (2013).
81. Yuan, F. *et al.* EGFRvIII-positive glioblastoma contributes to immune escape and malignant progression via the c-Fos-MDK-LRP1 axis. *Cell Death Dis.* **16**, 453 (2025).
82. Weller, M. *et al.* Rindopepimut with temozolomide for patients with newly diagnosed, EGFRvIII-expressing glioblastoma (ACT IV): a randomised, double-blind, international phase 3 trial. *Lancet Oncol.* **18**, 1373–1385 (2017).
83. Liu, X. *et al.* The Development of Immunotherapy for the Treatment of Recurrent Glioblastoma. *Cancers* **15**, 4308 (2023).
84. Zhou, Y., Shi, F., Zhu, J. & Yuan, Y. An update on the clinical trial research of immunotherapy for glioblastoma. *Front. Immunol.* **16**, 1582296 (2025).
85. Tang, J., Karbhari, N. & Campian, J. L. Therapeutic Targets in Glioblastoma: Molecular Pathways, Emerging Strategies, and Future Directions. *Cells* **14**, 494 (2025).
86. Várady, G., Cserepes, J., Németh, A., Szabó, E. & Sarkadi, B. Cell surface membrane proteins as personalized biomarkers: where we stand and where we are headed. *Biomark. Med.* **7**, 803–819 (2013).
87. Ghosh, D. *et al.* A Cell-Surface Membrane Protein Signature for Glioblastoma. *Cell Syst.* **4**, 516-529.e7 (2017).
88. Shen, Y., Thng, D. K. H., Wong, A. L. A. & Toh, T. B. Mechanistic insights and the clinical prospects of targeted therapies for glioblastoma: a comprehensive review. *Exp. Hematol. Oncol.* **13**, 40 (2024).
89. Kowalski-Chauvel, A. *et al.* Alpha-6 integrin promotes radioresistance of glioblastoma by modulating DNA damage response and the transcription factor Zeb1. *Cell Death Dis.* **9**, 872 (2018).
90. Mahdi, A., Aittaleb, M. & Tissir, F. Targeting Glioma Stem Cells: Therapeutic Opportunities and Challenges. *Cells* **14**, 675 (2025).

91. He, J., Liu, Y. & Lubman, D. M. Targeting glioblastoma stem cells: cell surface markers. *Curr. Med. Chem.* **19**, 6050–6055 (2012).
92. Chen, L., Shi, L., Wang, W. & Zhou, Y. ABCG2 downregulation in glioma stem cells enhances the therapeutic efficacy of demethoxycurcumin. *Oncotarget* **8**, 43237–43247 (2017).
93. Nakai, E. *et al.* Enhanced MDR1 expression and chemoresistance of cancer stem cells derived from glioblastoma. *Cancer Invest.* **27**, 901–908 (2009).
94. Cui, M., Cheng, C. & Zhang, L. High-throughput proteomics: a methodological mini-review. *Lab. Investig. J. Tech. Methods Pathol.* **102**, 1170–1181 (2022).
95. Rose, M. *et al.* Surfaceome Proteomic of Glioblastoma Revealed Potential Targets for Immunotherapy. *Front. Immunol.* **12**, 746168 (2021).
96. Lee, S. T., Strunk, K. M. & Spritz, R. A. A survey of protein tyrosine kinase mRNAs expressed in normal human melanocytes. *Oncogene* **8**, 3403–3410 (1993).
97. Mossie, K. *et al.* Colon carcinoma kinase-4 defines a new subclass of the receptor tyrosine kinase family. *Oncogene* **11**, 2179–2184 (1995).
98. Park, S.-K., Lee, H.-S. & Lee, S.-T. Characterization of the Human Full-Length PTK7 cDNA Encoding a Receptor Protein Tyrosine Kinase-Like Molecule Closely Related to Chick KLG. *J. Biochem. (Tokyo)* **119**, 235–239 (1996).
99. Lu, X. *et al.* PTK7/CCK-4 is a novel regulator of planar cell polarity in vertebrates. *Nature* **430**, 93–98 (2004).
100. Puppo, F. *et al.* Protein tyrosine kinase 7 has a conserved role in Wnt/β-catenin canonical signalling. *EMBO Rep.* **12**, 43–49 (2011).
101. Andreeva, A. *et al.* PTK7-Src signalling at epithelial cell contacts mediates spatial organization of actomyosin and planar cell polarity. *Dev. Cell* **29**, 20–33 (2014).
102. Dessaux, C., Ganier, L., Guiraud, L. & Borg, J.-P. Recent insights into the therapeutic strategies targeting the pseudokinase PTK7 in cancer. *Oncogene* **43**, 1973–1984 (2024).
103. Hayes, M., Naito, M., Daulat, A., Angers, S. & Ciruna, B. Ptk7 promotes non-canonical Wnt/PCP-mediated morphogenesis and inhibits Wnt/β-catenin-dependent cell fate decisions during vertebrate development. *Development* **140**, 1807–1818 (2013).
104. Mottard, K., Cokaiko, J., Rogister, B. & Neirinckx, V. Therapeutic targeting of the protein tyrosine kinase-7 in cancer: an overview. *The Oncologist* **30**, oyae290 (2025).
105. Raivola, J. *et al.* Multiomics characterization implicates PTK7 in ovarian cancer EMT and cell plasticity and offers strategies for therapeutic intervention. *Cell Death Dis.* **13**, 714 (2022).
106. Lee, H. K., Chauhan, S. K., Kay, E. & Dana, R. Flt-1 regulates vascular endothelial cell migration via a protein tyrosine kinase-7–dependent pathway. *Blood* **117**, 5762–5771 (2011).
107. Chauhan, S. K. *et al.* PTK7+ Mononuclear Cells Express VEGFR2 and Contribute to Vascular Stabilization by Upregulating Angiopoietin-1. *Arterioscler. Thromb. Vasc. Biol.* **35**, 1606–1615 (2015).
108. Lee, J. Y. *et al.* Identification and targeting of protein tyrosine kinase 7 (PTK7) as an immunotherapy candidate for neuroblastoma. *Cell Rep. Med.* **4**, 101091 (2023).
109. Jie, Y. *et al.* PTK7-Targeting CAR T-Cells for the Treatment of Lung Cancer and Other Malignancies. *Front. Immunol.* **12**, 665970 (2021).
110. Katoh, M. Antibody-drug conjugate targeting protein tyrosine kinase 7, a receptor tyrosine kinase-like molecule involved in WNT and vascular endothelial growth factor signalling: effects on cancer stem cells, tumor microenvironment and whole-body homeostasis. *Ann. Transl. Med.* **5**, 462 (2017).
111. Long, R. *et al.* Antibody-drug conjugates in cancer therapy: applications and future advances. *Front. Immunol.* **16**, 1516419 (2025).
112. Kong, C. *et al.* MTX-13, a Novel PTK7-Directed Antibody-Drug Conjugate with Widened Therapeutic Index Shows Sustained Tumor Regressions for a Broader Spectrum of PTK7-Positive Tumors. *Mol. Cancer Ther.* **22**, 1128–1143 (2023).
113. Mitra, A. *et al.* From bench to bedside: the history and progress of CAR T cell therapy. *Front. Immunol.* **14**, 1188049 (2023).
114. Lhoumeau, A.-C., Puppo, F., Prébet, T., Kodjabachian, L. & Borg, J.-P. PTK7: a cell polarity receptor with multiple facets. *Cell Cycle Georget. Tex* **10**, 1233–1236 (2011).
115. Suryadevara, C. M. *et al.* Temozolomide lymphodepletion enhances CAR abundance and correlates with antitumor efficacy against established glioblastoma. *Oncoimmunology* **7**, e1434464 (2018).
116. Wen, C., Wang, Y. & Wang, Y. Aptamers in Drug Delivery Development. *Mater. Today* **88**, 855–870 (2025).
117. Mahmoudian, F. *et al.* Aptamers as an approach to targeted cancer therapy. *Cancer Cell Int.* **24**, 108 (2024).
118. Su, M. *et al.* An aptamer-drug conjugate for promising cancer therapy with comprehensive evaluation from rodents to non-human primates. *Signal Transduct. Target. Ther.* **10**, 316 (2025).
119. Atchison, R. W., Casto, B. C. & Hammon, W. McD. Adenovirus-Associated Defective Virus Particles. *Science* **149**, 754–756 (1965).

120. Xu, X. *et al.* Adeno-associated virus (AAV)-based gene therapy for glioblastoma. *Cancer Cell Int.* **21**, 76 (2021).
121. Issa, S. S., Shaimardanova, A. A., Solovyeva, V. V. & Rizvanov, A. A. Various AAV Serotypes and Their Applications in Gene Therapy: An Overview. *Cells* **12**, 785 (2023).
122. Wang, J.-H., Gessler, D. J., Zhan, W., Gallagher, T. L. & Gao, G. Adeno-associated virus as a delivery vector for gene therapy of human diseases. *Signal Transduct. Target. Ther.* **9**, 78 (2024).
123. Meier, A. F., Fraefel, C. & Seyffert, M. The Interplay between Adeno-Associated Virus and its Helper Viruses. *Viruses* **12**, 662 (2020).
124. Lau, C.-H. & Suh, Y. In vivo genome editing in animals using AAV-CRISPR system: applications to translational research of human disease. *F1000Research* **6**, 2153 (2017).
125. Maitland, M. L. *et al.* First-in-Human Study of PF-06647020 (Cofetuzumab Pelidotin), an Antibody-Drug Conjugate Targeting Protein Tyrosine Kinase 7, in Advanced Solid Tumors. *Clin. Cancer Res. Off. J. Am. Assoc. Cancer Res.* **27**, 4511–4520 (2021).
126. Chen, B. *et al.* Antibody–drug conjugates in cancer therapy: current landscape, challenges, and future directions. *Mol. Cancer* **24**, 279 (2025).
127. Liu, M., Li, L., Jin, D. & Liu, Y. Nanobody-A versatile tool for cancer diagnosis and therapeutics. *Wiley Interdiscip. Rev. Nanomed. Nanobiotechnol.* **13**, e1697 (2021).
128. Verhaar, E. R., Woodham, A. W. & Ploegh, H. L. Nanobodies in cancer. *Semin. Immunol.* **52**, 101425 (2021).
129. Jug, A., Bratkovič, T. & Ilaš, J. Biolayer interferometry and its applications in drug discovery and development. *TrAC Trends Anal. Chem.* **176**, 117741 (2024).
130. Zarogoulidis, P. *et al.* Suicide Gene Therapy for Cancer - Current Strategies. *J. Genet. Syndr. Gene Ther.* **4**, 16849 (2013).
131. Hossain, J. A., Marchini, A., Fehse, B., Bjerkvig, R. & Miletic, H. Suicide gene therapy for the treatment of high-grade glioma: past lessons, present trends, and future prospects. *Neuro-Oncol. Adv.* **2**, vdaa013 (2020).
132. Kardani, K. *et al.* Immunocompetent murine glioblastoma stem-like cell models exhibiting distinct phenotypes. *Neuro-Oncol. Adv.* **7**, vdae215 (2025).
133. Okada, H. *et al.* Gene therapy against an experimental glioma using adeno-associated virus vectors. *Gene Ther.* **3**, 957–964 (1996).
134. Mizuno, M., Yoshida, J., Colosi, P. & Kurtzman, G. Adeno-associated virus vector containing the herpes simplex virus thymidine kinase gene causes complete regression of intracerebrally implanted human gliomas in mice, in conjunction with ganciclovir administration. *Jpn. J. Cancer Res. Gann* **89**, 76–80 (1998).
135. Dho, S. H., Cho, M., Woo, W., Jeong, S. & Kim, L. K. Caspases as master regulators of programmed cell death: apoptosis, pyroptosis and beyond. *Exp. Mol. Med.* **57**, 1121–1132 (2025).
136. Tomicic, M. T., Thust, R. & Kaina, B. Ganciclovir-induced apoptosis in HSV-1 thymidine kinase expressing cells: critical role of DNA breaks, Bcl-2 decline and caspase-9 activation. *Oncogene* **21**, 2141–2153 (2002).
137. Beltinger, C. *et al.* Herpes simplex virus thymidine kinase/ganciclovir-induced apoptosis involves ligand-independent death receptor aggregation and activation of caspases. *Proc. Natl. Acad. Sci. U. S. A.* **96**, 8699–8704 (1999).
138. Lv, G. *et al.* Multiple functions of HMGB1 in cancer. *Front. Oncol.* **14**, 1384109 (2024).
139. Widmann, C., Gibson, S. & Johnson, G. L. Caspase-dependent Cleavage of Signalling Proteins during Apoptosis. *J. Biol. Chem.* **273**, 7141–7147 (1998).
140. Zhou, Z., Chen, Y. & Qian, X. Target-Specific Exosome Isolation through Aptamer-Based Microfluidics. *Biosensors* **12**, 257 (2022).
141. Oishi, T. *et al.* Efficacy of HSV-TK/GCV system suicide gene therapy using SHED expressing modified HSV-TK against lung cancer brain metastases. *Mol. Ther. - Methods Clin. Dev.* **26**, 253–265 (2022).
142. Li, Y., Zhao, L. & Li, X.-F. Hypoxia and the Tumor Microenvironment. *Technol. Cancer Res. Treat.* **20**, 15330338211036304 (2021).
143. Casazza, A. *et al.* Tumor stroma: a complexity dictated by the hypoxic tumor microenvironment. *Oncogene* **33**, 1743–1754 (2014).
144. Haddad, A. F. *et al.* Mouse models of glioblastoma for the evaluation of novel therapeutic strategies. *Neuro-Oncol. Adv.* **3**, vdab100 (2021).
145. PTK7 (PTK7 protein tyrosine kinase 7). https://atlasgeneticsoncology.org/gene/41901/ptk7-%28ptk7-protein-tyrosine-kinase-7%29?utm_source=chatgpt.com.
146. van Solinge, T. S., Nieland, L., Chiocca, E. A. & Broekman, M. L. D. Advances in local therapy for glioblastoma - taking the fight to the tumour. *Nat. Rev. Neurol.* **18**, 221–236 (2022).
147. Duerinck, J. *et al.* Intracranial administration of anti-PD-1 and anti-CTLA-4 immune checkpoint-blocking monoclonal antibodies in patients with recurrent high-grade glioma. *Neuro-Oncol.* **26**, 2208–2221 (2024).
148. Tang, X. *et al.* B7-H3 as a Novel CAR-T Therapeutic Target for Glioblastoma. *Mol. Ther. Oncolytics* **14**, 279–287 (2019).
149. Vitanza, N. A. *et al.* Intraventricular B7-H3 CAR T Cells for Diffuse Intrinsic Pontine Glioma: Preliminary First-in-Human Bioactivity and Safety. *Cancer Discov.* **13**, 114–131 (2023).

Appendix

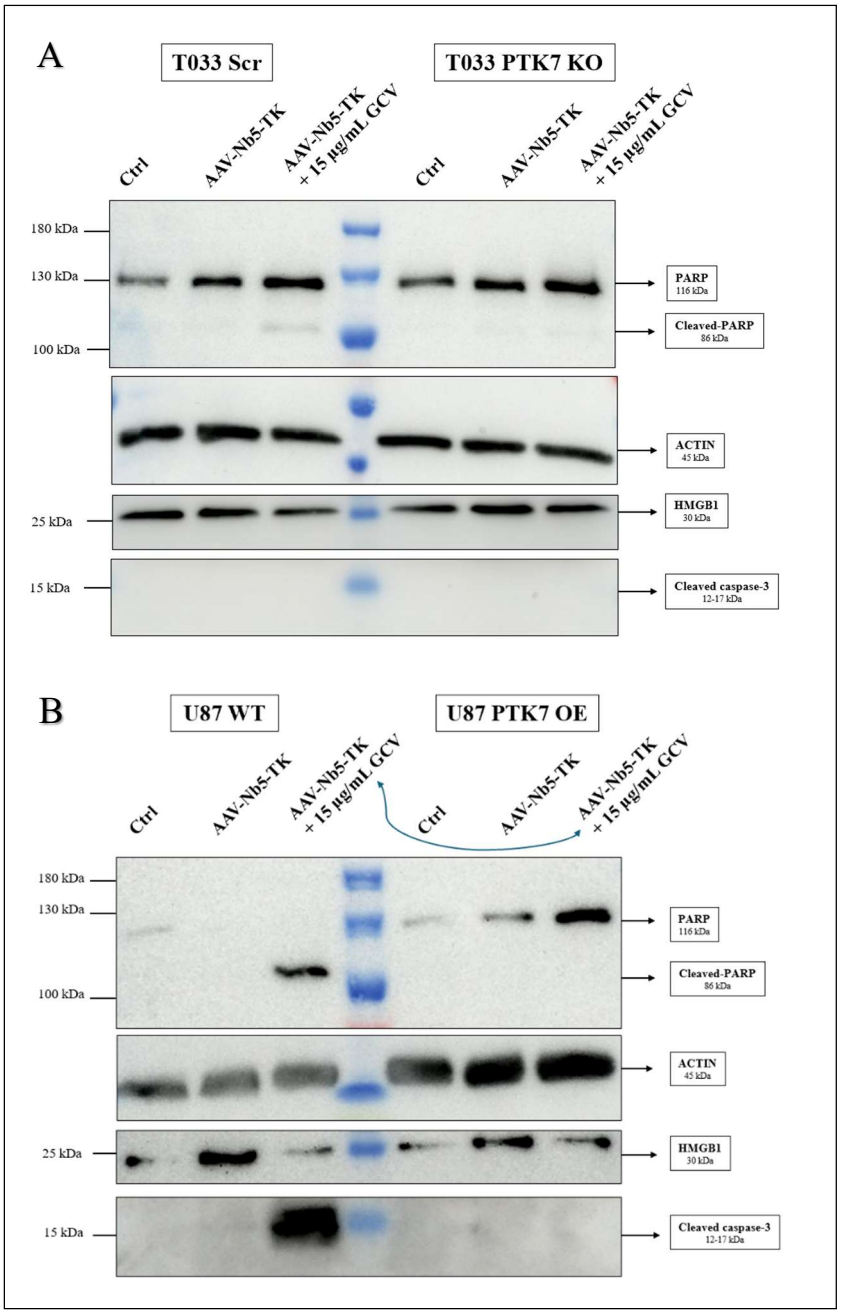

Supplementary Figure S1. Variability of protein expression across independent western blot experiments. Representative western blots analyses of cleaved CASP-3, PARP and HMGB1 under the same experimental conditions as described in Figure 12. (**A**) in T033 cells, cleaved CASP-3 signal was undetectable in this replicate despite similar experimental conditions. (**B**) Conversely, in U87 cells, cleaved CASP-3 signal was more prominent in this replicate compared to the main figure. HMGB1 also showed variability across experiments. These results highlight inter-experimental variability in protein detection while overall trends remain consistent.

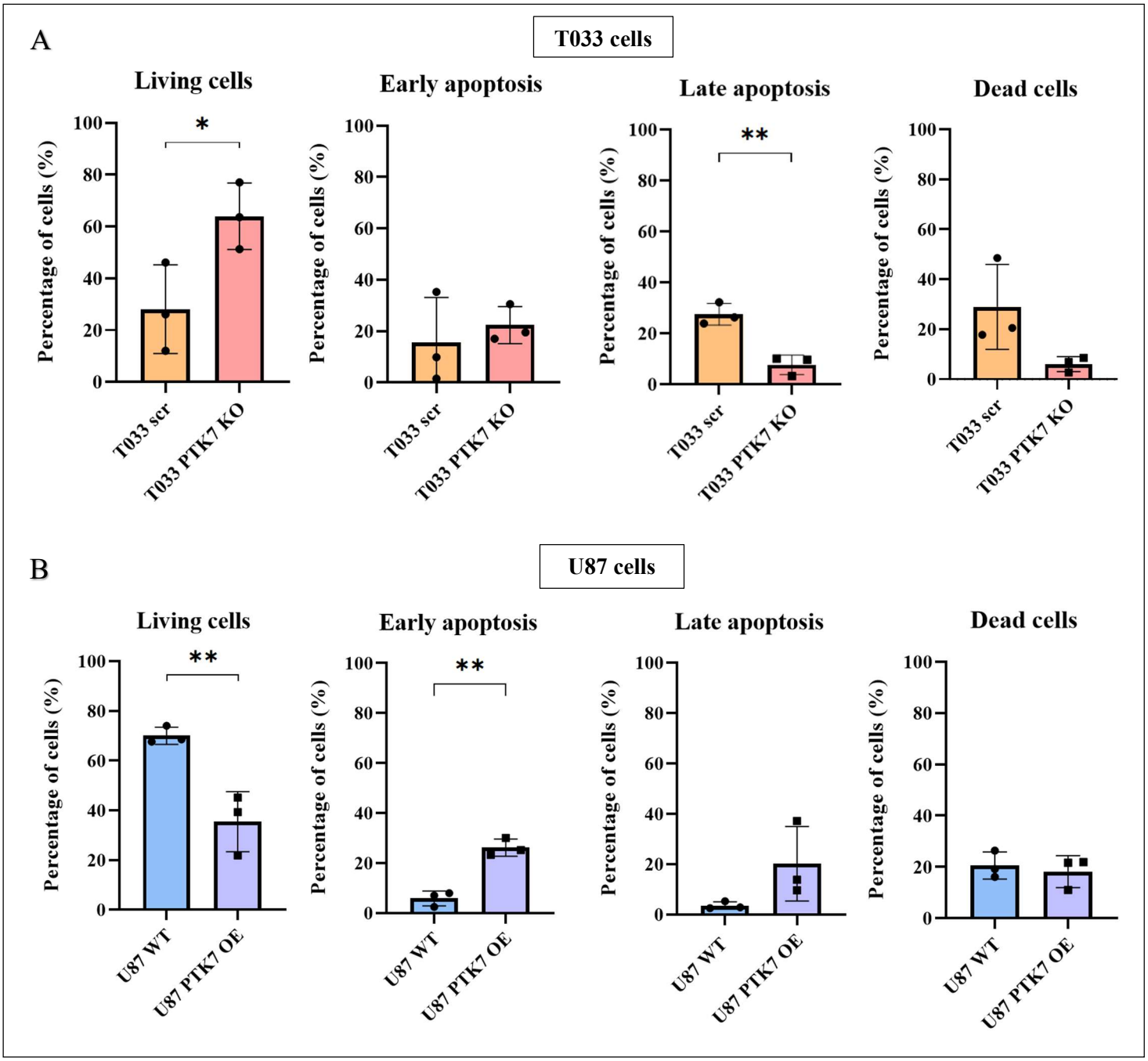

Supplementary Figure S2. Detailed quantification of cell death populations following Annexin V/DAPI staining. Representative histograms of cell death populations corresponding to living, early apoptotic, late apoptotic and necrotic/dead (**A**) T033, and (**B**) U87 cells following combined treatment. Data are represented as mean ± SEM from independent biological replicates. It confirms a significant increase in apoptotic populations and a significant decrease in living cells in $PTK7^{+}$ cells following treatment.

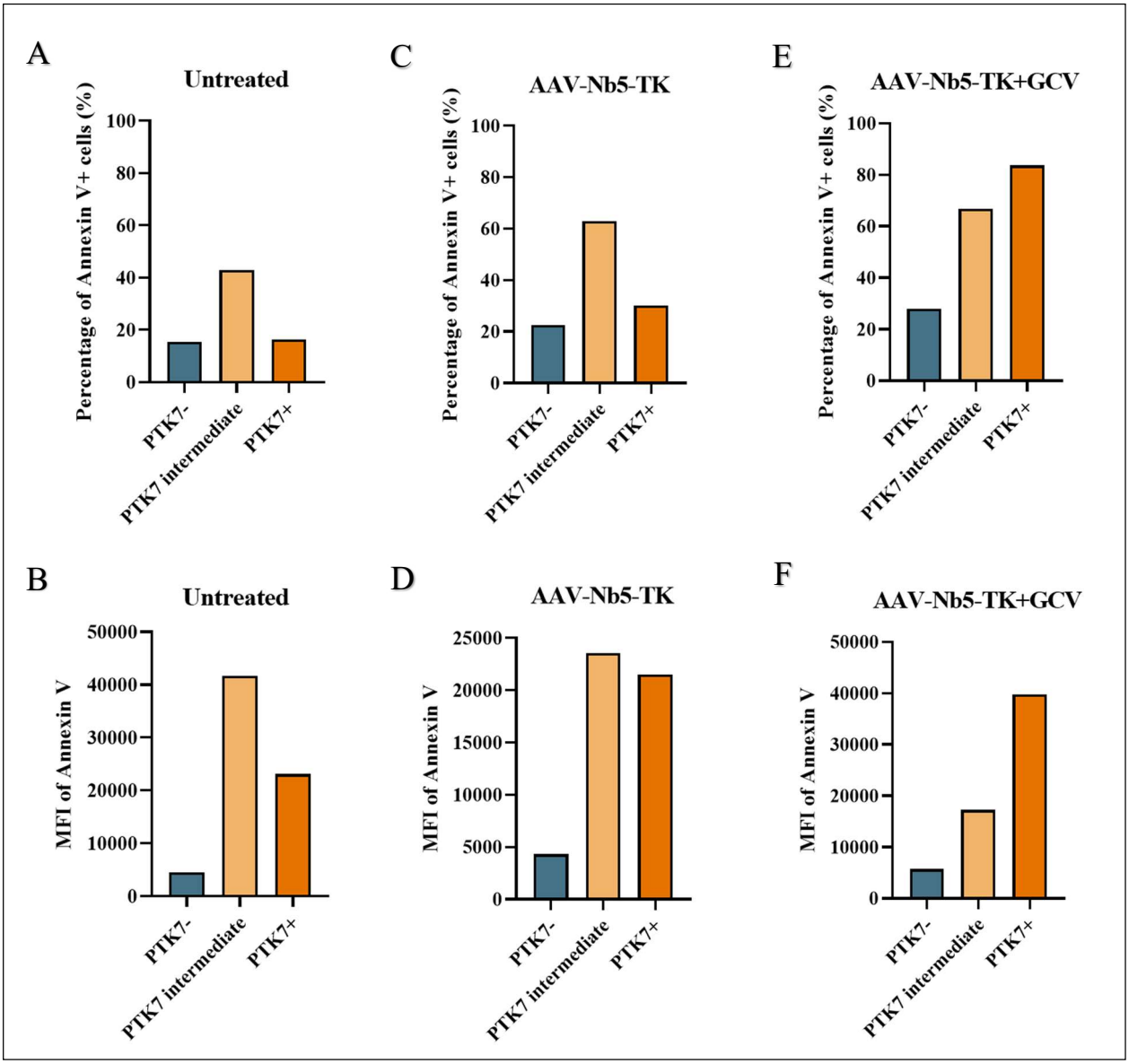

Supplementary Figure S3. Analysis of treatment-induced cell-death in T033 co-culture including PTK7 intermediate population. Quantification of (**A**) the percentage of Annexin V^+ cells and (**B**) MFI under untreated conditions. Quantification of (**C**) the percentage of Annexin V^+ cells and (**D**) MFI following AAV-Nb5-TK transduction. Quantification of (**E**) the percentage of Annexin V^+ cells and (**F**) MFI following AAV-Nb5-TK +GCV treatment.